

**UC Davis**

**UC Davis Electronic Theses and Dissertations**

**Title**

Examining Nitrate Leaching Potential and Nitrogen Cycle Dynamics under Agricultural Managed Aquifer Recharge in the Central Valley of California

**Permalink**

<https://escholarship.org/uc/item/940757hq>

**Author**

Murphy, Nicholas Paul

**Publication Date**

2021

Peer reviewed|Thesis/dissertation

Examining Nitrate Leaching Potential and Nitrogen Cycle Dynamics under Agricultural  
Managed Aquifer Recharge in the Central Valley of California

By

NICHOLAS PAUL MURPHY  
DISSERTATION

Submitted in partial satisfaction of the requirements for the degree of

DOCTOR OF PHILOSOPHY

in

Hydrologic Sciences

in the

OFFICE OF GRADUATE STUDIES

of the

UNIVERSITY OF CALIFORNIA

DAVIS

Approved:

---

Helen E. Dahlke, Chair

---

William R. Horwath

---

Majdi Abou Najm

Committee in Charge

2022

Copyright © 2022 by Nicholas P. Murphy

All rights reserved. No part of this dissertation may be reproduced or used in any manner without written permission of the copyright owner except with appropriate citation for use in a review. For more information, address: [npmurphy@ucdavis.edu](mailto:npmurphy@ucdavis.edu)

## **ACKNOWLEDGEMENTS**

Thank you to my advisor Helen Dahlke for her mentorship, wisdom, and support throughout my Ph.D. You pushed me to critically examine the existing scientific literature, finding opportunities to increase our knowledge and ability to sustainably manage groundwater resources in the future. I have watched you grow as a professor and mentor, evident by the exponential growth of your lab group in the past five years, in both amazing scientists and exciting, interdisciplinary research. Thank you for helping me develop the research skills I needed to succeed and giving me the freedom to pursue my own passions and interests within projects. Thank you to my dissertation committee for the valuable feedback regarding my research, you always provided thoughtful discussions that improved my research focus.

Thank you to my family, who supported me through the tough times, and cheered me on through the good times. In particular this includes my mother Kim, who encouraged me to move as far across the country from her as possible to pursue my dreams. Thank you to all my wonderful friends on both coasts (I'm lucky to say they are too many to name) who gave support to see me through the completion of my Ph.D.

Thank you to the Hydrologic Sciences Graduate Group at UC Davis, and all of my peers, teachers and mentors, I will always appreciate the educational and professional opportunities and connections I've gained here.

## TABLE OF CONTENTS

ACKNOWLEDGEMENTS.....	ii
ABSTRACT.....	x
1 INTRODUCTION.....	1
2 Chapter 1: Influence of Agricultural Managed Aquifer Recharge on nitrate transport – the role of soil texture and flooding frequency.....	6
CHAPTER 1 ABSTRACT .....	7
2.1 INTRODUCTION .....	8
2.2 MATERIALS AND METHODS .....	13
2.2.1 <i>Field Experiments</i> .....	13
2.2.1.1 <i>Study sites</i> .....	13
2.2.1.2 <i>Field instrumentation and modeling</i> .....	14
2.2.2 <i>Laboratory Experiments</i> .....	16
2.2.2.1 <i>Soil column experiments</i> .....	16
2.2.2.2 <i>Soil incubations and NO<sub>3</sub><sup>-</sup>-N mass balance calculations</i> .....	18
2.3 RESULTS .....	20
2.3.1 <i>Field Trials</i> .....	20
2.3.2 <i>Soil Column Experiments</i> .....	22
2.3.2.1 <i>Soil NO<sub>3</sub><sup>-</sup>-N mass balance and transport</i> .....	22
2.3.2.2 <i>Mineralization incubations and nitrate mass balance</i> .....	28
2.4 DISCUSSION.....	30
2.4.1 <i>Field Scale residual NO<sub>3</sub><sup>-</sup>-N profile trends</i> .....	30
2.4.2 <i>Biogeochemical Processes under varying flooding frequencies</i> .....	31
2.4.3 <i>Implications for field-scale nitrate leaching</i> .....	33

2.5 CONCLUSIONS .....	36
<b>3 Chapter 2: Comparison of reactive transport and non-equilibrium modeling approaches for the estimation of nitrate leaching under large water application events .....</b>	<b>38</b>
<b>CHAPTER 2 ABSTRACT.....</b>	<b>39</b>
<b>3.1 INTRODUCTION .....</b>	<b>40</b>
<b>3.2 MODEL THEORY AND STRUCTURE.....</b>	<b>47</b>
3.2.1 <i>Water Flow and Solute Transport.....</i>	48
3.2.2 <i>Biogeochemical reactions.....</i>	50
<b>3.3 MATERIALS AND METHODS.....</b>	<b>51</b>
3.3.1 <i>Experimental Design.....</i>	51
3.3.2 <i>Initial and Boundary Conditions.....</i>	52
3.3.3 <i>Model Sensitivity Analysis.....</i>	53
3.3.4 <i>Model Calibration.....</i>	53
<b>3.4 RESULTS.....</b>	<b>55</b>
3.4.1 <i>Hydrologic Calibration of the HP1-MIM model.....</i>	55
3.4.2 <i>Biogeochemical Calibration of the HP1-MIM model.....</i>	58
3.4.3 <i>Model Comparison.....</i>	63
<b>3.5 DISCUSSION.....</b>	<b>71</b>
3.5.1 <i>Model Sensitivity Analysis and Calibration.....</i>	71
3.5.2 <i>Conditionalization for Environmental Factors.....</i>	73
3.5.3 <i>Modeling Physical &amp; Chemical Non-Equilibrium Dynamics.....</i>	76
<b>3.6 CONCLUSION.....</b>	<b>77</b>
<b>4 Chapter 3: A multi-scenario analysis examining the effect of flooding frequency and flooding magnitude on nitrate leaching under large water application events.... ..</b>	<b>79</b>
<b>CHAPTER 3 ABSTRACT.....</b>	<b>80</b>

<b>4.1 INTRODUCTION .....</b>	<b>81</b>
<b>4.2 MATERIALS AND METHODS .....</b>	<b>86</b>
<b>4.2.1 Study Sites.....</b>	<b>86</b>
<b>4.2.2 Model Theory and Development.....</b>	<b>87</b>
<b>4.2.3 Model Calibration and Validation.....</b>	<b>88</b>
<b>4.2.4 Multi-scenario Analysis.....</b>	<b>90</b>
<b>4.3 RESULTS.....</b>	<b>92</b>
<b>4.3.1 Hydrologic Calibration.....</b>	<b>92</b>
<b>4.3.2 Biogeochemical Model Performance.....</b>	<b>94</b>
<b>4.3.3 Multi-Scenario Analysis.....</b>	<b>98</b>
<b>4.4 DISCUSSION.....</b>	<b>108</b>
<b>4.4.1 Multi-Scenario Analysis – Ag-MAR Best Management Practices.....</b>	<b>108</b>
<b>4.4.1.1 Flooding Frequency.....</b>	<b>109</b>
<b>4.4.1.2 Flooding Magnitude.....</b>	<b>110</b>
<b>4.4.1.3 Climate.....</b>	<b>112</b>
<b>4.4.2 Overarching Ag-MAR Considerations.....</b>	<b>113</b>
<b>4.4.3 Model Calibration and Validation.....</b>	<b>115</b>
<b>4.5 CONCLUSION.....</b>	<b>118</b>
<b>Appendix 1: Supplementary information for Chapter 1.....</b>	<b>119</b>
<b>Appendix 2: Supplementary information for Chapter 2.....</b>	<b>131</b>
<b>Appendix 3: Supplementary information for Chapter 3.....</b>	<b>137</b>
<b>REFERENCES .....</b>	<b>146</b>

## Figure List

Figure 2.1: Study locations and experimental setup. (a) fine sandy loam experimental field design; (b) sand experimental field design; and (c) Experimental laboratory column design, where $\theta$ – volumetric water content sensor, PW – pore water sampler, DO – dissolved oxygen sensor.....	14
Figure 2.2: Initial characterization of field soils with depth for (a) texture, (b) $\text{NO}_3^-$ -N, (c) $\text{NH}_4^+$ -N, (d) TC and (e) TN. LF – Low frequency treatment (1-2 weeks), HF – High frequency treatment (72 hours).....	23
Figure 2.3: Comparison of before (blue bars) and after (red bars) $\text{NO}_3^-$ -N loads in the soil profiles of the soil column experiments, (a) sand LF, (b) sand HF, (c) fine sandy loam LF and (d) fine sandy loam HF. Error bars represent one standard deviation of $\text{NO}_3^-$ -N in soil profile. P-values represent the statistical significance that the before and after values measured in the respective soil layer are not equal.....	24
Figure 2.4: Observed $\text{NO}_3^-$ -N concentrations in discharge through time, (a) sand LF, (b) sand HF, (c) fine sandy loam LF, and (d) fine sandy loam HF.....	25
Figure 2.5: Initial soil nitrate mass and amount of nitrate leached during each water application (WA) during the low frequency (a) and high frequency (b) column experiments using sand and fine sandy loam soils. Percentages represent the percent of initially present $\text{NO}_3^-$ -N (grey bar) leached in each WA. ....	27
Figure 2.6: Mineralization rates for the (a) sand and (b) fine sandy loam.....	29
Figure 2.7: Total nitrate mass balance for soil columns. Error bars represent one standard deviation of the aggregated error for all components of a single column.....	29
Figure 3.1: Examples of N cycling modeling approaches: (a) non-reactive modeling approach, (b) zero-order, first-order, or complex conditional approach, depending on functional dependence of biogeochemical equations 1 – 4, and (c) complex conditional modeling approach utilizing physical nonequilibrium (MIM dynamics). See Table 3.1 for the modeling approaches used in this paper, and their associated biogeochemical reactions. ....	43
Figure 3.2: Simulated modeling results vs. observed data for recharge and cumulative recharge at the bottom of the model domain (80 cm depth), using calibrated van Genuchten parameters. (a) and (b) represent the observed laboratory data compared to the simulated model recharge and cumulative recharge, respectively, for the fine sandy loam soil. (c) and (d) represent the same data for the sand soil. ....	56
Figure 3.3: Local sensitivity analysis of fine sandy loam hydraulic parameters. The shaded area represents the change in cumulative discharge at the bottom of the model due to a 40% parameter variation. (a) residual water content ( $\theta_r$ ), (b) saturated water content ( $\theta_s$ ), (c) alpha ( $\alpha$ ), (d) n, (e) saturated hydraulic conductivity ( $K_s$ ), (f) tortuosity (L). ....	57

Figure 3.4: Local sensitivity analysis of sand hydraulic parameters. The shaded area, in colors corresponding to material layers in the model, represents the change in cumulative discharge at the bottom of the model due to a 40% parameter variation. Note that for the sand soil two sets of parameters were calibrated for the upper soil layer (layer 1: 0-60 cm) and lower soil layer (layer 2: 60-80 cm). (a) residual water content ( $\theta_r$ ), (b) saturated water content ( $\theta_s$ ), (c) alpha ( $\alpha$ ), (d) n, (e) saturated hydraulic conductivity ( $K_s$ ), (f) tortuosity (L)..... 58

Figure 3.5: Biogeochemical validation metrics for simulated vs. observed model fit for the fine sandy loam. (a) cumulative  $\text{NO}_3^-$  leached from the profile, (b)  $\text{NO}_3^-$  leached from the profile, (c) residual  $\text{NO}_3^-$  in soil profile at the end of model simulation, (d) residual  $\text{NH}_4^+$  in soil profile at end of model simulation. Grey shaded areas show one standard deviation of error for the initial  $\text{NO}_3^-$  concentrations in the soil profile and the estimated mineralization rate constants..... 61

Figure 3.6: Biogeochemical validation metrics for simulated vs. observed model fit for the sand. (a) cumulative  $\text{NO}_3^-$  leached from the profile, (b)  $\text{NO}_3^-$  leached from the profile, (c) residual  $\text{NO}_3^-$  in soil profile at the end of model simulation, (d) residual  $\text{NH}_4^+$  in soil profile at end of model simulation. Grey shaded areas show one standard deviation of error for the initial  $\text{NO}_3^-$  concentrations in the soil profile and the estimated mineralization rate constants..... 62

Figure 3.7: Comparison of selected N mass balance components simulated with the NR, ZK, FK, HP1, and HP1-MIM models for the fine sandy loam. (a) cumulative  $\text{NO}_3^-$  leached at the bottom of model domain, (b) residual  $\text{NO}_3^-$  in soil profile, (c) residual  $\text{NH}_4^+$  in soil profile. -ND represents a model which does not incorporate denitrification in the biogeochemical processes. 66

Figure 3.8: Comparison of selected N mass balance components simulated with the NR, ZK, FK, HP1, and HP1-MIM models for the sand. (a) cumulative  $\text{NO}_3^-$  leached from the bottom of model domain, (b) residual  $\text{NO}_3^-$  in soil profile, (c) residual  $\text{NH}_4^+$  in soil profile. -ND represents a model which does not incorporate denitrification in the biogeochemical processes. .... 68

Figure 3.9: N mass balance for fine sandy loam with biogeochemical processes shown for models – (a) NR, (b) ZK, (c) FK, (d) HP1, (e) ZK-ND, (f) FK-ND, (g) HP1-MIM..... 70

Figure 3.10: N mass balance for sand with biogeochemical processes shown for models – (a) NR, (b) ZK, (c) FK, (d) HP1, (e) ZK-ND, (f) FK-ND, (g) HP1-MIM. .... 70

Figure 4.1: Soil temperature and precipitation data used for the fine sandy loam field site. Data used from CIMIS Station 71. (a) Soil temperature and precipitation from the 2015/16 season, representative of a dry winter. (b) Soil temperature and precipitation from the 2016/17 season, representative of a wet winter..... 91

Figure 4.2: Soil temperature and precipitation data used for the sand field site. Data used from CIMIS Station 206. (a) Soil temperature and precipitation from the 2015/16 season, representative of a dry winter. (b) Soil temperature and precipitation from the 2016/17 season, representative of a wet winter..... 92

Figure 4.3: Hydrologic calibration metric for the (a) fine sandy loam and (b) sand soils. Comparison of modeled versus observed volumetric water content. Blue line represents modeled results. Black line represents observed field data. Blue triangles represent Ag-MAR flooding events..... 93

Figure 4.4: Model performance for the fine sandy loam field site. (a) residual  $\text{NO}_3^-$  in the soil profile at the end of model simulation for FSL-core 1, (b) residual  $\text{NO}_3^-$  in the soil profile at the end of model simulation for FSL-core 2. Model uncertainty represents the one standard deviation of error in the mineralization and denitrification kinetic rate parameters..... 96

Figure 4.5: Model performance for the sand field site. (a) residual  $\text{NO}_3^-$  in the soil profile at the end of model simulation for core 1 (S-core1), (b) residual  $\text{NO}_3^-$  in the soil profile at the end of model simulation for core 2 (S-core2), (c) residual  $\text{NO}_3^-$  in the soil profile at the end of model simulation for core 3 (S-core 3). Model uncertainty represents one standard deviation error in mineralization and denitrification kinetic rate parameters. .... 97

Figure 4.6: Flooding frequency scenarios for the fine sandy loam soil at 15 cm flooding magnitude. (a) sum of  $\text{NO}_3^-$  leached from model domain during Ag-MAR flooding season, (b) residual  $\text{NO}_3^-$  in soil profile following Ag-MAR flooding season, (c) amount of mineralization occurring during Ag-MAR flooding season, (d) amount of denitrification occurring during Ag-MAR flooding season, as a function of flooding frequency. .... 100

Figure 4.7: Flooding frequency scenarios for the sand soil at 15 cm flooding magnitude. (a) sum of  $\text{NO}_3^-$  leached from model domain during Ag-MAR flooding season, (b) residual  $\text{NO}_3^-$  in soil profile following Ag-MAR flooding season, (c) amount of mineralization occurring during Ag-MAR flooding season, (d) amount of denitrification occurring during Ag-MAR flooding season, as a function of flooding frequency. .... 102

Figure 4.8: Flooding magnitude scenarios for the fine sandy loam soil at the 7-day flooding frequency. (a) sum of  $\text{NO}_3^-$  leached from model domain during Ag-MAR flooding season, (b) residual  $\text{NO}_3^-$  in soil profile following Ag-MAR flooding season, (c) amount of mineralization occurring during Ag-MAR flooding season, (d) amount of denitrification occurring during Ag-MAR flooding season, as a function of flooding magnitude. .... 104

Figure 4.9: Flooding magnitude scenarios for the sand soil at the 7-day flooding frequency. (a) sum of  $\text{NO}_3^-$  leached from model domain during Ag-MAR flooding season, (b) residual  $\text{NO}_3^-$  in soil profile following Ag-MAR flooding season, (c) amount of mineralization occurring during Ag-MAR flooding season, (d) amount of denitrification occurring during Ag-MAR flooding season, as a function of flooding magnitude. .... 106

Figure 4.10: Concentration of  $\text{NO}_3^-$  in the bulk applied recharge during an Ag-MAR season, as a function of flooding magnitude and flooding frequency for the fine sandy loam site. The thick dashed line represents the  $5 \text{ mg L}^{-1} \text{ NO}_3^- \text{-N}$  concentration threshold..... 107

Figure 4.11: Concentration of  $\text{NO}_3^-$  in the bulk applied recharge during an Ag-MAR season, as a function of flooding magnitude and flooding frequency for the sand site. The thick black line

represents the 10 mg L<sup>-1</sup> NO<sub>3</sub><sup>-</sup>-N concentration threshold and the dashed line represents the 5 mg L<sup>-1</sup> NO<sub>3</sub><sup>-</sup>-N concentration threshold..... 108

### Table List

Table 2.1: Sand and fine sandy loam field core NO<sub>3</sub>--N loads. The root zone (RZ) is defined as the first 100 cm of the core and while Full denotes the entire 400 cm profile or core length.....21

Table 3.1: Modeling approaches and their associated reactions as pictured in Figure 1.....43

Table 4.1: Biogeochemical processes simulated with the HP1-MIM model and their conditionalization parameters.  $k_{min}$  is the first order rate constant for mineralization,  $q$  is discharge,  $k_{nit}$  is the first order rate constant for nitrification,  $T$  is soil temperature,  $\omega$  is the mass transfer coefficient, and %PSF is the percent pore space filled with water..... 88

Table 4.2: Calibrated van Genuchten parameters for the fine sandy loam and sand.....94

## ABSTRACT

Dependence on groundwater for irrigation and consumptive use has resulted in the widespread depletion of groundwater aquifers across the world. In most of the semi-arid Southwest of the United States, groundwater is increasingly being regulated in efforts to sustainably manage this limited resource. Various Managed Aquifer Recharge (MAR) techniques are used to increase the sustainable management of groundwater resources. Agricultural Managed Aquifer Recharge (Ag-MAR) is a promising form of managed aquifer recharge, where farmland is flooded during the winter using excess surface water resources from runoff in order to recharge the underlying groundwater aquifer. In addition to increasing the security of groundwater resources and improving general drought resilience, Ag-MAR may have additional beneficial outcomes including flood risk reduction, drought preparedness, maintenance of environmental flows in aquatic ecosystems, prevention of saltwater intrusion in coastal aquifer systems, mitigating land subsidence as well as water quality benefits such as flushing salts from the shallow vadose zone. One main concern surrounding Ag-MAR implementation is the potential for increased nitrate ( $\text{NO}_3^-$ ) leaching from historically cultivated agricultural land. When ingested in high concentrations,  $\text{NO}_3^-$  has been linked to methaemoglobinaemia (“blue baby syndrome”), miscarriages, and non-Hodgkin’s lymphoma. In order to evaluate the general viability of Ag-MAR as an appropriate MAR technique that presents minimal risk to agricultural production systems and groundwater contamination, a thorough understanding of nitrogen cycle dynamics under Ag-MAR must be developed. This dissertation focuses on evaluating the hydrologic and biogeochemical processes driving  $\text{NO}_3^-$  leaching and nitrogen cycling in the shallow vadose zone, under varying soil textures and Ag-MAR best management practices. First, I present field and laboratory experiments, which

examine how different recharge practices affect  $\text{NO}_3^-$  leaching, mineralization and denitrification processes in different soil textures. Results show that short-lived, pulsed Ag-MAR flooding events cause  $\text{NO}_3^-$  leaching and organic N mineralization, whereby the dominant soil texture of an Ag-MAR site impacts both the timing of  $\text{NO}_3^-$  leaching, and the conditions for biogeochemical processes under Ag-MAR. Specifically, reducing time between flooding events for Ag-MAR reduces mineralization/nitrification, which in turn decreases mass of  $\text{NO}_3^-$  leached. This has implications for the development of Ag-MAR best management practices (BMPs), suggesting that in a N mineralization dominated system, short flooding frequencies may decrease mineralization/nitrification and  $\text{NO}_3^-$  leaching potential of Ag-MAR. Next, I developed a dual-porosity, mobile-immobile zone (MIM), reactive transport model using HP1 (HYDRUS-1D and PHREEQC), simulating  $\text{NO}_3^-$  leaching and biogeochemical processes under large water application events using observed datasets from the previous field and laboratory experiments. When comparing this HP1-MIM model to traditional  $\text{NO}_3^-$  leaching models, I find that the incorporation of environmental factors, and physical non-equilibrium dynamics improve model performance when estimating cumulative  $\text{NO}_3^-$  leached from the shallow vadose zone, and the amount of  $\text{NO}_3^-$  in the residual soil profile following water application events. Finally, I use this reactive transport model to perform a multi-scenario analysis, examining  $\text{NO}_3^-$  leaching potential, residual  $\text{NO}_3^-$  in the soil profile after water application events, and biogeochemical rates during water application events, over a variety of Ag-MAR best management practices (flooding frequency, flooding magnitude) and climate scenarios (dry year, wet year) to determine what Ag-MAR practices minimize  $\text{NO}_3^-$  leaching to the groundwater. For this analysis, I estimate the range of  $\text{NO}_3^-$  leached under Ag-MAR for two soil textures. Results of this analysis indicate that soil texture has a large influence on the moisture and oxygen regime of the soil,

which in turn defines whether the soil system is dominated by denitrification or mineralization during and after Ag-MAR events. This has implications regarding Ag-MAR best management practices, and the general viability of Ag-MAR implementation. Across all soil types, we see the ability of high-magnitude water applications to dilute the mass of  $\text{NO}_3^-$  being leached below the shallow vadose zone to low concentrations in the bulk recharge. This indicates that under proper management,  $\text{NO}_3^-$  leaching during high magnitude water applications can be minimized.

## INTRODUCTION

In semi-arid regions such as California, groundwater is a critical resource, contributing between 38 - 46% of the state's total water supply (DWR, 2019). In addition to supporting California's \$46 billion agricultural economy, many rural communities are fully dependent on groundwater resources for their water supply (Mehta et al. 2018). As a result of increased demand, groundwater resources have been continually over drafted in California, ranging from 1.2 – 2.5 km<sup>3</sup> of yearly overdraft (Hanak et al. 2017). Groundwater overdraft can result in undesirable effects, including declines in groundwater-level, subsidence, seawater intrusion, reductions in groundwater-storage, a decrease in the interconnection between groundwater and surface water systems, and water quality degradation (Konikow et al. 2005). The Sustainable Groundwater Management Act (SGMA) was passed in 2014 in an effort to set in place a plan to achieve groundwater sustainability by 2040. SGMA resulted in the creation of Groundwater Sustainability Agencies (GSAs), with the purpose of addressing groundwater sustainability at the local basin-scale. Over the past four year, these GSAs have developed Groundwater Sustainability Plans (GSPs) outlining objectives, milestones and actions to be implemented over a 20 year horizon to reach long-term sustainability by 2040, through a variety of groundwater resource management strategies. As part of these GSPs, many GSAs are implementing or planning groundwater recharge projects, designed to contribute towards the sustainable use of groundwater at a regional scale.

Managed Aquifer Recharge (MAR) projects can contribute to these efforts, attempting to mitigate groundwater overdraft and increase groundwater sustainability through a variety of implementation methods (Dahlke et al. 2018). One method in particular, Agricultural Managed Aquifer Recharge (Ag-MAR), has developed over the last decade as a strategy to achieve

groundwater sustainability. Over 3.6 million acres of suitable agricultural land has been identified in California, often equipped with water conveyance infrastructure, making Ag-MAR projects a cost-effective MAR option, in comparison to traditional MAR techniques such as injection wells or infiltration ponds (O'Geen et al. 2015, Kocis & Dahlke 2017, Dahlke et al. 2018). While Ag-MAR decision support tools such as the Soil Agricultural Groundwater Banking Index (SAGBI) have rated soils in California based upon their suitability for Ag-MAR recharge projects using five factors including soil profile percolation rate, root zone residence time, chemical limitations, topography, and soil surface conditions, it acknowledges its omission of important factors, specifically nitrate ( $\text{NO}_3^-$ ) leaching potential (O'Geen et al. 2015). One of the largest concerns regarding widespread implementation of Ag-MAR is the increased potential for groundwater contamination, specifically from legacy  $\text{NO}_3^-$  stored in the vadose zone.

Nitrate accumulation in the vadose zone has occurred as a result inefficient fertilization over the course of many years of agricultural production. Research shows the accumulation of residual  $\text{NO}_3^-$  in the shallow vadose zone is the result of a combination of fertilizer over-application and irrigation inefficiency, which is pushing  $\text{NO}_3^-$  below the rooting depth of crops, where it slowly accumulates and is transported towards the groundwater table through inefficient irrigation and natural precipitation (Di & Cameron, 2002a, Harter et al. 2005). This legacy  $\text{NO}_3^-$  is at risk of being leached under Ag-MAR, where large amounts of water are applied over short periods of time (Botros et al. 2012, Onsoy et al. 2005).

There has been a significant amount of research regarding  $\text{NO}_3^-$  transport through the vadose zone in an agricultural setting under varying irrigation practices, including drip (Baram et al. 2016, Lv et al. 2019, Phogat et al. 2014), sprinkler (Baram et al. 2016, Gheysari et al. 2009), and flood irrigation (Di et al. 2002a, Wang et al. 2010). Generally, this research supports the idea

that N supply from the vadose zone is transport-limited, with more efficient irrigation leading to lower  $\text{NO}_3^-$  leaching from the soil profile. This becomes less applicable when considering Ag-MAR, which involves large water applications which cannot be optimized for irrigation efficiency. Because Ag-MAR involves water amounts much larger than applied during typical irrigation events, we observe hydrologic and biogeochemical conditions in the soil profile atypical to the conditions observed during the growing season under traditional irrigation systems. Previous N transport research is therefore unlikely to represent the timing and magnitude of  $\text{NO}_3^-$  leaching and N cycling processes occurring under Ag-MAR flooding events.

Nitrogen cycling involves several organic and inorganic nitrogen compounds, and transformations depend on environmental conditions including soil moisture, soil temperature, microbial communities, pH and oxygen content (Booth et al. 2005, Cookson et al. 2007, Yu et al. 2009, Kuypers et al. 2018). To date, there are only a handful of studies which focus on N cycling and  $\text{NO}_3^-$  leaching under large water application events (Di et al. 2002, Mack et al. 2005, Waterhouse et al. 2021), and research gaps exist regarding the relationship between  $\text{NO}_3^-$  leaching potential, and the biogeochemical processes occurring during these high magnitude flooding events. An understanding must be developed of the relationship between  $\text{NO}_3^-$  leaching potential, and relevant biogeochemical processes (mineralization, denitrification) which may produce, mobilize or consume inorganic-N during Ag-MAR.

While there are a significant number of numerical modeling studies on  $\text{NO}_3^-$  leaching under typical agricultural management and irrigation practices, they often simplify nitrogen cycling dynamics, modeling  $\text{NO}_3^-$  as a conservative tracer (van der Laan et al. 2014, Karandish et al. 2017, Ajdary et al. 2007), or by using zero- or first-order kinetics (Li et al. 2015, Akbariyeh et al. 2018, Deb et al. 2015, Hanson et al. 2006, Hassan et al. 2008). Few studies have modeled

NO<sub>3</sub><sup>-</sup> leaching under Ag-MAR (Waterhouse et al. 2021), and further gaps exist regarding important N cycling processes and the incorporation of environmental conditions, including mineralization and denitrification dynamics as a function of temperature, moisture, and oxic/anoxic conditions. Additionally, to our knowledge, no studies have attempted to develop Ag-MAR best management practices (BMPs), which if optimized, may provide recommendations regarding Ag-MAR site development, in an effort to design Ag-MAR projects which minimize NO<sub>3</sub><sup>-</sup> leaching, while maximizing groundwater recharge.

Through a variety of field and laboratory experiments, paired with numerical modeling, this dissertation focuses on investigating nitrogen cycle dynamics and NO<sub>3</sub><sup>-</sup> leaching potential under Ag-MAR.

*Chapter 1 explores the relationship between soil texture and flooding frequency, and how these variables impact nitrate leaching potential under pulsed, Ag-MAR events.* Using a combination of field and laboratory experiments, high-resolution datasets are collected which measure the timing and magnitude of NO<sub>3</sub><sup>-</sup> leaching from the shallow vadose zone over the course of an Ag-MAR season. Soil texture is shown to impact the timing and magnitude of NO<sub>3</sub><sup>-</sup> leaching, and over 100% of the initially present NO<sub>3</sub><sup>-</sup> measured in the soil profile is flushed during some Ag-MAR treatments, indicating nitrogen mineralization can increase the mobile NO<sub>3</sub><sup>-</sup> available in the soil for leaching under subsequent Ag-MAR or irrigation events. Results show that decreasing the flooding frequency of Ag-MAR water applications decreases the potential mineralization, and subsequently decreases the amount of NO<sub>3</sub><sup>-</sup> leached during flooding events.

*Chapter 2 uses the high-resolution datasets collected in Chapter 1 to develop a reactive*

*transport model, capable of modeling N cycling processes and nitrate leaching through the incorporation of environmental conditionalization, and physical non-equilibrium dynamics.*

When compared to traditional  $\text{NO}_3^-$  leaching model schemes, the HP1-MIM model (HYDRUS-1D & PHREEQC) indicates superior model performance in estimating the observed  $\text{NO}_3^-$  leached under Ag-MAR events and the residual  $\text{NO}_3^-$  present in the soil profile following an Ag-MAR season across different soil textures.

*Chapter 3 presents a multi-scenario analysis evaluating the effect of different Ag-MAR best management practices (e.g. flooding frequency, flooding magnitude) on nitrate leaching as a function of soil texture and climate.* We see distinct management recommendations with regards to the interactions between soil texture, flooding frequency, and estimated  $\text{NO}_3^-$  leached. Results from this analysis show that the dilution effect is observed in both soil textures under high-magnitude flooding applications, indicating the potential for low  $\text{NO}_3^-$  concentrations in the bulk recharge. Under proper management,  $\text{NO}_3^-$  leaching during high magnitude water applications can be minimized, if a site supports large water applications depending on crop tolerance to flooding, water availability, and water conveyance.

## **Chapter 1: Influence of Agricultural Managed Aquifer Recharge on nitrate transport – the role of soil texture and flooding frequency**

Nicholas P Murphy<sup>1,\*</sup>, Hannah Waterhouse<sup>1</sup>, Helen E. Dahlke<sup>1</sup>

Affiliations: <sup>1</sup> Department of Land, Air and Water Resources, University of California, Davis, Davis, CA, 95616, USA. Corresponding author: [npmurphy@ucdavis.edu](mailto:npmurphy@ucdavis.edu)

### Core Ideas:

- Short-lived Ag-MAR flooding events cause nitrate leaching and organic N mineralization
- Soil texture impacts the timing of nitrate leaching under Ag-MAR
- Soil texture impact the conditions for biogeochemical processes under Ag-MAR
- Reducing time between flooding events for Ag-MAR reduces nitrate produced by mineralization

Abbreviations: Ag-MAR, agricultural managed aquifer recharge; NO<sub>3</sub><sup>-</sup>, nitrate; NH<sub>4</sub><sup>+</sup>, ammonium; TN, total nitrogen; TC, total carbon; DO, dissolved oxygen; NUE, nitrogen use efficiency; BMPs, Best Management Practices; WA, water application

## ABSTRACT

Agricultural Managed Aquifer Recharge (Ag-MAR) is a concept in which farmland is flooded during the winter using excess surface water to recharge the underlying groundwater. In this study, we show how different recharge practices affect nitrate ( $\text{NO}_3^-$ ) leaching and mineralization/denitrification processes in different soil systems. Two contrasting soil textures (sand, fine sandy loam) from the Central Valley, California were repeatedly flooded with 15 cm of water at varying time intervals in field and soil column experiments. Nitrogen species ( $\text{NO}_3^-$ ,  $\text{NH}_4^+$ , total nitrogen), total carbon, dissolved oxygen, and moisture content were measured throughout the experiments. Results show that when flooding occurs at longer intervals (every 1-2 weeks), N mineralization increases, leading to an increase of mobile  $\text{NO}_3^-$  in the upper root zone and leaching of significant quantities of  $\text{NO}_3^-$  from both soil textures ( $137.3\% \pm 6.6\%$  (sand) and  $145.7\% \pm 5.8\%$  (fine sandy loam) of initial residual soil  $\text{NO}_3^-$ ) during subsequent flooding events. Laboratory mineralization incubations show that long flooding intervals promote mineralization and production of excess  $\text{NO}_3^-$  at rates of  $0.11\text{-}3.93 \text{ mg N kg}^{-1} \text{ wk}^{-1}$  (sand) and  $0.08\text{-}3.41 \text{ mg N kg}^{-1} \text{ wk}^{-1}$  (fine sandy loam). Decreasing the flooding frequency to 72 hours reduces potential mineralization, decreasing the amount of  $\text{NO}_3^-$  leached during flooding events ( $31.7\% \pm 3.8\%$  (sand) and  $64.7\% \pm 10.4\%$  (fine sandy loam) of initial residual soil  $\text{NO}_3^-$ ). The results indicate that implementing recharge as repeated events over a long (multiple weeks) time horizon might increase the total amount of  $\text{NO}_3^-$  potentially available for leaching to groundwater.

## 2.1 INTRODUCTION

Dependence on groundwater for irrigation and consumptive use has resulted in the widespread depletion of groundwater aquifers across the world (Wada et al., 2014, Dalin et al., 2019). In most of the semi-arid Southwest of the United States, groundwater is increasingly being regulated in efforts to sustainably manage this limited resource. Sustainably managing groundwater in California has increased the interest in and use of managed aquifer recharge (MAR) technologies that purposefully recharge water to aquifers for subsequent recovery or environmental benefit (Dillon et al., 2009).

Agricultural Managed Aquifer Recharge (Ag-MAR) is a promising form of managed aquifer recharge, where farmland is flooded during the winter using excess surface water in order to recharge the underlying groundwater aquifer (Kocis & Dahlke, 2017). Over 3.6 million hectares of suitable farmland that is connected to water conveyance systems have been identified for Ag-MAR throughout the Central Valley of California (O'Geen et al., 2015). Some of these lands support infiltration rates in excess of 50 cm per day, raising questions on how Ag-MAR could be implemented on suitable but fertilized agricultural fields such that nitrate ( $\text{NO}_3^-$ ) leaching from the root zone to the groundwater is minimized.

The risk of  $\text{NO}_3^-$  leaching to the underlying groundwater stems from nitrogen (N) accumulation in the soil profile as a result of repeated fertilizer applications and incomplete N uptake by crops (Di & Cameron, 2002a). Over-application of N fertilizer has been reported as a major contributing factor to the accumulation of  $\text{NO}_3^-$  in the soil profile (0 – 400 cm) as shown by Zhou et al. (2016), who observed a residual  $\text{NO}_3^-$  load of 453 – 2155 kg N ha<sup>-1</sup> in the North China Plain and Loess Plateau, China. Harter et al. (2005) observed the accumulation of 218 – 477 kg N ha<sup>-1</sup> in the deep vadose zone (1,600 cm depth) under a citrus orchard in California.

These residual  $\text{NO}_3^-$  loads in the root zone or deep vadose zone are at risk of being leached when large amounts of water (e.g.  $>10 - 15$  cm/day) are applied for Ag-MAR, which could potentially lead to water quality degradation of underlying groundwater resources (Botros et al., 2012; Onsoy et al., 2005).

Research regarding  $\text{NO}_3^-$  transport in the vadose zone has been conducted in agricultural settings under various irrigation practices, such as drip (Baram et al., 2016; Lv et al., 2019; Phogat et al., 2014), sprinkler (Baram et al., 2016; Gheysari et al., 2009), and flood irrigation (Di & Cameron, 2002b; Wang et al., 2010). These studies have concluded that N supply from the vadose zone to the groundwater is transport-limited rather than source-limited, with the most efficient irrigation systems (drip and sprinkler) leaching lower amounts of  $\text{NO}_3^-$  from the soil profile. Drip irrigation paired with optimized N fertilization has shown to reduce  $\text{NO}_3^-$  leaching by 90% compared to conventional flood irrigation practices (Lv et al., 2019; Di et al., 2002a; Wang et al., 2010). Flood irrigation is an irrigation method similar to Ag-MAR, often with a smaller ponding depth and shorter application duration than is applied during Ag-MAR. As such, these studies provide insights into how larger water applications and ponded conditions might influence  $\text{NO}_3^-$  leaching. Wang et al. (2010) flooded a winter-wheat, summer maize cropping systems on a silt loam soil in the North China Plain every 72 hours with two, 25 cm water applications and found that  $62\% \pm 7\%$  of the  $\text{NO}_3^-$  within the upper 200 cm of the soil profile was leached. Lv et al. (2019) reported that flood irrigation of tomato fields in a silt loam at an agricultural experimental station in Tianjin City, China showed low N use efficiency (NUE) resulting in 50% of total N input being leached ( $300 \text{ kg N ha}^{-1}$  per season). Hence, in many irrigated agricultural regions, precision irrigation and/or deficit irrigation are increasingly used to minimize  $\text{NO}_3^-$  leaching and to trap residual  $\text{NO}_3^-$  in or below the root zone (Baram et al., 2016;

Gheysari et al., 2009; Waddell et al., 2000). AgMAR, therefore, represents a significant hydrologic regime shift from current growing season irrigation practices in semi-arid climates.

To date, not many studies exist that have investigated the impact of Ag-MAR on  $\text{NO}_3^-$  leaching and nitrogen (N) transformation processes in the root zone. Among the few studies that do exist, Bachand et al. (2014) concluded that while  $\text{NO}_3^-$  will initially be leached to the groundwater under Ag-MAR, there is the potential to improve groundwater quality over time through subsequent flooding applications with low-N water. Waterhouse et al. (2020) assessed the root zone residual  $\text{NO}_3^-$  load of farm fields representing different soil textures, crop types, and management practices to quantify the risk of groundwater contamination under Ag-MAR, concluding that wine grape vineyards on permeable soils had the lowest observed  $\text{NO}_3^-$  leaching risk. They noted that further research is needed regarding the relationship between  $\text{NO}_3^-$  leaching, Ag-MAR practices (e.g. frequency and duration of floodwater applications), and soil texture.

Soil texture has been shown to significantly impact both the hydrologic flow properties and conditions favorable to biogeochemical transformations. Soil texture impacts infiltration rates and residence time of applied water and thus  $\text{NO}_3^-$  mobilization, potential sorption of N species, oxygen content, oxidation-reduction potential, and microbial activity, all factors which may affect biogeochemical processes (Aronsson & Bergström, 2001; Bergström & Johansson 1991; Sogbedji et al., 2000; Kaiser et al., 1992). Gaines et al. (2008) examined the impact of soil texture and organic matter content on  $\text{NO}_3^-$  leaching potential and found that increased fractions of silt, clay and organic matter in a soil decrease the amount of  $\text{NO}_3^-$  leaching observed. Mineralization of organic N is the conversion of organic N to  $\text{NH}_4^+$ , which can be subsequently undergo nitrification, the conversion of  $\text{NH}_4^+$  to  $\text{NO}_3^-$ . Net mineralization (the conversion of

organic N to inorganic N), hereby referred to generally as mineralization, can under favorable temperature ( $>25^{\circ}\text{C}$ ) and moisture conditions ( $\sim 55\%$  water holding capacity), increase inorganic N concentrations within the soil profile which are then susceptible to leaching (Linn & Doran 1984, Cambardella et al., 1999, Cabrera et al., 1993). Conversely, the transition from an oxic to an anoxic soil environment impacts the potential for denitrification, which can decrease the  $\text{NO}_3^-$  leaching potential of a soil due to the transformation of  $\text{NO}_3^-$  to nitrogen gas ( $\text{N}_2$ ).

Nitrate leaching and N transformation processes have been studied in more detail in traditional MAR systems such as storm water or treated wastewater infiltration basins (Abiye et al., 2009; Schmidt et al., 2011; Gorski et al., 2019; Ben Moshe et al., 2020, Goren et al., 2014). Depending on the infiltration rate of the native soil, Schmidt et al. (2011) observed a 30-60% removal of  $\text{NO}_3^-$  in agricultural storm runoff recharged in a 3-hectare infiltration basin. Soil aquifer treatment (SAT) systems, a special form of MAR aimed at infiltrating wastewater or reclaimed water can result in dramatic water quality improvements by forcing soil systems towards favorable (e.g. anoxic) biogeochemical conditions. The physical and biochemical processes that occur during passage of the wastewater through the biologically active infiltration interface in the top meter of the infiltration basin sediments are key to N removal due to denitrification (Miller et al., 2006). SAT research has further highlighted the utility of controlled soil column experiments in examining spatially and temporally complex soil conditions and their impact on biogeochemical transformations (Ben Moshe et al., 2020, Goren et al., 2014, Quanrud et al., 1996). However, traditional MAR and SAT systems are often focused on remediating  $\text{NO}_3^-$  loads or other contaminants from the infiltrating recharge water, as opposed to Ag-MAR where the  $\text{NO}_3^-$  leaching potential stems from the residual  $\text{NO}_3^-$  stored in the soil matrix or vadose zone.

While traditional MAR systems have similar end goals to Ag-MAR, major hydrologic

differences exist between these systems. In contrast to MAR infiltration basins, which often maintain a constant head of several meters for several weeks creating a thick saturated layer beneath the basin surface (Schmidt et al., 2011; Gorski et al., 2019), previous Ag-MAR projects often had smaller heads (10-50 cm). In addition, on agricultural fields planted with perennial crops the water was applied in short-lived pulses on high-infiltration capacity soils to avoid waterlogged conditions that could potentially harm the crops. These pulsed water applications create more distinct wetting-drying cycles and dynamic changes in environmental conditions and biogeochemical processes than are found in continuously flooded systems (Dahlke et al., 2018). For these highly dynamic systems, not much is known about the effect that soil texture or Ag-MAR flooding frequency (how often water is applied for recharge) have on  $\text{NO}_3^-$  leaching potential.

The aim of this research is to quantify  $\text{NO}_3^-$  leaching and N transformation processes in the soil and shallow vadose zone of agricultural soils subject to different Ag-MAR practices. Our study specifically investigates the following questions: (1) what effect does soil texture have on  $\text{NO}_3^-$  leaching and N transformation processes during Ag-MAR? (2) what effect does varying flood frequency have on  $\text{NO}_3^-$  leaching and N transformation processes during Ag-MAR? We hypothesize that soil texture and flooding frequency are controlling factors on the amount of residual soil  $\text{NO}_3^-$  that is being leached from the root zone, since both parameters influence the wetting and drainage, oxygen, and redox regime of the soil and with that the environmental conditions favoring specific N transformation processes such as denitrification or mineralization. Soil texture is hypothesized to be particularly influential on the amount of  $\text{NO}_3^-$  leached from the profile, with coarser textures allowing more leaching than finer textured soils. Flooding frequency is hypothesized to impact mineralization/nitrification and denitrification potential in

both soils, as environmental conditions change as a function of wetting/drying cycle timing. To evaluate the posed questions and hypotheses, we used data from field experiments at two almond orchards in the Central Valley of California and laboratory soil column experiments, in which we tested the effects of flooding frequency and soil texture in a controlled environment. In addition, we completed incubation experiments to gain a mechanistic understanding of N transformation processes and rates for these soil textures.

## **2.2 MATERIALS AND METHODS**

### **2.2.1 Field experiments**

#### *2.2.1.1 Study Sites*

Two almond orchards were investigated during the winters of 2015/2016 and 2016/2017, both located in the Central Valley of California. The first site is located south of Delhi, California (37°24'12"N, 120°47'19"W) while the second is located southwest of Modesto, California (37°36'26"N, 121° 4'21"W) (Figure 2.1). The soil at Delhi is a sand (Delhi sand series, mixed, thermic, Typic Xeropsamments), a rapidly draining soil with high infiltration rates (average profile  $K_{\text{sat}} \sim 30 \text{ cm hr}^{-1}$ ). The presence of a hardpan layer around 100 cm depth was previously observed at Delhi, however deep ripping of the hardpan occurred prior to the original planting of the orchard in the early 2000s. The soil at Modesto is a fine sandy loam, a moderately draining soil derived from granitic alluvium (Dinuba series, coarse-loamy, mixed, active, thermic Typic Haploxeralfs) (Soil Series USDA). Hereafter, the two field sites will be referenced to as sand (Delhi) and fine sandy loam (Modesto). The two sites are rated as “Excellent” (sand) and “Moderately Good” (fine sandy loam) by the Soil Agricultural Groundwater Banking Index (SAGBI, O’Geen et al., 2015), a recently proposed measure of Ag-MAR soil suitability. The mean annual precipitation at both sites varied between 17.8 and 36.1 cm from 2015 – 2018: 2015

was a critical dry year and 2017 the 2<sup>nd</sup> wettest year on the 100-year climate record in California. The majority of precipitation at both sites occurs during the winter months (Nov-Apr), and the mean annual temperature is 17.25°C (January 2015 - 2018) (Soil Series USDA, CIMIS Station 206).

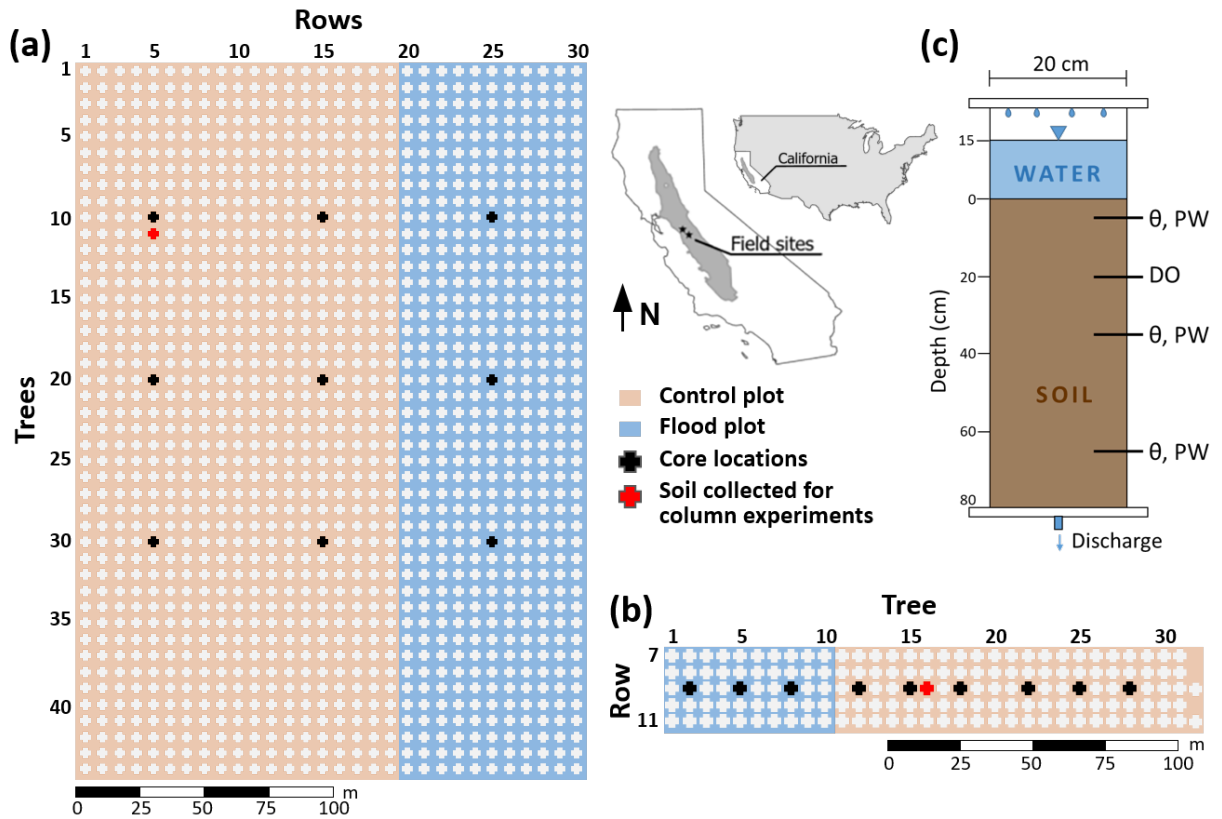


Figure 2.0: Study locations and experimental setup. (a) fine sandy loam experimental field design; (b) sand experimental field design; and (c) Experimental laboratory column design, where  $\theta$  – volumetric water content sensor, PW – pore water sampler, DO – dissolved oxygen sensor.

### 2.2.1.2 Field Instrumentation and Monitoring

Two treatments were tested at each orchard: a flood treatment (i.e., Ag-MAR) in which 61 cm of water were applied during December – January (2015/16 and 2016/17) in 3 – 4 separate flooding events, with 15.24 – 25.4 cm of applied water during each event (Supplementary Material; Table S2.1), and the grower standard irrigation practices, defined as the control. The

average  $\text{NO}_3^-$ -N concentration of the applied water was  $9.63 \text{ mg L}^{-1}$  for the sand field site, and  $1.45 \text{ mg L}^{-1}$  for the fine sandy loam field site. The variation in  $\text{NO}_3^-$  concentration of the applied water between sites is reflective of the water source that was used for flooding, the fine sandy loam site used local surface water, and the sand site used pumped groundwater in lieu of available surface water resources. Soil cores (5 cm diameter) were collected using a direct push drill method (Geoprobe Systems, Salina, KS, USA) before and after winter flooding events, to a depth of 300 – 400 cm.

Cores were analyzed for soil texture, nitrate-nitrogen ( $\text{NO}_3^-$ -N), ammonium-nitrogen ( $\text{NH}_4^+$ -N), total carbon (TC), and total nitrogen (TN). Soil samples were prepared for N analysis using 0.5M  $\text{K}_2\text{SO}_4$  extractions, whereby 15g of soil (corrected for soil water content) were extracted with 36mL  $\text{K}_2\text{SO}_4$ , with extracted supernatant representing soil extractable N. All  $\text{NO}_3^-$ -N and  $\text{NH}_4^+$ -N samples in both field and laboratory experiments were analyzed using the vanadium (III) reduction (Doane & Horwath, 2003) and the Berthelot reaction (Forster 1995; Verdouw et al., 1978), respectively. TC and TN soil samples were ball milled and analyzed using the Costech ECS 4010. Soil samples taken before and after recharge events were analyzed in triplicate samples for  $\text{NO}_3^-$ -N,  $\text{NH}_4^+$ -N, and TN, in 10 cm intervals, which allowed constraining both the organic-N and inorganic-N pools within the soil matrix.

## 2.2.2 Laboratory Experiments

### 2.2.2.1 Soil Column Experiments

Laboratory soil column experiments were designed to corroborate data collected from field scale experiments and to quantify  $\text{NO}_3^-$  leaching and major N transformation processes in the root zone induced by the application of large water amounts typical for Ag-MAR practices. Large soil columns (80 cm tall, 20 cm in diameter) were built from polyvinyl chloride (PVC) pipe (Fig. 2.1). This column size was chosen to minimize sidewall flow (1:4 width to depth ratio) and to encompass some of the heterogeneity of the  $\text{NO}_3^-$  distribution observed within the field cores. The soils for the laboratory experiments were excavated in 10 cm intervals from the control treatment at both field sites in order to represent pre-flooding conditions. The columns were packed with the soil collected from the field sites in 10 cm intervals, to a depth of 80 cm and a measured average bulk density of  $1.58 \text{ g cm}^{-3}$  (sand) and  $1.65 \text{ g cm}^{-3}$  (fine sandy loam). Prior to and after completion of the flooding experiments, soil samples were taken at 10 cm intervals to constrain both the organic-N and inorganic-N pools within the soil matrix. Soil samples were analyzed in triplicate samples for  $\text{NO}_3^-$ -N,  $\text{NH}_4^+$ -N, and TN using the standard protocols as detailed above.

Each soil column was equipped with three volumetric soil water content (VWC) sensors at 5, 35 and 65 cm depth (Acclima TDR-310S), a dissolved oxygen ( $\text{O}_2$ ) sensor at 20 cm depth (PreSens, Fibox 4, Regensburg, Germany), and three discrete pore water sampling ports at 5, 35 and 65 cm depth (Soil Moisture, Model 190D4, Santa Barbara, California). VWC was measured continuously at 1 min intervals. Discharge from the soil column was continuously measured in 5 min intervals using a tipping bucket rain gauge (Acurite, Model 00899, Lake Geneva, WI). A vacuum of 1.5 - 2 inHg (50.80 - 67.73 mbar) was applied to the bottom of the soil columns in

order to represent the matric potential and prevent the buildup of an artificial water table (Lewis & Sjöstrom, 2010). From the discharge, 50-ml water samples were collected at flow-dependent intervals ranging from 5 to 60 minutes, and then analyzed for  $\text{NO}_3^-$ -N and  $\text{NH}_4^+$ -N.

Two flooding frequency treatments, Low Frequency (LF; flooding every 1-2 weeks) and High Frequency (HF; flooding every 72 hours), and two soil textures, sand (Delhi site) and fine sandy loam (Modesto site) were tested with the soil column experiments for a total of four treatments. During each column experiment, three water applications (WAs) of each 15 cm were made to each soil column (hereafter referred to as WA1, WA2 and WA3 respectively). Each 15 cm of water added represented 0.47 pore volumes of the 80 cm column for the sand, and 0.51 pore volumes for the fine sandy loam. The LF treatment was a true replicate of the water applications made at both field sites, consisting of three consecutive WAs in total with a 168 hour (one week) break between WA 1 and 2, and a 336 hour (two week) break between WA 2 and 3. In the HF treatment three WAs were made, each 72 hours apart. An individual WA consisted of applying tap water (with non-detect concentrations of  $\text{NO}_3^-$ ) equivalent to 15 cm of water depth over a period of 0.5 hours onto the soil surface of the column using a perforated bucket to minimize erosion. Twenty-four hours before the start of the column experiments, the soil columns were brought up to the same VWC as was observed at each field site prior to the start of the Ag-MAR field experiments (sand: 0.1-0.15  $\text{cm}^3/\text{cm}^3$ , fine sandy loam: 0.2-0.25  $\text{cm}^3/\text{cm}^3$ ), by applying a water application of ~8 cm such that soil volumetric water contents increased to between 0.1 - 0.2  $\text{cm}^3 \text{ cm}^{-3}$ .

### 2.2.2.2 Soil Incubations and $\text{NO}_3^-$ -N mass balance calculations

Mineralization and denitrification incubations were performed on field soils in order to constrain transformation rates under ideal conditions. Net mineralization potential, the rate at which a soil converts organic-N into inorganic-N, was evaluated using methods outlined in Wade et al. (2018), where 10 g of soil from each 10 cm soil layer was air-dried and sieved through a 2-mm sieve. Initial inorganic-N levels were measured in each soil layer according to the methods described in Section 2.1.2 before samples were brought up to 55% water holding capacity, in order to maximize aerobic microbial activity (Linn & Doran, 1984), and incubated for two weeks. Inorganic-N levels were re-measured and mineralization rates were calculated as the difference in N concentrations between the initial and ending time of the experiment.

Denitrification incubations were measured on soil subsamples according to the acetylene-inhibition method described in Smith et al., (1978), using the method outlined in Groffman et al. (1999). Gas samples were collected at 30 minutes, 90 minutes, and 1 day incubation time. Samples were analyzed by gas chromatography for  $\text{N}_2\text{O}$  (Model GC-2014; Shimadzu Scientific Instruments, Kyoto, Japan).

In order to evaluate  $\text{NO}_3^-$  leaching potential, i.e. the potential for soil residual  $\text{NO}_3^-$  to be transported out of the soil profile, a  $\text{NO}_3^-$  mass balance for each soil column was calculated.

Total mass of specific N species ( $\text{NO}_3^-$ -N,  $\text{NH}_4^+$ -N) in the soil (solid samples) was calculated as:

$$M_{soil} = \sum_{i=1}^n C_n V_n \rho_n \quad (1)$$

where  $M_{soil}$  is the mass of the N species within the soil column ( $\mu\text{g}$ ),  $n$  is the soil layer of the column (10 cm intervals to a depth of 80 cm),  $C$  is the concentration of the N species in the soil ( $\mu\text{g g}^{-1}$  soil),  $V$  is the volume of the soil layer ( $\text{cm}^3$ ) and  $\rho$  is the density of the soil ( $\text{g cm}^{-3}$ ). Mass

loads of  $\text{NO}_3^-$  leaving the column as leachate (liquid samples) were calculated by:

$$M_{eff} = \sum_{i=1}^n q_t C_t \Delta t \quad (2)$$

where  $M_{eff}$  is the mass of  $\text{NO}_3^-$ -N leaving the column during a flooding event,  $C_t$  is the concentration in an effluent sample ( $\mu\text{g N mL}^{-1}$ ),  $q_t$  is the flow rate out of the column ( $\text{mL min}^{-1}$ ) and  $\Delta t$  is the timestep associated with  $C_t$  and  $q_t$ . The mass balance for  $\text{NO}_3^-$  within the soil column is then represented by the typical mass balance equation:

$$I - O = \Delta S \quad (3)$$

where  $I$  represents the biogeochemical creation or addition of  $\text{NO}_3^-$  to the system,  $O$  represents the biogeochemical consumption or leaching of  $\text{NO}_3^-$  from the system, and  $\Delta S$  represents the change of storage of  $\text{NO}_3^-$  mass within the system. When considering the  $\text{NO}_3^-$  mass balance, the only input considered in this mass balance is the creation of  $\text{NO}_3^-$  through mineralization and subsequent nitrification (conversion of organic N to ammonium, and conversion of ammonium to  $\text{NO}_3^-$  measured in the soil profile). The water used for flooding contained negligible amounts of N species ( $<0.05 \text{ mg L}^{-1} \text{ NO}_3^-$ -N,  $\text{NH}_4^+$ -N). Outputs considered can include N transformations such as immobilization and denitrification, or physical processes such as  $\text{NO}_3^-$  leaching measured in the effluent (i.e.  $M_{eff}$ ). Change in storage is represented by the difference between the before and after N profiles in the soil column experiments.

## 2.3 RESULTS

### 2.3.1 Field Trials

The two almond orchards were flooded with 61 - 66.4 cm (about 2 ft) of water during the winters (Dec-Jan) of 2015/16 and 2016/17 (Supplementary material, Table S2.2). Soil moisture in the flood treatment for the sand reached saturation ( $0.4 \text{ cm}^3 \text{ cm}^{-3}$ ) and returned back to pre-flooding soil water content ( $0.1 - 0.15 \text{ cm}^3 \text{ cm}^{-3}$ ) within 12 hours after Ag-MAR water application. Infiltration rates for the fine sandy loam were less rapid than for the sand, and an estimated 81-96% of the applied water for Ag-MAR left the root zone, depending on the year (Supplementary material, Table S2.3). Moisture sensors showed that flooding events on the fine sandy loam took between 48-72 hours to return from saturation ( $0.35 - 0.4 \text{ cm}^3 \text{ cm}^{-3}$ ) to pre-flooding soil water content ( $0.15 - 0.2 \text{ cm}^3 \text{ cm}^{-3}$ ).

The data from the field experiments show large amounts of variance in  $\text{NO}_3^-$ , across both treatments and year. The  $\text{NO}_3^-$ -N load within the 400 cm soil cores taken from the sand site before the flooding events ranged between 68.0 and 570.1  $\text{kg ha}^{-1}$  in the flood treatment and between 446.9 and 1501.3  $\text{kg ha}^{-1}$  in the control (plots only receiving winter precipitation) in 2015/16. In 2016/17,  $\text{NO}_3^-$ -N load ranged between 60.2 and 244.7  $\text{kg ha}^{-1}$  in the flood treatment and between 612.1 and 1718.0  $\text{kg ha}^{-1}$  in the control (Table 2.1). Total  $\text{NO}_3^-$ -N loads in the 400 cm soil cores taken from the flood-irrigated fine sandy loam before Ag-MAR flooding were lower than the sand, between 26.0 and 99.1  $\text{kg ha}^{-1}$  in the Ag-MAR treatment and 21.3 and 201.6  $\text{kg ha}^{-1}$  in the control in 2015/16. In 2016/17, the observed range was between 29.5 and 437.9  $\text{kg ha}^{-1}$  in the Ag-MAR treatment and between 119.7 and 127.5  $\text{kg ha}^{-1}$  in the control (Table 2.1). Two-sample and traditional t-tests ( $\alpha = 0.05$ ) were used to evaluate significance of the differences of  $\text{NO}_3^-$  in the soil core data between flood and control plots, and the before and after

flooding season soil cores, respectively. While the differences in the field data are mostly non-significant, there are general directional trends which can be identified.

The two sites exhibited opposing trends in the  $\text{NO}_3^-$  profiles resulting from the Ag-MAR flooding events in the 2015/16 field experiments. The sand shows a general decrease in  $\text{NO}_3^-$ -N load in the soil profile after Ag-MAR flooding, while the fine sandy loam shows a general increase in  $\text{NO}_3^-$ -N load following flooding events. These trends are not as apparent in the 2016/17 season, where the sand profile shows no strong directional shift following Ag-MAR flooding events, and the fine sandy loam shows only a slight increase in  $\text{NO}_3^-$ -N load after flooding (Table 2.1). The high variance of  $\text{NO}_3^-$ -N measured across the field sites results in a lack of significant conclusions that can be made regarding  $\text{NO}_3^-$ -N leaching due to Ag-MAR flooding events from the field data. Additionally, in the case of the fine sandy loam, where there is a net increase in  $\text{NO}_3^-$  between the before and after residual soil profile, an estimation of  $\text{NO}_3^-$  leached during Ag-MAR is not possible, highlighting the importance of controlled, high resolution laboratory experiments

Table 2.1: Sand and fine sandy loam field core  $\text{NO}_3^-$ -N loads. The root zone (RZ) is defined as the first 100 cm of the core and while Full denotes the entire 400 cm profile or core length.

<b>Sand (2015 – 2016)</b>						
	<b><math>\text{NO}_3^-</math>-N load Before Flood (RZ)</b>	<b><math>\text{NO}_3^-</math>-N load After Flood (RZ)</b>	<b>Change</b>	<b><math>\text{NO}_3^-</math>-N load Before Flood (Full profile)</b>	<b><math>\text{NO}_3^-</math>-N load After Flood (Full profile)</b>	<b>Change</b>
	kg ha <sup>-1</sup>	kg ha <sup>-1</sup>	%	kg ha <sup>-1</sup>	kg ha <sup>-1</sup>	%
<b>Flood Avg.</b> (n = 3)	44.12 ± 28.55	5.41 ± 0.65	-82 ± 15	286.03 ± 257.49	115.36 ± 54.39	-23 ± 85
<b>Control Avg.</b> (n = 6)	182.39 ± 186.79	9.72 ± 3.97	-90 ± 9	668.84 ± 275.92	644.12 ± 252.80	1 ± 40
<b>Sand (2016-2017)</b>						
<b>Flood Avg.</b> (n = 3)	19.78 ± 5.01 <sup>o</sup>	15.98 ± 6.71	-11 ± 16	124.74 ± 104.03	88.62 ± 31.25	6 ± 83
<b>Control Avg.</b> (n = 2)	52.81 ± 4.01 <sup>o,*</sup>	9.25 ± 2.16 <sup>*</sup>	-83 ± 3	1165.08 ± 781.98	354.45 ± 111.96	-65 ± 14

Fine sandy loam (2015 – 2016)						
<b>Flood Avg.</b> (n = 3)	13.98 ± 4.59	22.99 ± 20.04	56 ± 142	59.70 ± 36.88	114.98 ± 69.64	107 ± 113
<b>Control Avg.</b> (n = 6)	12.02 ± 5.30*	32.39 ± 11.12*	209 ± 149	122.03 ± 70.66	118.11 ± 70.63	20 ± 79
Fine sandy loam (2016 – 2017)						
<b>Flood Avg.</b> (n = 2)	53.20 ± 49.06	65.24 ± 0.06	113 ± 197	233.70 ± 288.74	66.61 ± 1.99	23 ± 152
<b>Control Avg.</b> (n = 2)	64.35 ± 8.96	49.96 ± 14.11	-23 ± 11	123.6 ± 5.54	316.59 ± 391.19	164 ± 329

° indicates significance of a two-sample t-test comparing initial NO<sub>3</sub><sup>-</sup>-N load between flood and control plots.

\* indicates significant difference between the before and after NO<sub>3</sub><sup>-</sup>-N load within a plot.

## 2.3.2 Soil Column Experiments

### 2.3.2.1 Soil NO<sub>3</sub><sup>-</sup>-N Mass Balance and Transport

#### *Initial Nitrogen Distribution in the Soil Profile*

The initial soil NO<sub>3</sub><sup>-</sup>-N and NH<sub>4</sub><sup>+</sup>-N concentrations for the sand LF column ranged from 1.09 to 4.58 mg kg<sup>-1</sup> for NO<sub>3</sub><sup>-</sup>-N, and 0.15 to 0.76 mg kg<sup>-1</sup> NH<sub>4</sub><sup>+</sup>-N (Fig. 2.2). The highest concentrations were located in the top 10 cm, while the lowest were found in the 30-50 cm range. The soil for the fine sandy loam LF column showed concentrations ranging from 0.09 to 3.12 mg kg<sup>-1</sup> NO<sub>3</sub><sup>-</sup>-N, and 0.237 to 0.531 mg kg<sup>-1</sup> NH<sub>4</sub><sup>+</sup>-N. Nitrate concentrations for the fine sandy loam decreased with increasing depth, while ammonium concentrations were greatest at 20-60 cm depth (Fig. 2.2).

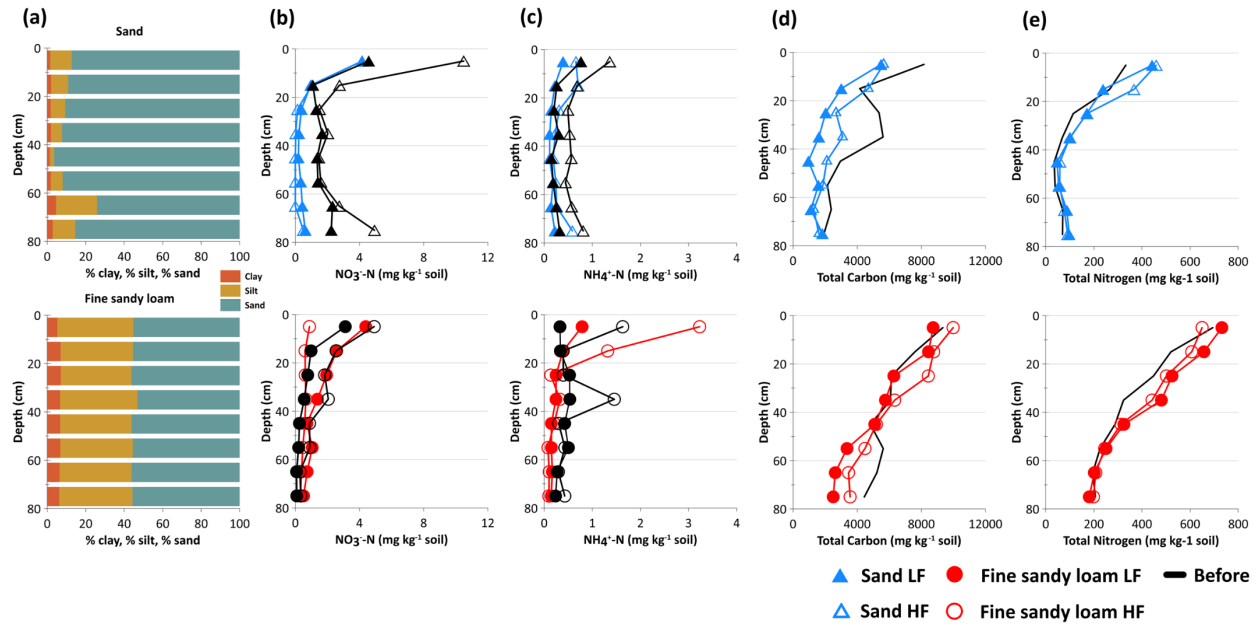


Figure 2.1: Initial characterization of field soils with depth for (a) texture, (b)  $\text{NO}_3^-$ -N, (c)  $\text{NH}_4^+$ -N, (d) TC and (e) TN. LF – Low frequency treatment (1-2 weeks), HF – High frequency treatment (72 hours)

The initial soil  $\text{NO}_3^-$ -N and  $\text{NH}_4^+$ -N concentrations for sand HF ranged from 1.50 to 9.13  $\text{mg kg}^{-1}$   $\text{NO}_3^-$ -N, and 0.49 to 1.36  $\text{mg/kg}$   $\text{NH}_4^+$ -N. The fine sandy loam HF concentrations ranged from 0.29 to 4.91  $\text{mg kg}^{-1}$   $\text{NO}_3^-$ -N, and 0.29 to 2.20  $\text{mg kg}^{-1}$   $\text{NH}_4^+$ -N (Fig. 2.3). This is an average total increase of  $60\% \pm 28\%$  for the sand and  $127\% \pm 15.8\%$  for the fine sandy loam in initial  $\text{NO}_3^-$  mass compared to the LF initial conditions in the soil profile before flooding.

#### *$\text{NO}_3^-$ -N breakthrough in effluent*

The  $\text{NO}_3^-$  breakthrough curves of the fine sandy loam LF and HF column experiments were similar in shape but the peak concentration reached during WA1 in the HF experiment was twice the peak concentration during the LF experiment (Fig. 2.4c, d). Interestingly, the fine sandy loam LF experiment showed a distinct secondary peak during WA1 and WA2 around 30 hours after water application. During the fine sandy loam HF experiment, the late secondary peak seen in the LF experiment (Fig. 2.4c,d) was missing. Effluent concentrations in the fine

sandy loam HF were much lower in WA2 & WA3, never exceeding 1 mg L<sup>-1</sup> NO<sub>3</sub><sup>-</sup>-N, with long periods of zero NO<sub>3</sub><sup>-</sup>-N concentration.

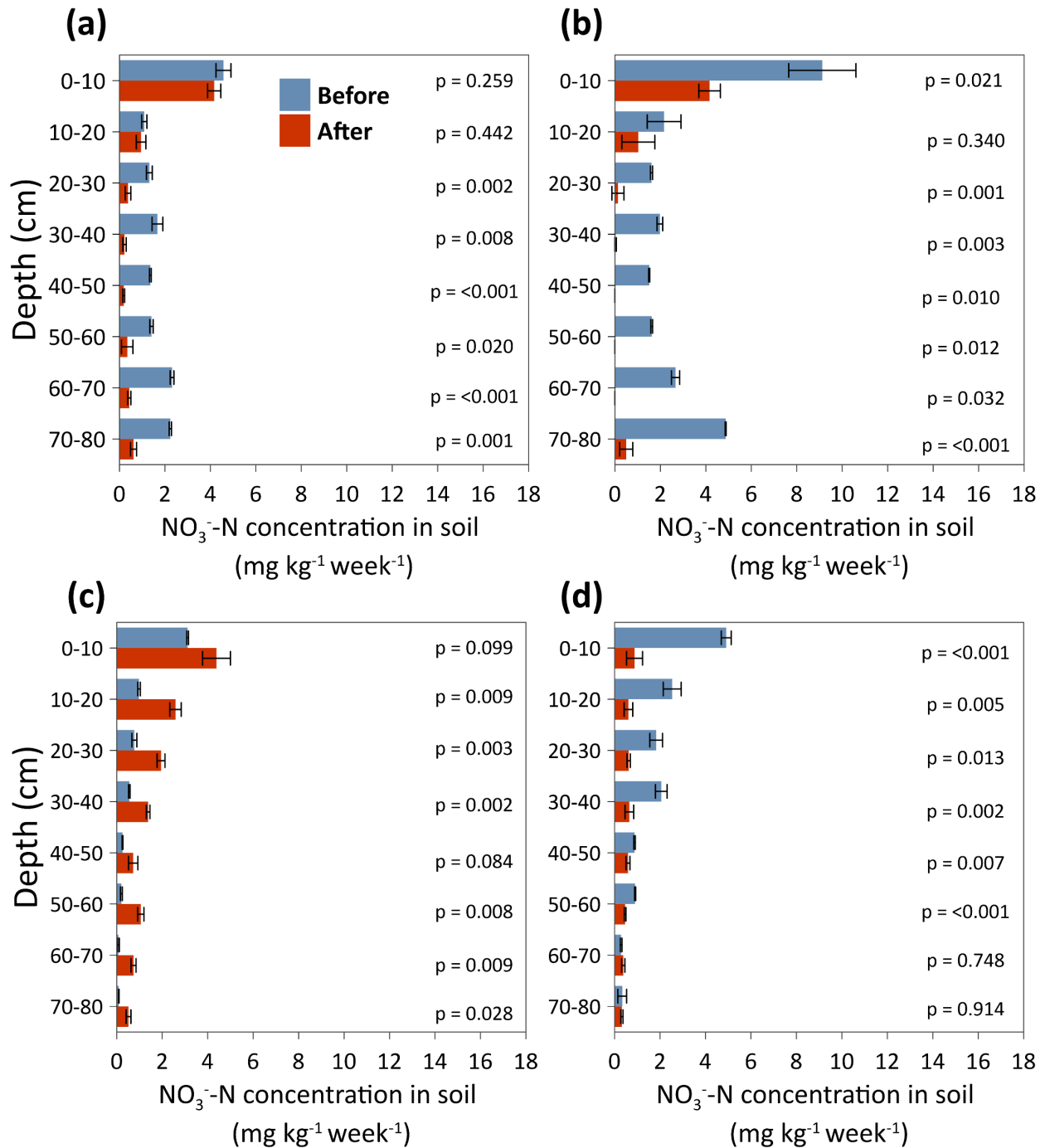


Figure 2.2: Comparison of before (blue bars) and after (red bars) NO<sub>3</sub><sup>-</sup>-N loads in the soil profiles of the soil column experiments, (a) sand LF, (b) sand HF, (c) fine sandy loam LF and (d) fine sandy loam HF. Error bars represent one standard deviation of NO<sub>3</sub><sup>-</sup>-N in soil profile. P-

values represent the statistical significance that the before and after values measured in the respective soil layer are not equal.

Both of the sand LF and HF experiments showed narrow peaks in the  $\text{NO}_3^-$  breakthrough curve in WA1 with peak  $\text{NO}_3^-$ -N concentrations in the effluent of  $18.4 \text{ mg L}^{-1}$  and  $26.72 \text{ mg L}^{-1}$  during the sand LF and sand HF, respectively (Fig. 2.4a,b). The sand HF did show the same shift in the  $\text{NO}_3^-$  peak as observed in sand LF WA2 and WA3, but the sand HF peaks were of lower magnitude (LF WA2 & WA3  $\text{NO}_3^-$ -N peaks were  $7.58$  and  $9.27 \text{ mg L}^{-1}$  compared to HF WA2 and WA3  $\text{NO}_3^-$ -N peaks of  $2.35$  and  $2.93 \text{ mg L}^{-1}$ ) (Fig. 2.4a,b).

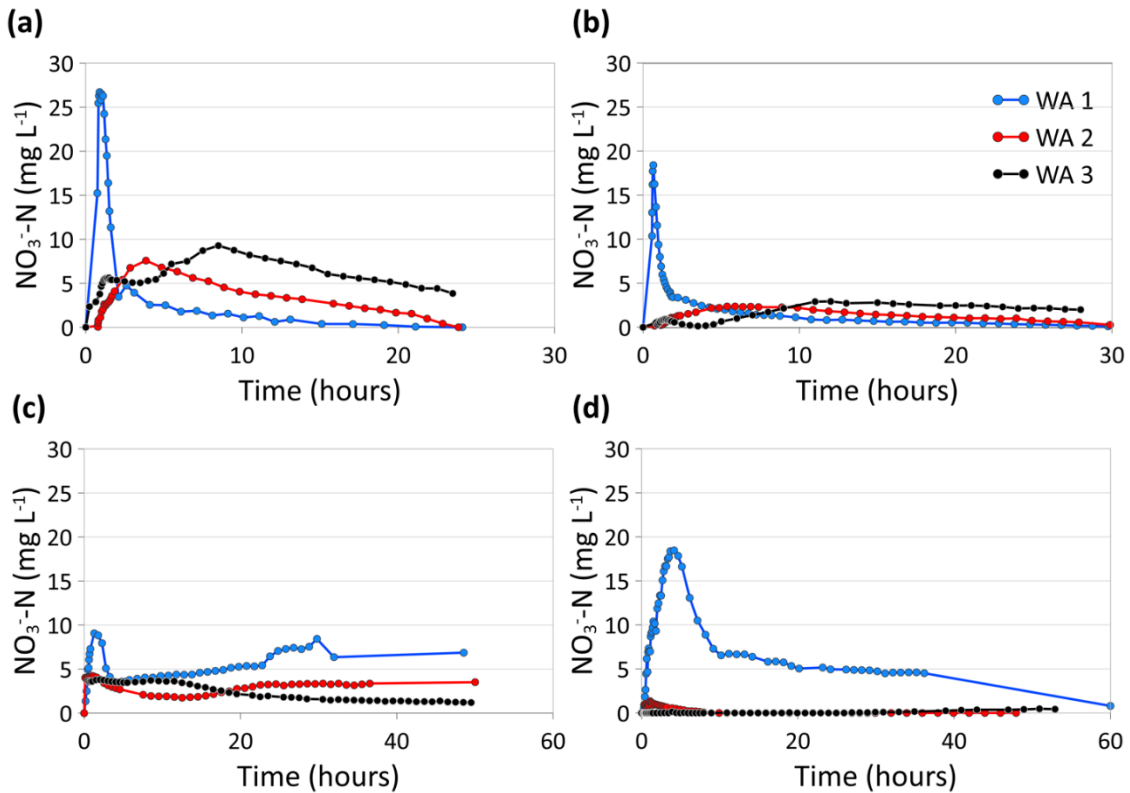


Figure 2.3: Observed  $\text{NO}_3^-$ -N concentrations in discharge through time, (a) sand LF, (b) sand HF, (c) fine sandy loam LF, and (d) fine sandy loam HF.

### *Effluent and residual soil NO<sub>3</sub><sup>-</sup>-N mass balance*

The same directional trends in the residual soil NO<sub>3</sub><sup>-</sup>-N of the 2015/2016 field experiments (Section 3.1) were observed in the corresponding LF soil column experiments (Fig. 2.3). For the fine sandy loam, there was a greater amount of NO<sub>3</sub><sup>-</sup>-N measured in the soil profile post-flooding than was initially present. In contrast, the sand profile showed a general decrease in NO<sub>3</sub><sup>-</sup>-N measured in the soil profile post-flooding (Fig. 2.3). However, effluent loads measured during the soil column experiments indicate that both sites were leaching discernible quantities of NO<sub>3</sub><sup>-</sup> from the upper root zone (top 80 cm) (Fig. 2.4). Both soil textures leached over 100% of the initially present NO<sub>3</sub><sup>-</sup>-N during the LF soil column experiments (Fig. 2.5).

The effluent mass balance of the fine sandy loam LF experiment showed that  $145.7\% \pm 5.8\%$  (47.1 mg NO<sub>3</sub><sup>-</sup>-N) of the initially measured NO<sub>3</sub><sup>-</sup> (32.4 mg NO<sub>3</sub><sup>-</sup>-N) in the soil profile leached after three WAs (73.0%, 45.2%, and 27.5% leached during WA1, WA2, and WA3 respectively) (Fig. 2.5a). The fine sandy loam HF effluent concentrations showed that the majority of the initially measured soil NO<sub>3</sub><sup>-</sup> (73.5mg NO<sub>3</sub><sup>-</sup>-N) leached during WA1 (62.8% of the initial NO<sub>3</sub><sup>-</sup> load), with only 1.0% and 0.9% leached during WA2 and WA3 (Fig. 2.5b) for a total of  $64.7\% \pm 10.4\%$  (47.6 mg NO<sub>3</sub><sup>-</sup>-N) (Fig. 2.5b).

For the sand LF column experiment the total amount of NO<sub>3</sub><sup>-</sup> leached was slightly lower than the fine sandy loam LF, with  $137.3\% \pm 6.6\%$  (112.4 mg NO<sub>3</sub><sup>-</sup>-N) of the initially measured NO<sub>3</sub><sup>-</sup> (81.9 mg NO<sub>3</sub><sup>-</sup>-N) leached after three WAs (72.7%, 25.5% and 39.2% leached during WA1, WA2, and WA3 respectively (Fig. 2.5a). Overall, NO<sub>3</sub><sup>-</sup> mass loss from the sand HF column was lower than from sand LF. The percent of NO<sub>3</sub><sup>-</sup> leached from the initial sand HF profile (130.9 mg NO<sub>3</sub><sup>-</sup>-N) during each WA was 24.5%, 3.0%, and 4.2 % of the initial NO<sub>3</sub><sup>-</sup> mass for a total of  $31.7\% \pm 3.8\%$  (41.6 mg NO<sub>3</sub><sup>-</sup>-N) (Fig. 2.5b).

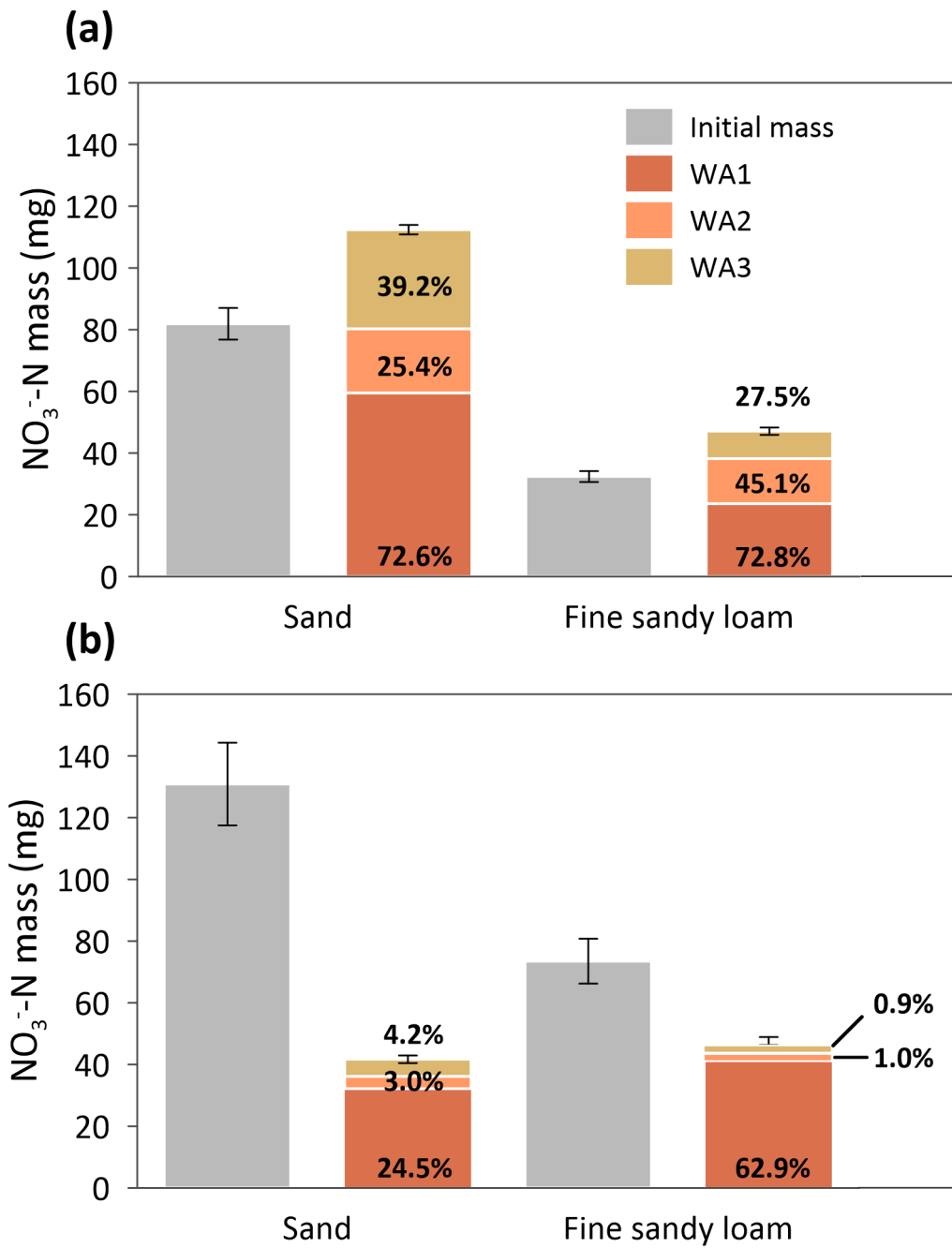


Figure 2.4: Initial soil nitrate mass and amount of nitrate leached during each water application (WA) during the low frequency (a) and high frequency (b) column experiments using sand and fine sandy loam soils. Percentages represent the percent of initially present  $\text{NO}_3^-$ -N (grey bar) leached in each WA.

### 2.3.2.2 Net mineralization incubations and nitrate mass balance

Both soil profiles showed similar net mineralization rates, both in the maximum rate and in the depth distribution (Fig. 2.6). The highest net mineralization rates observed were  $3.93 \text{ mg N kg}^{-1} \text{ wk}^{-1}$  (sand) and  $3.41 \text{ mg N kg}^{-1} \text{ wk}^{-1}$  (fine sandy loam) in the top soil (0 – 10 cm), which decreased to  $0.11 \text{ mg N kg}^{-1} \text{ wk}^{-1}$  (sand) and  $0.08 \text{ mg N kg}^{-1} \text{ wk}^{-1}$  (fine sandy loam) at 50 – 70 cm depth. For the sand, the 50 – 70 cm depth showed indications of immobilization rather than mineralization, with a C:N ratio ranging from 53-61.

To account for the difference between the excess  $\text{NO}_3^-$  leached ( $137.3\% \pm 6.6\%$  or  $112.4 \text{ mg NO}_3^- \text{-N}$ ) during the sand LF column experiment and the change in residual  $\text{NO}_3^-$  left in the soil after flooding (a decrease of  $43.8 \text{ mg NO}_3^- \text{-N}$ ), the mass balance required a net mineralization contribution of  $64.0 \pm 8.2 \text{ mg N}$  (Fig. 2.7). The net mineralization incubation assays for the sand determined a total mineralization potential of  $103 \text{ mg N}$  for the duration of the flooding experiment. The fine sandy loam LF mass balance required an even greater amount of  $81.6 \pm 10.9 \text{ mg N}$  to explain the discrepancy between the  $145.7\% \pm 5.8\%$  ( $47.1 \text{ mg NO}_3^- \text{-N}$ ) of  $\text{NO}_3^-$  leached during the fine sandy loam LF experiment and the change in residual  $\text{NO}_3^-$  left in the soil after flooding (an increase of  $34.5 \text{ mg NO}_3^- \text{-N}$ ) (Fig. 2.7). The total mineralization potential determined for the fine sandy loam from the assays was  $133 \text{ mg N}$  for the duration of the flooding experiment. When scaled for mineralization potential as a function of water content (Paul et al., 2003), the mineralization potential was  $46.57 \pm 14.29 \text{ mg N}$  and  $68.55 \pm 19.34 \text{ mg N}$  for the sand and fine sandy loam. This indicates that the positive mass balance for both soil textures may be explained by mineralization processes (Fig. 2.7). The HF experiments both showed a decrease in residual  $\text{NO}_3^-$  left in the soil after flooding. In general, they both have lower mineralization potential, and a higher denitrification potential, due to increased frequency

of the water applications and higher water contents in the columns, conditions more conducive to denitrification (Butterbach-Bahl et al., 2013) (Fig. 2.7).

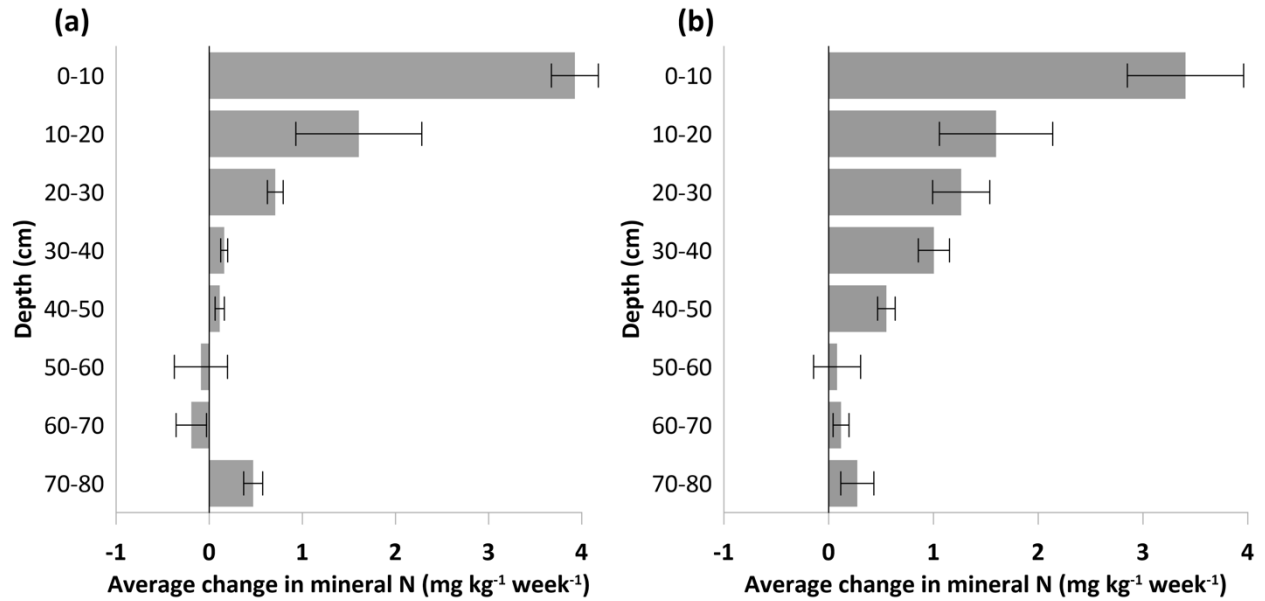


Figure 2.5: Mineralization rates for the (a) sand and (b) fine sandy loam.

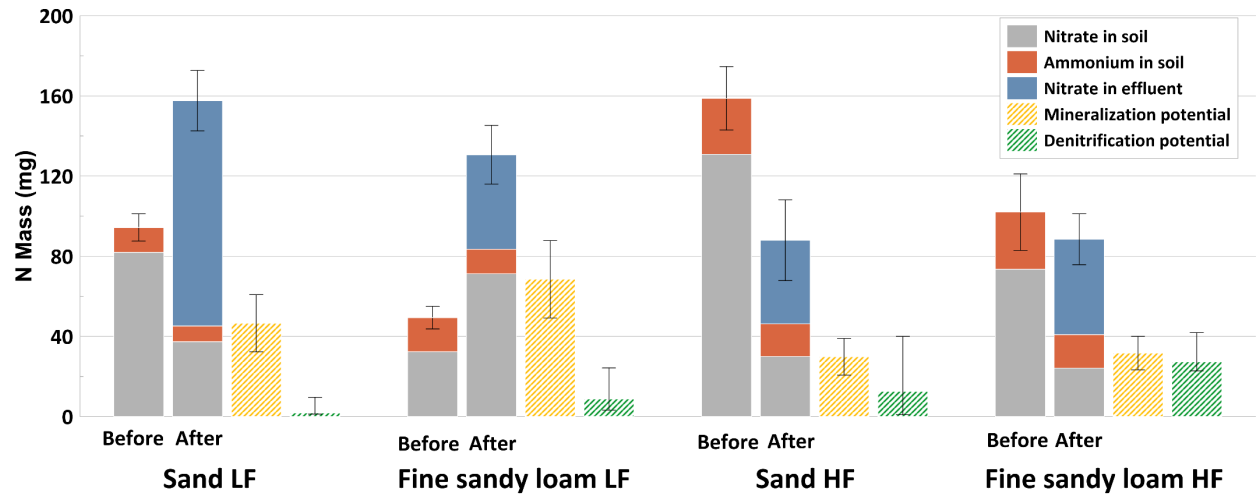


Figure 2.6: Total mineral N mass balance for soil columns. Error bars represent one standard deviation of the aggregated error for all components of a single column.

## 2.4 DISCUSSION

### 2.4.1 Field scale residual $\text{NO}_3^-$ -N profile trends

Wetting-drying cycles have been shown to impact microbial activity, and semi-arid regions like California particularly exhibit pulses of increased microbial activity during significant precipitation events following long, dry periods (Noy-Meir 1973; Austin et al., 2004). Our results indicate that the soil residual  $\text{NO}_3^-$  content after Ag-MAR can either increase or decrease in response to the pulsed water applications and related soil moisture-dependent N transformation processes. The 2015/2016 water year was ranked as a below average precipitation year in California and marked the final year of a four-year drought. In contrast, the 2016/17 water year was the second wettest year in a 100-year record (California DWR, 2017). Thus, variation in precipitation between the 2015/16 and 2016/17 Ag-MAR field experiments may have distinctly impacted biogeochemical processes and their potential rates and magnitudes at the field scale as indicated in Table 2.1. While there is a lack of statistically significant trends between treatments and years in the field data, the finer texture soil (i.e. fine sandy loam) showed a clear increase in residual soil  $\text{NO}_3^-$  after flooding. Similar trends have been observed in previous studies by Chau et al. (2011) and Gregorich et al. (1991) who found greater amounts of mineralization and microbial activity in finer textured soils following irrigation or precipitation events. They concluded that the fine sandy loam in conjunction with a low  $K_{\text{sat}}$  of  $3.3 \text{ mm hr}^{-1}$  in the deeper profile may create an environment where mineralization and nitrification processes are dominating over advective transport, resulting in a net increase of  $\text{NO}_3^-$  in the residual soil profile post-Ag-MAR. However, it is also important to note that in the flood treatment of the fine sandy loam residual  $\text{NO}_3^-$  increase was less than the increase observed in the control, indicating that the flood treatment likely experienced more  $\text{NO}_3^-$  leaching than the control. This is further supported by our soil column experiments, where the fine sandy loam LF shows a net increase in

residual  $\text{NO}_3^-$  in the soil profile, but also a large amount of  $\text{NO}_3^-$  exported out of the column with the effluent.

#### **2.4.2 Biogeochemical processes under varying flooding frequencies**

During the LF treatment, over 100% of the initially present  $\text{NO}_3^-$  was leached from the soil columns, indicating that organic N mineralization was occurring at significant rates in between flooding events. Under ideal conditions (i.e., 55% water holding capacity,  $\sim 0.16 - 0.25 \text{ cm}^3 \text{ cm}^{-3}$  depending on soil layer) both soils would have the potential to mineralize inorganic N at a profile average rate of  $7.0 \text{ mg N kg}^{-1} \text{ wk}^{-1}$  for the sand and  $8.3 \text{ mg N kg}^{-1} \text{ soil wk}^{-1}$  for the fine sandy loam. Mineralization at these rates well exceed the amounts needed to explain the positive N mass balance observed in the column experiments. Moisture conditions for mineralization were near ideal 24 – 48 hours after each WA (e.g. water content ranged between 55% and 100% of water holding capacity, Supplementary Fig. S2.3 & S2.4). Although  $72.6 \pm 4.3\%$  (sand) and  $72.8 \pm 3.7\%$  (fine sandy loam) of the initial soil  $\text{NO}_3^-$  was leached during WA1, we estimate that  $46.6 \pm 14.29 \text{ mg}$  (sand) and  $68.55 \pm 19.34 \text{ mg}$  (fine sandy loam) of new inorganic N was mineralized and subsequently nitrified between flooding events, which then became susceptible to leaching during subsequent WAs. This is further supported by the amounts of  $\text{NO}_3^-$  leached during LF WA2 and 3 ( $64.6\%$  and  $72.6\%$  of initial soil  $\text{NO}_3^-$  for the sand and fine sandy loam respectively), which combined with WA1 exceeded the initial soil  $\text{NO}_3^-$  amount by  $30.5 \text{ mg}$  (sand) and  $14.7 \text{ mg}$  (fine sandy loam), respectively.

When the timing between flooding events was decreased to 72 hours (HF treatment),  $24.5 \pm 2.9\%$  (sand) to  $62.9 \pm 5.6\%$  (fine sandy loam) of the initial soil  $\text{NO}_3^-$  was leached during WA1 and markedly lower  $\text{NO}_3^-$  concentrations were observed in the effluent during WA2 and WA3 than during the LF experiment. The total amounts of  $\text{NO}_3^-$  leached during HF WA2 and 3 only

accounted for 6.7% (sand) and 1.9% (fine sandy loam) of the initially present  $\text{NO}_3^-$ , indicating lower contributions from mineralization likely due to the shorter time periods between flooding events. This is further supported by the pore water  $\text{NO}_3^-$  data shown in Fig. S2.1 & S2.2 (Supplementary Material). The sand HF experiment clearly lacks the increase in pore water  $\text{NO}_3^-$  concentrations at the beginning of WAs 2 and 3 that were observed during the LF experiment, indicating that a breakthrough of recently mobilized  $\text{NO}_3^-$  through the column was not occurring during the HF experiment. Similar patterns were observed for the HF experiment conducted with the fine sandy loam (Supplementary Material, Fig. S2.2). These dynamics support the hypothesis that less mineralization occurred in the shorter frequency (72-hr) recharge experiment.

The  $\text{NO}_3^-$  mass balance of the HF experiments indicates that biogeochemical processes other than mineralization might have played a role. Although oxygen levels stayed well above 10% during the HF experiment (Supplementary Fig. S2.3 & S2.4), the  $\text{NO}_3^-$  mass balance indicates that there likely was a significant amount of denitrification occurring, possibly restricted to microsites (i.e. saturated immobile pore space) of the soil profile that provided conditions supportive of denitrification (Parkin, 1987, Groffman et al., 2009). In addition, temporary microbial immobilization of inorganic N to organic N within the soil profile might have occurred (Johnsson et al., 1987, Paul & Clark 1989, Romero et al., 2015). Based upon the denitrification potential incubations, and previous research concerning anaerobic microbial activity as a function of percent water filled pore space (Bateman et al., 2005), the estimated denitrification of the soil columns were 0.89 – 40.04 mg N (sand HF) and 22.83 – 41.91 mg N (fine sandy loam HF), respectively (Fig. 2.7). Several layers in both soil textures had negative rates of net mineralization in the incubations (Fig. 2.6), indicating that immobilization could also

play a role in transforming inorganic N into organic N following WAs, which could act as a temporary sink of  $\text{NO}_3^-$  (Azam et al., 1988, Recous et al., 1990, Burger et al., 2003).

The mineralization rates for the sand and fine sandy loam observed in this experiment are comparable to the rates found in other agricultural soils. Springob et al., (2003) found mineralization rates of  $0.42 - 5.39 \text{ mg N kg}^{-1} \text{ wk}^{-1}$  in sandy and sandy loam soils in the top 28cm, while Wade et al. (2016) found mineralization rates in the top 25cm of soil to be on average  $1.61 \text{ mg N kg}^{-1} \text{ wk}^{-1}$ , which are comparable to our soils which mineralized  $3.93 \text{ mg N kg}^{-1} \text{ wk}^{-1}$  (sand) and  $3.41 \text{ mg N kg}^{-1} \text{ wk}^{-1}$  (fine sandy loam) in the top soil (0 – 10 cm) (Fig. 2.6).

### **2.4.3 Implications for field-scale $\text{NO}_3^-$ leaching**

The soil column Ag-MAR experiments allowed for a controlled setting to investigate N cycling and N transport processes at finer temporal and spatial scales than was possible in the field. The column experiments confirmed our hypothesis that both soil texture and the time interval between water applications influence  $\text{NO}_3^-$  leaching amounts. We found that irrespective of soil texture or treatment, most  $\text{NO}_3^-$  was leached during the first water application, transporting 50%-97% of the total observed effluent  $\text{NO}_3^-$  mass out of the column. Although we conducted two sets of column experiments comparing two soil textures and flooding frequencies, the soil core data collected from the field sites highlight the huge variability in residual soil  $\text{NO}_3^-$  mass that can be observed just at the plot or field scale and the need for appropriate scaling techniques to reliably estimate  $\text{NO}_3^-$  leaching potential in agricultural soils subject to Ag-MAR at the field scale. Baram et al. (2016) showed that using the spatial average of all observed  $\text{NO}_3^-$  concentrations within a field can sufficiently capture the variability in N mass balance.

Our analysis showed that when scaled up to the field, the amount of  $\text{NO}_3^-$  leached from the soil columns in response to the 45 cm of applied water for the LF and HF experiments were

33.11 ( $0.72 \text{ kg ha}^{-1} \cdot \text{cm H}_2\text{O}$ ) and  $12.82 \text{ kg ha}^{-1}$  ( $0.28 \text{ kg ha}^{-1} \cdot \text{cm H}_2\text{O}$ )  $\text{NO}_3^-$ -N for the sand, while the fine sandy loam LF and HF were  $14.53$  ( $0.32 \text{ kg ha}^{-1} \cdot \text{cm H}_2\text{O}$ ) and  $14.90 \text{ kg ha}^{-1}$  ( $0.33 \text{ kg ha}^{-1} \cdot \text{cm H}_2\text{O}$ )  $\text{NO}_3^-$ -N, respectively. These amounts are comparable to a  $\text{NO}_3^-$  leaching study conducted by Onsoy et al. (2005) in a citrus orchard near Fresno, California, where intensive irrigation of  $174 \text{ cm yr}^{-1}$  resulted in  $93$  and  $275 \text{ kg ha}^{-1} \cdot \text{yr}$   $\text{NO}_3^-$ -N leached from the  $180 \text{ cm}$  root zone, which translates to  $0.53$  and  $1.58 \text{ kg ha}^{-1} \cdot \text{yr}$   $\text{NO}_3^-$ -N  $\cdot \text{cm H}_2\text{O}$  respectively, depending on fertilizer application rate ( $110 - 365 \text{ kg ha}^{-1} \cdot \text{yr}$   $\text{NO}_3^-$ -N). Bachand et al. (2016) reported an estimated  $\text{NO}_3^-$ -N loss of  $1.64 \text{ kg ha}^{-1} \cdot \text{cm H}_2\text{O}$  recharged on a mixture of sandy loam and loamy sand soils, growing alfalfa and wine grapes, in California's Central Valley.

For our soil column experiments,  $\text{NO}_3^-$  leaching for the sand LF and HF was estimated at  $0.72 \text{ kg ha}^{-1} \cdot \text{cm H}_2\text{O}$  and  $0.28 \text{ kg ha}^{-1} \cdot \text{cm H}_2\text{O}$  respectively, and the fine sandy loam LF and HF to be  $0.32 \text{ kg ha}^{-1} \cdot \text{cm H}_2\text{O}$  and  $0.33 \text{ kg ha}^{-1} \cdot \text{cm H}_2\text{O}$ , respectively. The sand soil column estimates are similar to the average  $\text{NO}_3^-$  leaching amount of  $0.77 \text{ kg ha}^{-1} \cdot \text{cm H}_2\text{O}$  we estimated for the 2016 field-collected soil cores. Our numbers are 30-50% of what Bachand et al. (2016) reported but are comparable to the  $\text{NO}_3^-$  leaching estimates Onsoy et al. (2005) estimated for the low fertilizer application rate treatment ( $110 \text{ kg ha}^{-1} \cdot \text{yr}$   $\text{NO}_3^-$ -N). Comparison of our  $\text{NO}_3^-$  leaching amounts to Onsoy et al. (2005) highlights that the nitrate leaching amounts observed during our winter recharge event are comparable in magnitude to the amount of  $\text{NO}_3^-$  leached during the growing season in the citrus orchard near Fresno, California. This opens the question, whether the combination of winter Ag-MAR and growing season irrigation would effectively double the annual amount of  $\text{NO}_3^-$  leached from the root zone or whether the increase in soil  $\text{NO}_3^-$  due to mineralization after Ag-MAR events could potentially reduce fertilizer needs in subsequent growing seasons.

Some answers can be provided to this question based on our field and column experiments. First, it is important to note that in all soil column experiments, regardless of treatment or soil texture, the  $\text{NO}_3^-$  concentration of the total recharge was always below the US EPA (Environmental Protection Agency) Maximum Contaminant Level of  $10 \text{ mg NO}_3^- \text{-N L}^{-1}$  (sand LF –  $7.22 \text{ mg L}^{-1}$ , sand HF –  $2.81 \text{ mg L}^{-1}$ , fine sandy loam LF –  $3.18 \text{ mg L}^{-1}$ , fine sandy loam HF –  $3.26 \text{ mg L}^{-1}$ ). Additionally, the bulk of  $\text{NO}_3^-$  transport comes at the beginning of the water application, often within the first few hours in coarse-textured soils.

These dynamics have several implications both for the Ag-MAR best practices to minimize  $\text{NO}_3^-$  leaching as well as growing season nitrogen management. Because the majority of the residual soil  $\text{NO}_3^-$  is leached at the beginning of Ag-MAR events, growing season nutrient needs need to be carefully managed on fields considered for winter Ag-MAR to reduce the residual  $\text{NO}_3^-$  content of the soil at the end of the growing season. Management practices that reduce the residual N at the end of a growing season (cover cropping, high nutrient use efficiency strategies, etc.) will be beneficial at Ag-MAR sites in decreasing the  $\text{NO}_3^-$  leaching potential from the root zone. At the same time, our results highlight that coarse textured or high  $K_{\text{sat}}$  soils promote fast and nearly complete (>70%) leaching of residual soil  $\text{NO}_3^-$  within hours of the first water application. Thus, it is unlikely that managing Ag-MAR systems for environmental conditions that promote denitrification, which often can be achieved by continuous flooding over several hours or days, will have much of an effect on reducing the leaching of  $\text{NO}_3^-$  already present in the soil at the beginning of the water application. However, prioritizing continuous flooding, and decreasing the time between water applications will likely decrease the mineralization potential and thus decrease total leached  $\text{NO}_3^-$  amounts.

While this research study highlighted the impact that the time interval between water applications may have on biogeochemical forcing, other Ag-MAR management variables exist which may influence  $\text{NO}_3^-$  leaching potential and site suitability for Ag-MAR projects. These include physically manageable factors, such as flooding duration, and timing within the season, and site-specific considerations, such as textural properties, hydrogeology, organic C:N pools, and the mineralization/denitrification potential of the site's soils. Future research should place emphasis on the development of models which can represent the biogeochemical processes observed under Ag-MAR more fully to evaluate best Ag-MAR practices (Waterhouse et al., 2021).

## 2.5 CONCLUSIONS

The field and soil column experiments conducted in this study highlight the importance of biogeochemical processes when considering  $\text{NO}_3^-$  leaching potential during winter groundwater recharge on agricultural fields (Ag-MAR). With  $137.3\% \pm 6.6\%$  (sand) and  $145.7\% \pm 5.8\%$  (fine sandy loam) of the initially present  $\text{NO}_3^-$  leached during low-frequency (1-2 week apart) flooding, our results show that using soil cores obtained in the field before and after winter recharge events to estimate  $\text{NO}_3^-$  leaching potential do not adequately capture total  $\text{NO}_3^-$  leaching amounts. This is because repeated, pulsed water applications for groundwater recharge, particularly if applied with long time intervals between events, provide environmental conditions promoting the mineralization of organic nitrogen to  $\text{NO}_3^-$ . Despite their contrasting soil texture, both soils studied here were capable of mineralizing organic nitrogen at a profile-average rate of  $7.0 - 8.3 \text{ mg N kg}^{-1} \text{ wk}^{-1}$ . Comparison of different flooding frequencies (e.g. 72-hr vs 1-week time intervals between flooding events) showed that longer time intervals resulted in increased N mineralization potential, and consequently higher amounts of  $\text{NO}_3^-$  leached during subsequent

flooding events. The column experiments further showed that the majority of the total  $\text{NO}_3^-$  leached over the course of the groundwater recharge event was leached during the first few hours of the first water application when environmental conditions were unfavorable for denitrification (such as anoxic conditions), a process that reduces  $\text{NO}_3^-$  to different gaseous nitrogen oxide products.

Our results helped identify and quantify important biogeochemical processes that need to be considered when assessing the environmental trade-offs of practicing Ag-MAR on agricultural fields in production. Specifically, our results indicate that winter flooding on agricultural fields for groundwater recharge produces environmental conditions that promote nitrogen transformation processes which can produce more residual soil  $\text{NO}_3^-$ . However, more research is needed comparing different soil textures and Ag-MAR practices to fully understand the impact of winter recharge (amounts, timing, flooding duration) on the organic C:N pools and nitrogen cycling processes, including  $\text{NO}_3^-$  leaching and mineralization/denitrification potential. Simulating these biogeochemical processes with reactive transport instead of conservative transport models should allow improving estimates of total  $\text{NO}_3^-$  leaching amounts during Ag-MAR, which can guide Ag-MAR best practice development.

## **Chapter 2: Comparison of reactive transport and non-equilibrium modeling approaches for the estimation of nitrate leaching under large water application events**

Nicholas P. Murphy<sup>1,\*</sup>, Helen E. Dahlke<sup>1</sup>

Affiliations: <sup>1</sup> Department of Land, Air and Water Resources, University of California, Davis, Davis, CA, 95616, USA. Corresponding author: [npmurphy@ucdavis.edu](mailto:npmurphy@ucdavis.edu)

Core Ideas:

- Incorporating environmental conditions improves simulated estimates of biogeochemical rates
- Incorporating physical non-equilibrium dynamics improves simulated estimates of residual soil nitrate following large water application events
- HP1-MIM is able to accurately estimate nitrate leaching potential across multiple soil textures

Abbreviations: Ag-MAR, agricultural managed aquifer recharge; NO<sub>3</sub><sup>-</sup>, nitrate; NH<sub>4</sub><sup>+</sup>, ammonium; BMPs, Best Management Practices

## ABSTRACT

In agricultural ecosystems, nitrate ( $\text{NO}_3^-$ ) leaching is the most widespread loss pathway and non-point source of nitrogen (N) to surface water and groundwater.  $\text{NO}_3^-$  leaching has been modeled extensively in rain-fed and irrigated agricultural systems using different approaches of varying complexity. However, most research has focused on optimizing growing season losses and less on  $\text{NO}_3^-$  leaching dynamics and N cycling under large water application events such as flood irrigation or off-season agricultural managed aquifer recharge (Ag-MAR), a practice that deliberately floods farm fields in the winter for groundwater recharge. In this study, we simulate observed  $\text{NO}_3^-$  leaching and biogeochemical processes under large water application events with a 1D non-equilibrium (e.g. mobile-immobile) reactive transport HP1 (HYDRUS-1D and PHREEQC) model to compare model performance to existing HYDRUS nitrate leaching modeling approaches (uniform flow, non-reactive, zero- and first-order kinetics). HYDRUS-1D is a variably saturated water flow and solute transport model that solves Richards' equation and Fickian-based advection dispersion transport equations. PHREEQC implements a N cycling model representing mineralization, nitrification and denitrification dynamics using conditional, kinetically controlled reactions. Results show that the incorporation of conditional environmental factors such as temperature, soil moisture, and a proxy for oxic/anoxic conditions (percent pore-space filled) improve model performance when estimating cumulative  $\text{NO}_3^-$  leached from the shallow vadose zone. The incorporation of physical non-equilibrium (i.e. mobile-immobile) dynamics improves model performance when estimating residual  $\text{NO}_3^-$  in the soil profile after water application events.

### 3.1 INTRODUCTION

An understanding of the nitrate ( $\text{NO}_3^-$ ) leaching potential in the vadose zone, and the subsequent contamination risk of underlying groundwater systems or connected surface water systems is essential for the sustainable management of water resources (Power et al. 1989). Nitrogen (N) cycling in the vadose zone is dependent on complex interactions between physical, atmospheric and hydrologic processes. Nitrogen cycling involves several organic and inorganic nitrogen compounds whose form and relative mobility can depend on environmental conditions including moisture, temperature, microbial communities, pH and oxygen (Booth et al. 2005, Cookson et al. 2007, Yu et al. 2009, Kuypers et al. 2018). Due to its mobility, abundance in the vadose zone, and associated health risks,  $\text{NO}_3^-$  is a constituent of growing concern in surface water systems and considered the most widespread nonpoint source pollutant in groundwater (Gurdak and Qi, 2012).

Most studies to date have investigated  $\text{NO}_3^-$  leaching in various environmental settings through experimental and modeling studies (Ritter et al. 1989, Padilla et al. 2018, Wang et al. 2019). Many of these studies have focused on optimizing growing season fertilization with reduction of  $\text{NO}_3^-$  leaching being a secondary objective (Errebhi et al. 1989). However, to date there are only a handful of studies that have focused on N cycling and  $\text{NO}_3^-$  leaching under naturally occurring large water applications events (e.g. >15 cm or 6 inches) that may occur as the result of natural flooding from rainfall or intentional flooding of agricultural fields for groundwater recharge (Di et al. 2002, Mack et al. 2005, Waterhouse et al. 2021).

In arid and semi-arid regions where rainfall often only occurs during the winter (i.e. crop dormancy) season, natural flooding from rainfall and intentional flooding of farm fields with excess surface water for groundwater recharge (also called agricultural managed aquifer

recharge, Ag-MAR) can have significant effects on  $\text{NO}_3^-$  leaching and N cycling processes in the root zone. The practice of Ag-MAR in particular is gaining interest in California and other groundwater dependent regions, however, questions remain regarding the  $\text{NO}_3^-$  leaching potential when applying large amounts of water to historically fertilized and cultivated fields.

The uncertainty surrounding  $\text{NO}_3^-$  leaching potential during Ag-MAR is still relatively uninvestigated. Because Ag-MAR involves applying water amounts that are much greater (e.g. >15 cm/event) than typical irrigation events (except for ponded systems such as rice, which remain continuously flooded but do not support substantial recharge), Ag-MAR creates hydrologic and biogeochemical conditions atypical to most agricultural systems such as ponded conditions, a more thorough and deeper wetting of the root zone, and longer drying periods compared to traditional irrigation systems. Therefore, previous N transport research is unlikely to represent the processes observed under Ag-MAR well. As a relatively new research area, previous Ag-MAR research has focused on assessing infiltration rates, crop tolerance and yield effects, and  $\text{NO}_3^-$  leaching risk through a variety of field and laboratory experiments (Dahlke et al. 2018, Waterhouse et al. 2020, Bachand et al. 2016, Murphy et al. 2021). Field and laboratory studies are vital to understanding the viability of Ag-MAR, however they are often limited by access to land and water availability, and high economic costs. Previous research examined the potential for biogeochemical transformations under repeated but distinct water application events, finding that mineralization, the microbial transformation of organic nitrogen to  $\text{NH}_4^+$ , which can be subsequently undergo nitrification, the conversion of  $\text{NH}_4^+$  to  $\text{NO}_3^-$  (hereby we use mineralization to generally refer to the complete conversion of organic N to inorganic  $\text{NO}_3^-$ ), and denitrification, the microbial process of reducing  $\text{NO}_3^-$  and nitrite ( $\text{NO}_2^-$ ) to gaseous forms of nitrogen such as nitrous oxide ( $\text{N}_2\text{O}$ ) and dinitrogen ( $\text{N}_2$ ), are important biogeochemical

processes occurring during Ag-MAR that should be considered when estimating total amounts of  $\text{NO}_3^-$  leached under Ag-MAR (Murphy et al. 2021). Similarly, Waterhouse et al. (2020) highlight the benefits of numerical modeling to increase our understanding of the timing and magnitude of  $\text{NO}_3^-$  leaching potential under Ag-MAR. Accurately modeling N cycle dynamics under Ag-MAR will be crucial to widespread implementation and the development of best management practices.

There exists a significant amount of research on the numerical modeling of  $\text{NO}_3^-$  leaching under typical agricultural management and irrigation practices. However,  $\text{NO}_3^-$  leaching and N cycling models vary in model and process complexity depending on the scale and scope of the study. There are various modeling codes that have been used to simulate N cycling processes and  $\text{NO}_3^-$  leaching in agricultural ecosystems including RZWQM, DSSAT, LEACHM, DRAINMOD, and HYDRUS. HYDRUS in particular is a popular code since it allows simulating saturated and unsaturated flow and solute transport under a variety of conditions including uniform or non-equilibrium flow and conservative and reactive transport (Šimůnek & van Genuchten 2008).

HYDRUS models developed for simulating  $\text{NO}_3^-$  leaching potential can be grouped into three categories based on model structure and complexity of the biogeochemical reactions that are incorporated: (1) non-reactive, (2) zero-order or first-order kinetic models, and (3) conditional kinetic models. Additionally, each of these model types can vary based on the representation of hydrologic flow processes, specifically whether they are represented as physical equilibrium (i.e. uniform flow) or physical non-equilibrium (i.e. mobile-immobile (MIM) dynamics). Within both saturated and unsaturated systems, these nitrogen cycling models often include the simulation of  $\text{NO}_3^-$ ,  $\text{NO}_2^-$ ,  $\text{NH}_4^+$ , gaseous nitrogen ( $\text{N}_2\text{O}$ ,  $\text{N}_2$ ), and organic

nitrogen (Org-N) as well as biogeochemical transformations such as mineralization, nitrification (oxidization of ammonia and other reduced nitrogen compounds to  $\text{NO}_2^-$  and  $\text{NO}_3^-$ ), denitrification, and physical processes such as leaching.

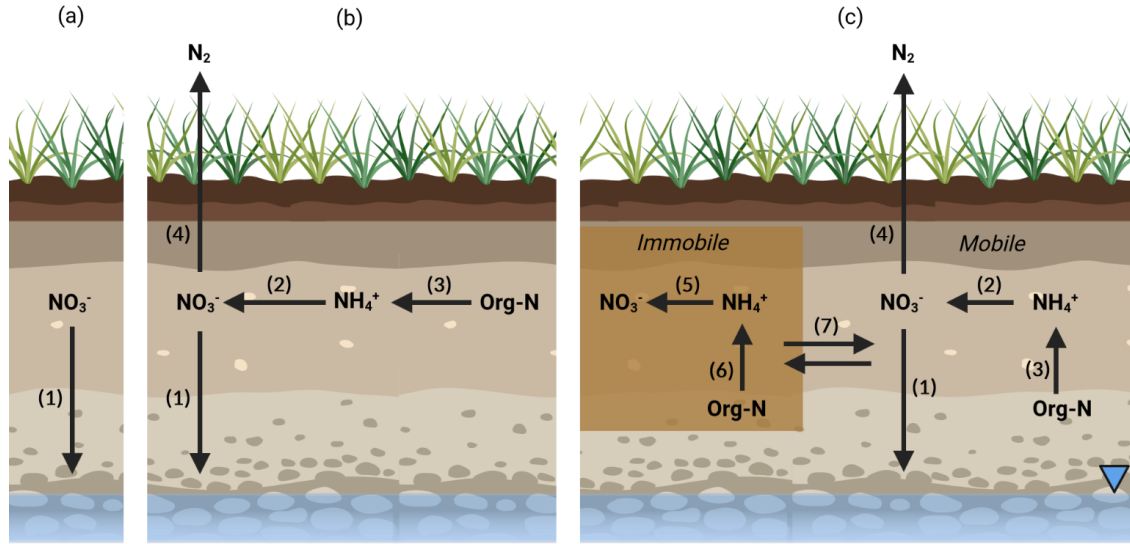


Figure 3.1: Examples of N cycling modeling approaches: (a) non-reactive modeling approach, (b) zero-order, first-order, or complex conditional approach, depending on functional dependence of biogeochemical equations 1 – 4, and (c) complex conditional modeling approach utilizing physical nonequilibrium (MIM dynamics). See Table 3.1 for the modeling approaches used in this paper, and their associated biogeochemical reactions.

Table 3.1: Modeling approaches and their associated reactions as pictured in Figure 3.1.

Model Type	Model Process	Functional Parameters/Variables
<b>NR (Non-reactive, uniform flow)</b> (Fig. 3.1a)	(1) Leaching	$f(q, [\text{NO}_3^-])$
<b>ZK (zero-order kinetic, uniform flow)</b> (Fig. 3.1b)	(1) Leaching (2) Nitrification (3) Mineralization (4) Denitrification	$f(q, [\text{NO}_3^-])$ $f(k_{\text{nit}})$ $f(k_{\text{min}})$ $f(k_{\text{denit}})$
<b>FK (first-order kinetic, uniform flow)</b> (Fig. 3.1b)	(1) Leaching (2) Nitrification (3) Mineralization (4) Denitrification	$f(q, [\text{NO}_3^-])$ $f(k_{\text{nit}}, [\text{NH}_4^+])$ $f(k_{\text{min}}, [\text{Org-N}])$ $f(k_{\text{denit}}, [\text{NO}_3^-])$
<b>HP1 (conditional kinetic, uniform flow)</b> (Fig. 3.1b)	(1) Leaching (2) Nitrification (3) Mineralization (4) Denitrification	$f(q, [\text{NO}_3^-])$ $f(k_{\text{nit}}, [\text{NH}_4^+], \%PSF)$ $f(k_{\text{min}}, [\text{Org-N}], \theta, T)$ $f(k_{\text{denit}}, [\text{NO}_3^-], \%PSF)$

<b>HP1-MIM (conditional kinetic, non-equilibrium flow, mobile-immobile dynamics)</b> (Fig. 3.1c)	(1) Leaching	$f(q, [NO_3^-])$
	(2) Mobile Nitrification	$f(k_{nit}, [NH_4^+]_{mob}, \%PSF)$
	(3) Mobile Mineralization	$f(k_{min}, [Org-N]_{mob}, \theta_{mob}, T)$
	(4) Immobile Nitrification	$f(k_{nit}, [NH_4^+]_{imm}, \%PSF)$
	(5) Immobile Mineralization	$f(k_{min}, [Org-N]_{imm}, T)$
	(6) Denitrification	$f(k_{denit}, [NO_3^-], \%PSF)$
	(7) Mass transfer (mobile- immobile phase)	$f(\omega_{mim})$

Non-reactive  $NO_3^-$  leaching models consider it as a non-reactive, mobile tracer. No biogeochemical transformations are considered, and  $NO_3^-$  leaves the system either through plant uptake, or physical processes such as advective-dispersive transport (Karandish et al. 2017, Ajdary et al. 2007). Application of these models often focuses on large scales, both spatially and temporally. Karandish et al. (2017) used a two-dimensional  $NO_3^-$  leaching model (HYDRUS-2D) to optimize irrigation and fertilization rates on a 0.08 ha, drip irrigated, sandy clay loam, maize field site in Sari, Iran. Although biogeochemical transformations such as mineralization and denitrification were omitted, plant uptake was considered. Ajdary et al. (2007) used a similar HYDRUS-2D model structure to represent field scale  $NO_3^-$  leaching dynamics as a function of soil texture and drip fertigation rates in a two-dimensional model on a drip irrigated, sandy clay loam, onion field in New Delhi, India, but did not incorporate mineralization, nitrification or denitrification processes. Other research has compared non-reactive  $NO_3^-$  leaching models to simple N mass balance models, and Darcy flux calculations for estimating its loss to groundwater. Baram et al. (2017) for example found that all three of these approaches estimated similar timings and magnitudes of N loss from almond orchards to groundwater (80-240 kg N ha<sup>-1</sup> yr<sup>-1</sup>). While non-reactive models are useful for large-scale applications, field and laboratory experiments have found significant amounts of both mineralization (Wade et al. 2016, Geisseler et al. 2019) and denitrification (Hofstra & Bouwman 2005) can occur in agricultural settings, indicating their importance for inclusion when estimating the  $NO_3^-$  leaching potential of a soil.

The second group of models consists of advection-dispersion models that simulate N cycling through simple one-directional kinetic reactions (Li et al. 2015, Akbariyeh et al. 2018, Deb et al. 2015, Hanson et al. 2006, Hassan et al. 2008). The spatial scale of applying these models is often smaller than the non-reactive model group, mainly focused on the field to watershed scale. Hanson et al. (2006) used first order kinetics in a HYDRUS model to represent the degradation of urea to  $\text{NH}_4^+$ , and the subsequent nitrification of  $\text{NH}_4^+$  to  $\text{NO}_3^-$  during various drip fertigation scenarios. They defined kinetic rates based on literature values and performed a multi-scenario analysis to investigate fertigation best management practices.

There also exist models which represent the N cycle as a series of complex conditional reactions dependent on other chemical species, such as multiple organic pools of varying lability, or environmental conditions, such as dissolved oxygen and oxidation-reduction potential (Porporato et al. 2003, Waterhouse et al. 2021). Porporato et al. (2003) developed a N cycling model which includes denitrification, mineralization and nitrification processes under a number of conditional factors. They used soil moisture, temperature and soil organic matter ratios to condition mineralization and immobilization rates. Denitrification is modeled to only occur at sufficiently high moisture levels. They also calibrated multiple soil organic matter pools, representing plant residue, microbial biomass, and humus, all with unique carbon and N compositions. The hydrologic side of the model is represented stochastically rather than deterministically. These complex model schemes require a significant amount of parameterization, and consequently the soil system is considered as a single pool, with no spatial discretization or heterogeneity. It is important to note that even when models use site-specific data for biogeochemical parameters, they often are not able to discretize spatially (Lotse et al. 1992, D'odorico et al. 2003). The HYDRUS and HP1 models discussed in this paper are able to

discretize biogeochemical parameters with depth. This is important due to the variation in mineralization, nitrification and denitrification rates observed for different soil horizons, where laboratory incubations have shown mineralization rates changing more than one order of magnitude over 10 cm depth (Murphy et al. 2021).

To our knowledge, only one complex conditional modeling approach investigating  $\text{NO}_3^-$  leaching under Ag-MAR exists. Waterhouse et al. (2021) developed a reactive transport model in TOUGHREACT to investigate  $\text{NO}_3^-$  leaching and denitrification potential, with an emphasis on deep subsurface (9 m deep vadose zone) dynamics. TOUGHREACT represents denitrification as a complex, microbially mediated redox reaction. However, the main focus was the development of theoretical stratigraphic profiles and flooding frequency scenarios to investigate N retention and denitrification potential in the deep vadose zone. Nitrogen mineralization dynamics were omitted, and the difficulty of deep vadose zone sampling meant validation of  $\text{NO}_3^-$  leaching estimates was not possible. Waterhouse et al. (2021) identified the need for future studies to include important N cycling processes such as mineralization, and to investigate their role under Ag-MAR.

The objective of this study is to develop the reactive transport model HP1, using HYDRUS-1D coupled to PHREEQC, to represent nitrogen cycle and  $\text{NO}_3^-$  leaching dynamics observed in the shallow vadose zone during field and laboratory large water application Ag-MAR experiments. In this study, we examine two specific questions: (1) How does a reactive transport model which incorporates parameter conditionalization (i.e. scaling dependent on environmental factors) compare to non-reactive, zero-order or first-order kinetic  $\text{NO}_3^-$  leaching models when simulating large water application events? (2) What effect does the incorporation of physical nonequilibrium (mobile-immobile soil dynamics) have on  $\text{NO}_3^-$  leaching modeling and

estimations of residual  $\text{NO}_3^-$  in the soil profile? To address these questions, we compare a non-reactive, uniform flow model (NR), a zero-order kinetic, uniform flow model (ZK), a first-order kinetic, uniform flow model (FK), a conditional kinetic, uniform flow model (HP1), and a conditional kinetic, mobile-immobile model (HP1-MIM). We hypothesize that our HP1-MIM model, which incorporates scaling factors for environmental conditions and physical and chemical non-equilibrium dynamics, will accurately capture both the  $\text{NO}_3^-$  leaching dynamics observed during large water application events and the N transformations occurring within the soil profile, compared to traditional NR, ZK, or FK models. Additionally, we hypothesize that the incorporation of mobile-immobile dynamics will improve the model performance, specifically with regards to the amount of residual  $\text{NO}_3^-$  simulated in the soil profile following Ag-MAR water application events, when comparing the HP1 and HP1-MIM models.

### **3.2 Model Theory and Structure**

HP1 is a coupled water flow and solute transport model, pairing HYDRUS-1D and PHREEQC (Jacques & Šimůnek, 2004). HYDRUS-1D simulates variably-saturated water flow in one dimension, while PHREEQC calculates biogeochemical reactions. The HP1 model is capable of simulating variably-saturated flow, the transport of multiple solutes through the soil profile, and relevant geochemical reactions, including interactions between the solid/gas/water phases, sorption dynamics and kinetic reactions. The reactive transport model presented in this research is a HP1 model with mobile-immobile (MIM) dynamics, hereby referred to as HP1-MIM. Fig. 3.1c represents this modeling approach, while Table 3.1 outlines the differences in number of parameters and processes between this model and commonly used  $\text{NO}_3^-$  leaching modeling approaches. Model parameters and governing rate equations for the biogeochemical

reactions of all models discussed in this paper are presented in the Supplementary Material (Table S3.1).

### 3.2.1 Water Flow & Solute Transport

HYDRUS-1D models variably-saturated water flow through the soil profile, by solving the 1D Richards Equation for vertical flow:

$$\frac{\partial \theta}{\partial t} = \frac{\partial}{\partial z} \left[ K(\theta) \left( \frac{\partial h}{\partial z} + 1 \right) \right] \quad (1)$$

where  $h$  is the water pressure head [L],  $\theta$  is the volumetric water content [ $L^3 L^{-3}$ ], and  $K$  is the unsaturated hydraulic conductivity [ $LT^{-1}$ ] (Diederik & Šimůnek 2005). Within HYDRUS-1D, solute transport is solved by a version of the advection-dispersion equation given in Šimůnek et al. (1998):

$$\frac{\partial \theta c_i}{\partial t} = \frac{\partial}{\partial z} \left( \theta D_i^w \frac{\partial c_i}{\partial z} \right) - \frac{\partial q c_i}{\partial z} - S c_{r,i} + R_i \quad (2)$$

where  $i$  is the aqueous species number,  $c_i$  is the aqueous concentration of solute  $i$  [ $M L^{-3}$ ],  $q$  is the volumetric flux density,  $S$  is a sink term in the water flow equation (1),  $c_r$  is the concentration of the sink term [ $M L^{-3}$ ],  $D^w$  is the dispersion coefficient in the liquid phase [ $L^2 T^{-1}$ ], and  $R_i$  is a source/sink term for chemical reactions simulated by PHREEQC (Diederik & Šimůnek 2005).

In this study we also incorporate the dual-porosity (mobile-immobile water) model for solute transport, allowing for the simulation of physical nonequilibrium solute transport

dynamics. The MIM model assumes that water present in micropores within the soil matrix is immobile and constant in time but dissolved solutes can move into and out of this immobile domain by molecular diffusion (e.g., van Genuchten and Wierenga, 1976). HP1-MIM simulates physical nonequilibrium solute transport while still maintaining uniform water flow by partitioning a fraction of the pore space as immobile and parameterizing a solute mass transport term so that the immobile-mobile phases interact throughout model simulations. This modifies the typical advection-dispersion equation presented above, and is characterized by the equations:

$$\frac{\partial \theta_{mo} c_{mo}}{\partial t} + f_{mo} \rho \frac{\partial s_{mo}}{\partial t} = \frac{\partial}{\partial z} \left( \theta_{mo} D_{mo} \frac{\partial c_{mo}}{\partial z} \right) - \frac{\partial q_{mo} c_{mo}}{\partial z} - R_{mo,i} - \gamma_s \quad (3a)$$

$$\frac{\partial \theta_{im} c_{im}}{\partial t} + (1 - f_{mo}) \rho \frac{\partial s_{im}}{\partial t} = \gamma_s - R_{im,i} \quad (3b)$$

$$\gamma_s = \omega_{mim} (c_{mo} - c_{im}) \quad (3c)$$

Where the subscripts *mo* and *im* refer to the mobile and immobile phases, respectively, *f* is the porosity of a phase, *s* is the sorbed concentration of a species, *i* is the aqueous species number, *c<sub>i</sub>* is the aqueous concentration of solute *i* [ML<sup>-3</sup>], *q* is the volumetric flux density, *c<sub>r</sub>* is the concentration of the sink term [ML<sup>-3</sup>], *D* is the dispersion coefficient in liquid phase [L<sup>2</sup>T<sup>-1</sup>], *R<sub>i</sub>* is a source/sink term for chemical reactions simulated by PHREEQC, *γ<sub>s</sub>* is the mass transfer term for solutes between the mobile and immobile regions [ML<sup>-3</sup>T<sup>-1</sup>], and *ω* is the mass transfer coefficient [T<sup>-1</sup>] (Diederik & Šimůnek 2008).

### 3.2.2 Biogeochemical reactions

Three main biogeochemical reactions are considered in our model: mineralization, nitrification, and denitrification. All of them are modeled through kinetic reactions, but in the HP1 model, each reaction is conditional under varying criteria.

Nitrogen mineralization potential has been shown to change significantly under varying temperature and moisture conditions (Cassman et al. 1980). The mineralization of organic N was represented in our model as a conditional first order kinetic reaction:

$$R_{min} = k_{min} F_T W_m [Org - N] \quad (4)$$

where  $R_{min}$  is the amount of mineralization [ $ML^{-3}T^{-1}$ ],  $k_{min}$  is the first order rate constant for mineralization [ $T^{-1}$ ],  $F_T$  is a dimensionless scalar representing the relationship between temperature and mineralization,  $W_m$  is a dimensionless scalar representing the relationship between water content and mineralization, and  $[Org-N]$  is the concentration of organic nitrogen [ $ML^{-3}$ ]. The relationship used by Miller & Geisseler (2018) to determine the temperature sensitivity of N mineralization in soil is defined as:

$$F_T = 241.9e^{-3.528\left(1-\frac{T}{50}\right)^2} \quad (5)$$

where  $F_T$  is the rate constant as a function of temperature in percent of the N mineralization rate at 25 °C,  $T$  is the measured soil temperature in degrees Celsius. The relationship between N mineralization rate and water content,  $W_m$ , was defined by Paul et al. (2003) as:

$$W_m = \frac{1}{1+6.63 \exp(-5.69RFWC)} \quad (6)$$

where  $W_m$  is a scaling factor dependent on the relative field water content,  $RFWC$ , which is determined as a function of the lower and upper limit of  $\theta$  observed for a soil layer.

Nitrification was represented in the model as a first order kinetic reaction:

$$R_{nit} = k_{nit}[NH_4^+] \quad (7)$$

$R_{nit}$  is the amount of nitrification [ $ML^{-3}T^{-1}$ ],  $k_{nit}$  is the first order rate constant for nitrification [ $T^{-1}$ ], and  $[NH_4^+]$  is the concentration of ammonium.

Denitrification was represented in the model as a conditional zero order kinetic reaction.

It has the general form:

$$R_{denit} = k_{denit} \quad (8)$$

Where  $R_{denit}$  is the amount of denitrification [ $ML^{-3}T^{-1}$ ],  $k_{denit}$  is the zero order rate constant for denitrification [ $T^{-1}$ ]. However, because denitrification is known to be favorable above specific volumetric water content thresholds (Bremner & Shaw 1958), a proxy was introduced such that denitrification only occurs if the percent of the total pore space is more than 70% filled with water. This proxy, known as percent pore space filled (%PSF) is common for estimating conditions favorable to denitrification (Linn & Doran, 1984).

### 3.3 MATERIALS AND METHODS

#### 3.3.1 Experimental Design

The reactive N transport model was developed and calibrated with high resolution datasets collected from laboratory column experiments replicating large water application events for Ag-MAR conducted at two field sites in Central California, USA. The experimental design, instrumentation and data collection is outlined in detail in Murphy et al. (2021). To summarize briefly, Ag-MAR experiments were conducted on two soil textures, a sand (Delhi sand series, mixed, thermic, Typic Xeropsamments) and a fine sandy loam (Dinuba series, coarse-loamy, mixed, active, thermic Typic Haploxeralfs) rated “Excellent” and “Moderately Good” respectively by the Soil Agricultural Groundwater Banking Index (O’Geen et al. 2015). Each soil

column (80 cm high, 20 cm diameter) experiment consisted of three discrete 15 cm water applications, spaced one to two weeks apart, representing past Ag-MAR field experiments (Murphy et al. 2021). Data included the measurement of organic and inorganic N ( $\text{NO}_3^-$ -N,  $\text{NH}_4^+$ -N, TN) within the soil matrix before and after water application events, and continuous measurements of discharge rates and  $\text{NO}_3^-$ -N concentration in the effluent along with measurements of volumetric water content, redox potential and dissolved oxygen.

### **3.3.2 Initial and Boundary Conditions**

The initial hydrologic conditions in the model were set based upon measured volumetric water content recorded prior to any water applications. Both the sand and fine sandy loam were near the residual water content before the first water application for Ag-MAR was made and therefore VWC was initially set to 0.08. The initial conditions for solute concentrations in the soil profile were based upon soil analyses measured in 10 cm intervals for  $\text{NO}_3^-$ -N,  $\text{NH}_4^+$ -N and DON.

For water flow, the upper boundary was set as atmospheric boundary, with the water applied as high magnitude precipitation events. The lower boundary was set as a variable pressure head, and a low negative pressure head was applied (-51 cm), mimicking the conditions in the laboratory column experiments, which were designed to prevent the buildup of an artificial water table (Murphy et al. 2021, Lewis & Sjöstrom 2010). For solute transport, the upper boundary was set as a concentration flux, while the lower boundary was set as a zero-concentration gradient. The water applied to the soil columns had non-detect concentrations of nitrogen species, and  $\text{NO}_3^-$  leaching was assumed to come solely from the solute concentrations within the soil profile.

### 3.3.3 Model Sensitivity Analysis

A local sensitivity analysis (Liu et al. 2018, Ben-Moshe et al. 2021) was applied, where  $f$  is a model with output  $O$ , which is dependent on a set of  $\beta$  model parameters:

$$O = f(\beta_1, \beta_2, \beta_3 \dots \beta_i \dots \beta_n) \quad (9)$$

Model output variation due to the variation of parameter  $\beta_i$  is represented as  $\delta_i$ , where:

$$\delta_i = \frac{\Delta O}{\Delta \beta} = \frac{f(\beta_1 \dots \beta_i \pm \Delta \beta_i \dots \beta_n) - f(\beta_1 \dots \beta_i \dots \beta_n)}{\Delta \beta_i} \quad (10)$$

Normalizing these variations in model output due to shifting parameters, we calculate the sensitivity index,  $SI$ :

$$SI_i = \delta_i \frac{\beta_i}{O} \quad (11)$$

Three sensitivity analyses were performed in order to evaluate the relative sensitivity of parameters to model validation metrics: the sensitivity of model parameters (1) to the hydrologic flow through the soils (Fig. 3.3 & 3.4), (2) to the amount of  $\text{NO}_3^-$  leached under water application events (Supplementary Material, Fig. S3.3 & S3.4), and (3) to the amount of residual  $\text{NO}_3^-$  and  $\text{NH}_4^+$  present in the soils after Ag-MAR (Supplementary Material, Fig. S3.3 & S3.4) were all assessed. A 40% shift was chosen to evaluate the local parameter sensitivity, Parameter sensitivity was calculated using multiple model output variables, including cumulative water recharged, cumulative  $\text{NO}_3^-$  leached, and the residual  $\text{NO}_3^-$  in the soil profile at 10 and 80 cm depth.

### 3.3.4 Model Calibration

UCODE, a set of inverse modeling codes was used to perform the HP1-MIM model calibration. Developed by the US Geological Society, UCODE is capable of solving inverse modeling tasks through parameter estimations, using non-linear regressions (Poeter & Hill

1999). UCODE was used in this study to estimate parameters which could not be measured during lab or field experiments.

The HP1-MIM model presented was calibrated in two discrete steps. The first calibration step included hydraulic parameters impacting the observed hydrologic flow of water through the model domain, based upon cumulative discharge data (Fig. 3.2). Next, relevant biogeochemical parameters were calibrated using the measured timing and magnitude of the cumulative  $\text{NO}_3^-$  leached from the soil column experiments, along with the residual  $\text{NO}_3^-$  and  $\text{NH}_4^+$  profiles measured following the water applications (Fig. 3.5 & 3.6).

The mobile and immobile phases were calibrated based upon high-resolution  $\text{NO}_3^-$  breakthrough observed during laboratory soil column experiments. This data showed that approximately 30% of the  $\text{NO}_3^-$  remains in immobile pore space following water application event. As a result, the  $\text{NO}_3^-$  is split initially with 30% present in the immobile pore space, and 70% present in the mobile pore space or a ratio,  $r$ , of 0.3:0.7. This ratio was calibrated manually for goodness of fit using the initial magnitude of  $\text{NO}_3^-$  breakthrough during the first water application. The ratio,  $r_{kin}$ , was used to represent the fraction of mineralization and nitrification occurring in the immobile and mobile pore spaces, respectively. It was set to the same mobile/immobile pore space ratio  $r$  (0.3:0.7) and was also calibrated manually, using the residual  $\text{NO}_3^-$  in the soil profile following the water applications. The sensitivity analysis, and model performance used to calibrate  $r$  and  $r_{kin}$  is included in the Supplementary Information (Fig. S3.1 & S3.2). The water content of the immobile pore space is not known, and was therefore set to be relatively small ( $\theta_{im}=0.024$ ), to serve as a proxy for physical nonequilibrium solute transport dynamics. The mass transfer coefficient ( $\omega_{mim}$ ) was calibrated to 1E-06, based upon observation data of residual  $\text{NO}_3^-$  in the soil profile.

## 3.4 RESULTS

### 3.4.1 Hydrologic Calibration of the HP1-MIM model

The RMSE values of the calibrated models were 1.07 cm-H<sub>2</sub>O and 1.23 cm-H<sub>2</sub>O for the fine sandy loam and sand, respectively (Fig. 3.2). Hydraulic parameters (Table 3.2) fell within typical ranges for their respective soil types, and the values for the fine sandy loam were similar to a separate study conducted by Waterhouse et al. (2021), which independently calibrated hydraulic parameters for the same soil (Schaap et al. 2001, Kosugi et al. 2002).

Table 3.2: Calibrated van Genuchten parameters for the fine sandy loam and sand.

Layer	$\theta_r$ [-]	$\theta_s$ [-]	$\alpha$ [cm <sup>-1</sup> ]	n [-]	K <sub>s</sub> [cm hr <sup>-1</sup> ]	l [-]
<b>Fine sandy loam</b>						
<b>1 (0 - 80cm)</b>	0.032	0.320	0.076	1.86	3.20	0.5
<b>Sand</b>						
<b>1 (0 - 60cm)</b>	0.028	0.345	0.025	1.78	23.56	0.5
<b>2 (60 - 80cm)</b>	0.036	0.320	0.025	2.00	3.66	0.5

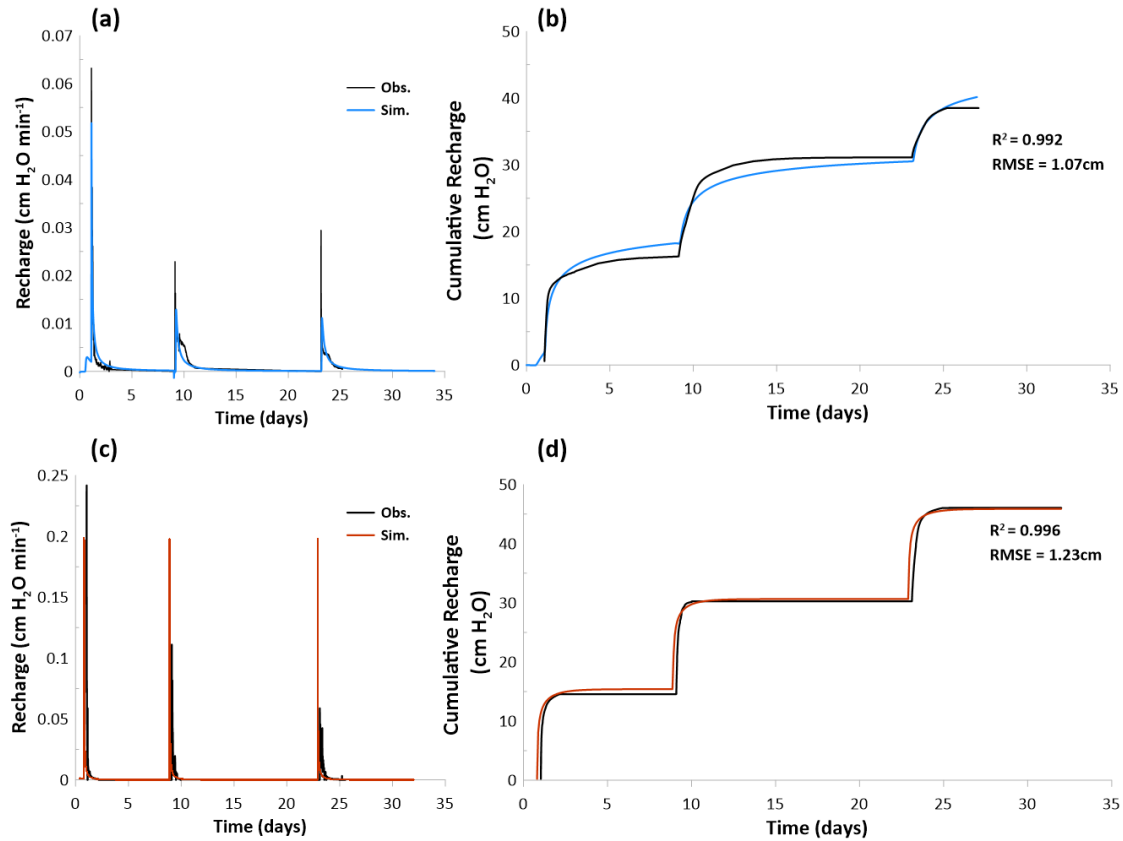


Figure 3.2: Simulated modeling results vs. observed data for recharge and cumulative recharge at the bottom of the model domain (80 cm depth), using calibrated van Genuchten parameters. (a) and (b) represent the observed laboratory data compared to the simulated model recharge and cumulative recharge, respectively, for the fine sandy loam soil. (c) and (d) represent the same data for the sand soil.

The fine sandy loam shows the highest sensitivity to parameters  $n$  (SI = +67%, -171%) and  $K_s$  (SI = +55%, -90%) (Fig. 3.3). The sand is split into two texture layers with differing hydraulic properties (Table 3.2). The sensitivity analysis of the sand profile shows a higher model sensitivity to the van Genuchten parameters of Layer 1 (0-60cm), compared to Layer 2 (60-80cm) (Fig. 3.4). The sand has the highest sensitivity to  $n_1$  (SI = +37%, -20%) and  $\theta_{s,1}$  (SI = +22%, -20%), with lower overall sensitivity than the fine sandy loam.

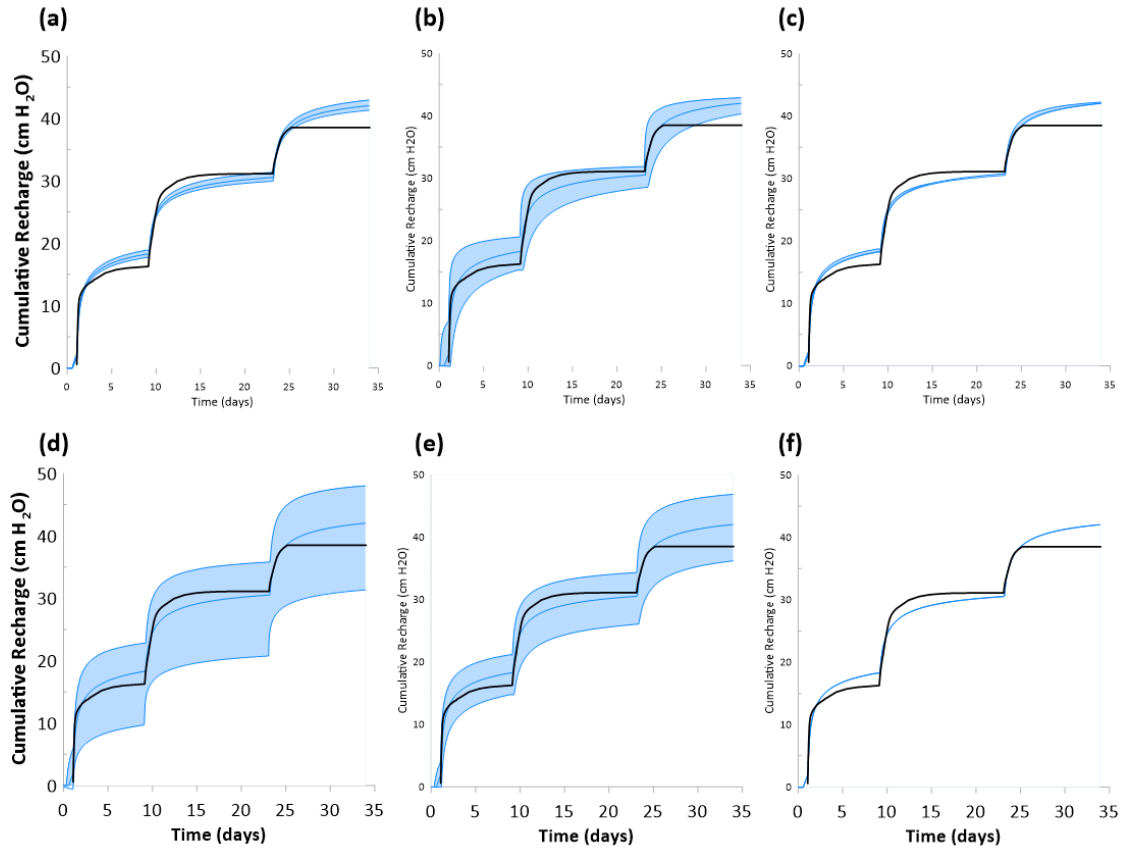


Figure 3.3: Local sensitivity analysis of fine sandy loam hydraulic parameters. The shaded area represents the change in cumulative discharge at the bottom of the model due to a 40% parameter variation. (a) residual water content ( $\theta_r$ ), (b) saturated water content ( $\theta_s$ ), (c) alpha ( $\alpha$ ), (d) n, (e) saturated hydraulic conductivity ( $K_s$ ), (f) tortuosity (L).

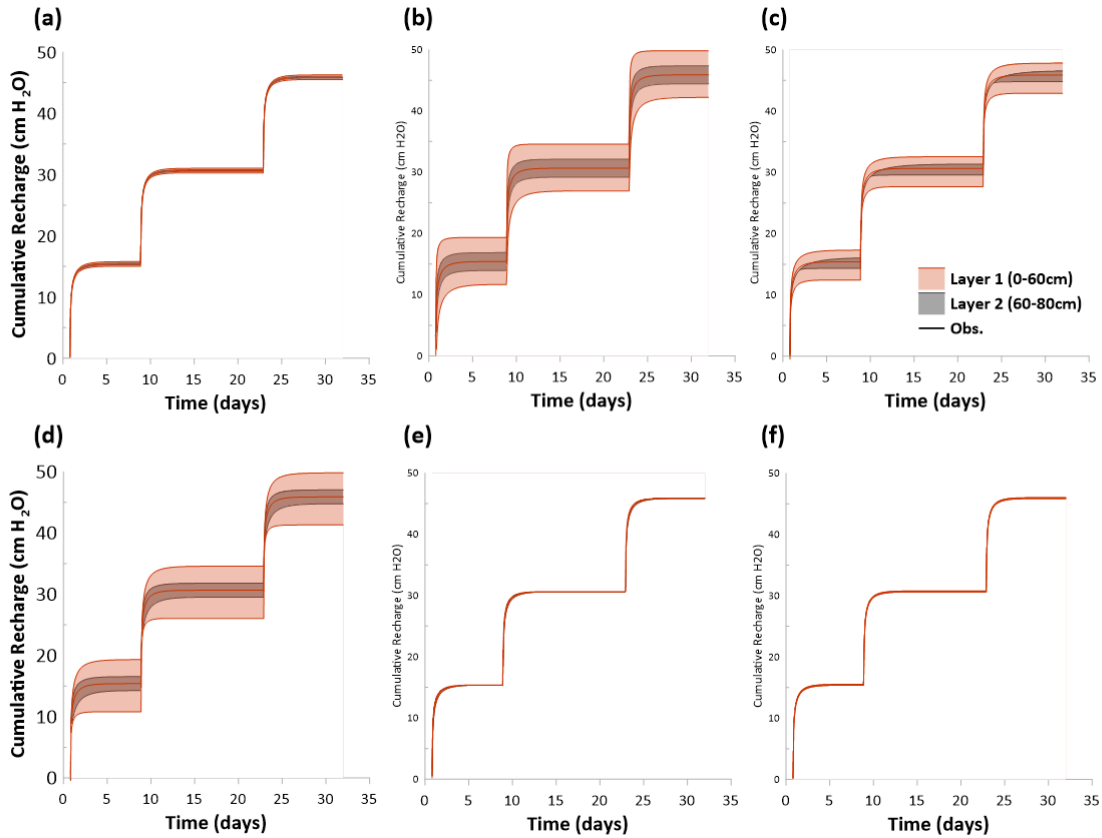


Figure 3.4: Local sensitivity analysis of sand hydraulic parameters. The shaded area, in colors corresponding to material layers in the model, represents the change in cumulative discharge at the bottom of the model due to a 40% parameter variation. Note that for the sand soil two sets of parameters were calibrated for the upper soil layer (layer 1: 0-60 cm) and lower soil layer (layer 2: 60-80 cm). (a) residual water content ( $\theta_r$ ), (b) saturated water content ( $\theta_s$ ), (c) alpha ( $\alpha$ ), (d)  $n$ , (e) saturated hydraulic conductivity ( $K_s$ ), (f) tortuosity ( $L$ ).

### 3.4.2 Biogeochemical Calibration of the HP1-MIM model

Nitrate data collected from the soil column experiments were used for the biogeochemical calibration of the model. Cumulative  $\text{NO}_3^-$  leached at the bottom of the model domain and residual  $\text{NO}_3^-$  in the soil profile were both used for model calibration and to determine model performance. Residual  $\text{NH}_4^+$  in the soil profile was also used, as it indicates goodness of fit regarding model representation of the timing and magnitude of N mineralization and nitrification processes. Laboratory incubation experiments resulted in detailed measurements

of the initial  $\text{NO}_3^-$  concentrations in the soil profile as well as = mineralization ( $k_{min}$ ) and denitrification ( $k_{denit}$ ) rates for both soils, spatially discretized into 10 cm intervals for the full 80 cm profiles. The site-specific mineralization and denitrification rate data was incorporated into the model, along with the measured uncertainty and further calibration was not necessary. Other parameters impacting biogeochemical transformation rates included the nitrification rate,  $k_{nit}$ , the ratio by which initially present soil  $\text{NO}_3^-$  is split between the mobile,  $r$ , and immobile pore-space,  $r_{kin}$ , the %PSF threshold, which serves as a proxy for oxic/anoxic conditions, and the mass transfer coefficient between the immobile and mobile pore space,  $\omega_{mim}$ . The %PSF threshold was set to 0.7 across both soil types (Machefert et al. 2004). Freundlich adsorption was incorporated into the model, using the Freundlich fitting parameters  $K_f$  ( $\text{cm}^3 \text{mg}^{-1}$ ) and  $n$  (-), based on literature values from a similar soil type ( $K_f$ :  $28.2 \text{ cm}^3 \text{mg}^{-1}$ ,  $n$ : 0.6) (Vogeler et al. 2011) for both the  $\text{NH}_4^+$  and Org-N pools. The purpose of this was to ensure that the  $\text{NH}_4^+$  and Org-N pools were not flushed from the soil profile during water application events, as they were observed to be relatively immobile based upon laboratory leachate data for both soils. Biogeochemical parameters were either estimated from reasonable literature values, or manually calibrated based on the model performance metrics outlined in the methods. Relevant biogeochemical parameters are reported in the Supplementary Materials, Table S3.1 & S3.2.

Both models capture well the general trends (i.e. timing and magnitude) of  $\text{NO}_3^-$  leaching during the Ag-MAR water applications, and the total amount of  $\text{NO}_3^-$  leached from the soil profile (Fig. 3.5, 3.6). However, in both soil types, we see a slight underestimation of the initial  $\text{NO}_3^-$  breakthrough during the first water application. The second water application captures the observed  $\text{NO}_3^-$  leaching within the model uncertainty and the third water application results in an overestimation of the individual  $\text{NO}_3^-$  leaching event. The fine sandy loam model estimates

between 13.5 – 22.1 kg ha<sup>-1</sup> of NO<sub>3</sub>-N is leached during the water applications, compared to the observed 15.0 kg ha<sup>-1</sup> NO<sub>3</sub>-N leached during laboratory experiments (Fig. 3.5). The sand model estimates between 29.2– 37.1 kg ha<sup>-1</sup>, compared to the observed 35.7 kg ha<sup>-1</sup> NO<sub>3</sub><sup>-</sup>-N leached during laboratory experiments (Fig. 3.6). The residual soil NO<sub>3</sub><sup>-</sup> trends are accurately captured in both the fine sandy loam and the sand model. For the fine sandy loam, we see a general increase in NO<sub>3</sub><sup>-</sup> in the soil profile following the three water applications, and model results capture the majority of this trend within the model uncertainty (Fig. 3.5). The sand shows a general decrease in the residual NO<sub>3</sub><sup>-</sup> load following the water applications, and again the model does a satisfactory job of representing the trend and magnitude of the residual NO<sub>3</sub><sup>-</sup> in the soil profile (Fig. 3.6).

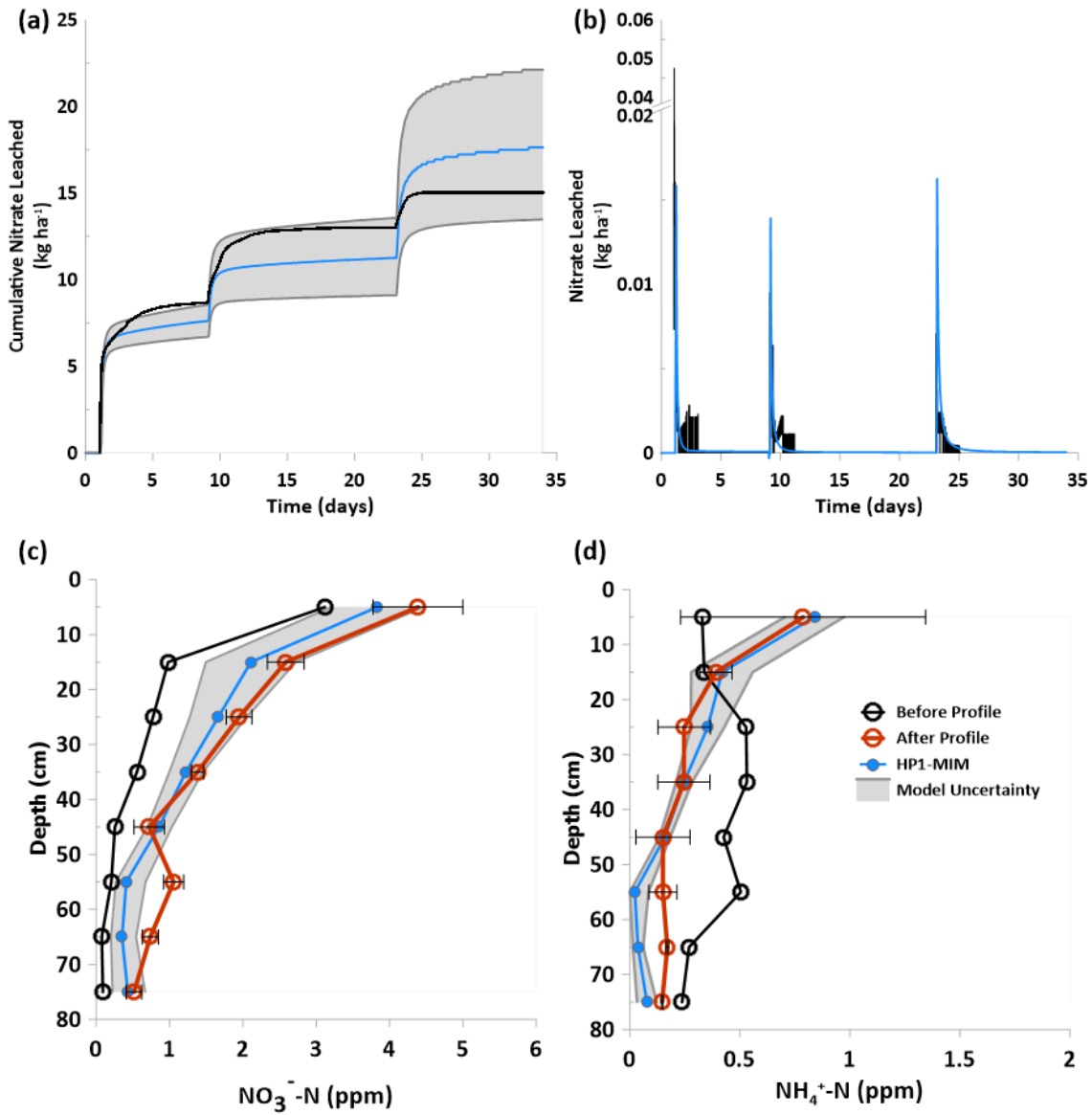


Figure 3.5: Biogeochemical validation metrics for simulated vs. observed model fit for the fine sandy loam. (a) cumulative NO<sub>3</sub><sup>-</sup> leached from the profile, (b) NO<sub>3</sub><sup>-</sup> leached from the profile, (c) residual NO<sub>3</sub><sup>-</sup> in soil profile at the end of model simulation, (d) residual NH<sub>4</sub><sup>+</sup> in soil profile at end of model simulation. Grey shaded areas show one standard deviation of error for the initial NO<sub>3</sub><sup>-</sup> concentrations in the soil profile and the estimated mineralization rate constants.

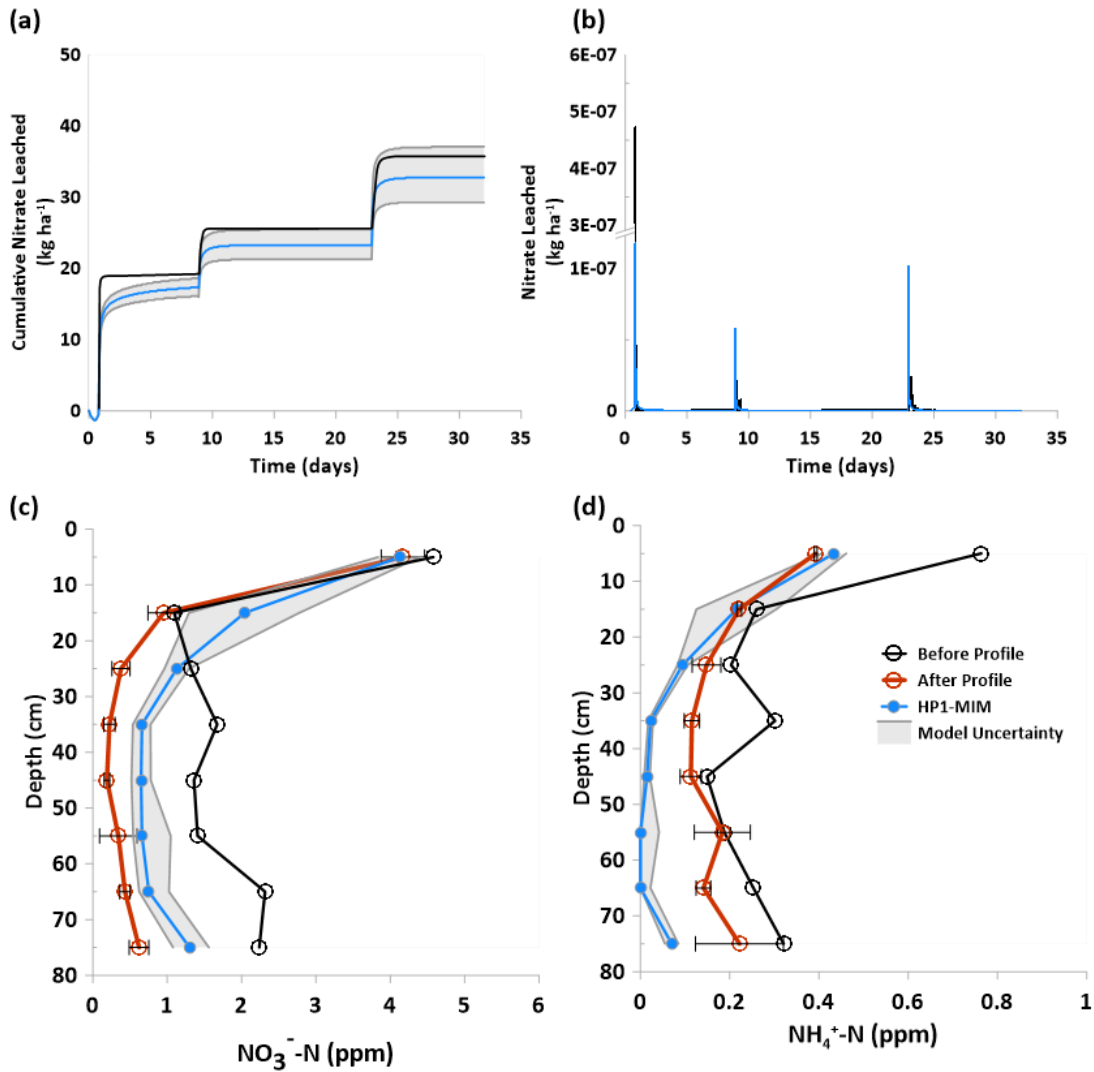


Figure 3.6: Biogeochemical validation metrics for simulated vs. observed model fit for the sand. (a) cumulative  $\text{NO}_3^-$  leached from the profile, (b)  $\text{NO}_3^-$  leached from the profile, (c) residual  $\text{NO}_3^-$  in soil profile at the end of model simulation, (d) residual  $\text{NH}_4^+$  in soil profile at end of model simulation. Grey shaded areas show one standard deviation of error for the initial  $\text{NO}_3^-$  concentrations in the soil profile and the estimated mineralization rate constants.

The sensitivity analysis shows for the fine sandy loam, the most sensitive parameters are  $[\text{NO}_3^-\text{-N}]_{ini}$  and  $k_{min}$ , although  $k_{denit}$  can also impact cumulative  $\text{NO}_3^-$  leaching (Supplemental Materials, Fig. S3.3). Conversely, cumulative  $\text{NO}_3^-$  leaching shows relatively low sensitivity to the  $k_{nit}$  and  $\omega_{mim}$  parameters (Supplemental Materials, Fig. S3.3). The sand model's most

sensitive parameters are also  $[NO_3^- - N]_{ini}$  and  $k_{min}$ , however  $\omega_{mim}$  shows a greater sensitivity compared to the fine sandy loam, with  $k_{nit}$  and  $k_{denit}$  having the lowest sensitivity (Supplementary Material, Fig. S3.4).

Overall, the residual soil profile for both soil types show a lack of sensitivity to all biogeochemical parameters besides  $k_{min}$ . (Supplementary Material, Figure S3.3 & S3.4). The residual soil profile shows a high sensitivity to  $k_{min}$ , particularly in the upper layers where it can shift the residual  $NO_3^-$  concentration by  $\sim 1.5$  ppm. There is a low sensitivity (predominantly at the 10-20 cm depth) to  $\omega_{mim}$ , which may impact how quickly  $NO_3^-$  located within the immobile pore space is transported to the mobile pore space, and available for leaching during subsequent water applications.

### 3.4.3 Model Comparison

To evaluate the performance of the newly developed HP1-MIM reactive N transport model, a comparison of simulated vs observed cumulative  $NO_3^-$  leached from the soil profile, residual soil  $NO_3^-$ , and residual soil  $NH_4^+$  was performed for the NR, ZK, FK, HP1, and HP1-MIM models (Figs. 3.9, 3.10). Two versions of the ZK and FK models are shown with denitrification either included (ZK and FK) or omitted (ZK-ND and FK-ND) from the biogeochemical processes modeled. All hydrologic parameters were kept constant across the models. Biogeochemically, all models have the same initial chemical concentrations in the soil profile. Nitrification and adsorption parameters were kept constant across all models. For the zero- and first-order kinetic models, the mineralization and denitrification incubation data was used to calculate site-specific rate constants for each soil texture. In summary, these models were

designed to be identical, except for the ways that mineralization and denitrification are represented.

As expected, the NR model showed the lowest cumulative amount of  $\text{NO}_3^-$  leached from the soil profile in response to three 15 cm water applications. In contrast the ZK-ND and FK-ND models overestimated the cumulative amount of  $\text{NO}_3^-$  leached by a factor of 3.5 which mainly can be attributed to the fact that denitrification was omitted. When measured laboratory rates for denitrification (under ideal conditions) were applied in the model, the ZK models for both soil textures greatly overestimate the magnitude of denitrification in the model, resulting in a major underestimation of both cumulative  $\text{NO}_3^-$  leached, and residual  $\text{NO}_3^-$  in the soil profile following water applications. This is a result of the models' inability to characterize the environmental conditions at which the denitrification occurs.

The observed cumulative  $\text{NO}_3^-$  amount leached after three water applications in the fine sandy loam was  $15.0 \text{ kg ha}^{-1} \text{ NO}_3^- \text{-N}$ , and residual  $\text{NO}_3^- \text{-N}$  and  $\text{NH}_4^+ \text{-N}$  concentrations in the soil profiles were 4.4 (10cm) to 0.5 ppm (80cm) and 0.8 (10cm) to 0.2 ppm (80cm), respectively. The NR model not only underestimated the cumulative  $\text{NO}_3^-$  leached ( $9.7 \text{ kg ha}^{-1} \text{ NO}_3^- \text{-N}$ ) but also the  $\text{NO}_3^-$  concentrations in the residual soil profile ( $\text{NH}_4^+$  not considered) as indicated by the total flushing of  $\text{NO}_3^-$  (0 ppm  $\text{NO}_3^- \text{-N}$ ) in the residual soil profile. The ZK-ND model overestimates the observed cumulative  $\text{NO}_3^-$  leached with  $52.2 \text{ kg ha}^{-1} \text{ NO}_3^- \text{-N}$ . The ZK-ND model represents the residual  $\text{NO}_3^-$  profile accurately in trend and magnitude, ranging from 4.4 (10cm) to 0.9 ppm  $\text{NO}_3^- \text{-N}$  (80cm), while slightly underestimating the residual  $\text{NH}_4^+$  profile, estimating 0.5 (10cm) to 0.4 ppm (80cm)  $\text{NH}_4^+ \text{-N}$ . If denitrification is included in the ZK model, it significantly underestimates cumulative  $\text{NO}_3^-$  leached, estimating  $2.0 \text{ kg ha}^{-1} \text{ NO}_3^- \text{-N}$ , and contains no residual  $\text{NO}_3^-$  in the soil profile. The FK-ND model also overestimates the amount of

cumulative  $\text{NO}_3^-$  leached, with  $47.9 \text{ kg ha}^{-1} \text{ NO}_3\text{-N}$ . The residual profiles of the FK-ND model look similar to the ZK-ND model, with an accurate representation of the observed trend, ranging from 3.7 (10cm) to 1.1 ppm  $\text{NO}_3^-$ -N (80cm) and 0.3 (10cm) to 0.1 ppm  $\text{NH}_4^+$ -N (80cm). However, the FK-ND model is underestimating the residual  $\text{NH}_4^+$  profile, and the top 10cm of the  $\text{NO}_3^-$  profile. If denitrification is included in the FK model, we again see a significant underestimation of  $\text{NO}_3^-$  leaching ( $4.6 \text{ kg ha}^{-1} \text{ NO}_3^-$ -N) and the residual  $\text{NO}_3^-$  profile, 0.2 (10cm) to 0.1 ppm  $\text{NO}_3^-$ -N (80cm). The HP1 model accurately represents the observed cumulative  $\text{NO}_3^-$  leaching trend ( $15.4 \text{ kg ha}^{-1} \text{ NO}_3^-$ -N) (Fig. 3.7), but significantly underestimates both the residual  $\text{NO}_3^-$ -N and  $\text{NH}_4^+$ -N in the soil profile after Ag-MAR, 1.0 (10cm) to 0.2 ppm (80cm)  $\text{NO}_3^-$ -N and 0.4 (10cm) to 0.04 ppm (80cm)  $\text{NH}_4^+$ -N. The HP1-MIM model provides the best overall model fit, accurately representing the magnitude and timing of the cumulative  $\text{NO}_3^-$  leached ( $17.64 \text{ kg ha}^{-1} \text{ NO}_3^-$ -N) as well as the residual  $\text{NO}_3^-$ -N and  $\text{NH}_4^+$ -N concentrations in the soil profile following water applications, 3.9 (10cm) to 0.4 ppm (80cm)  $\text{NO}_3^-$ -N and 0.8(10cm) to 0.1 ppm (80cm)  $\text{NH}_4^+$ -N (Fig. 3.7).

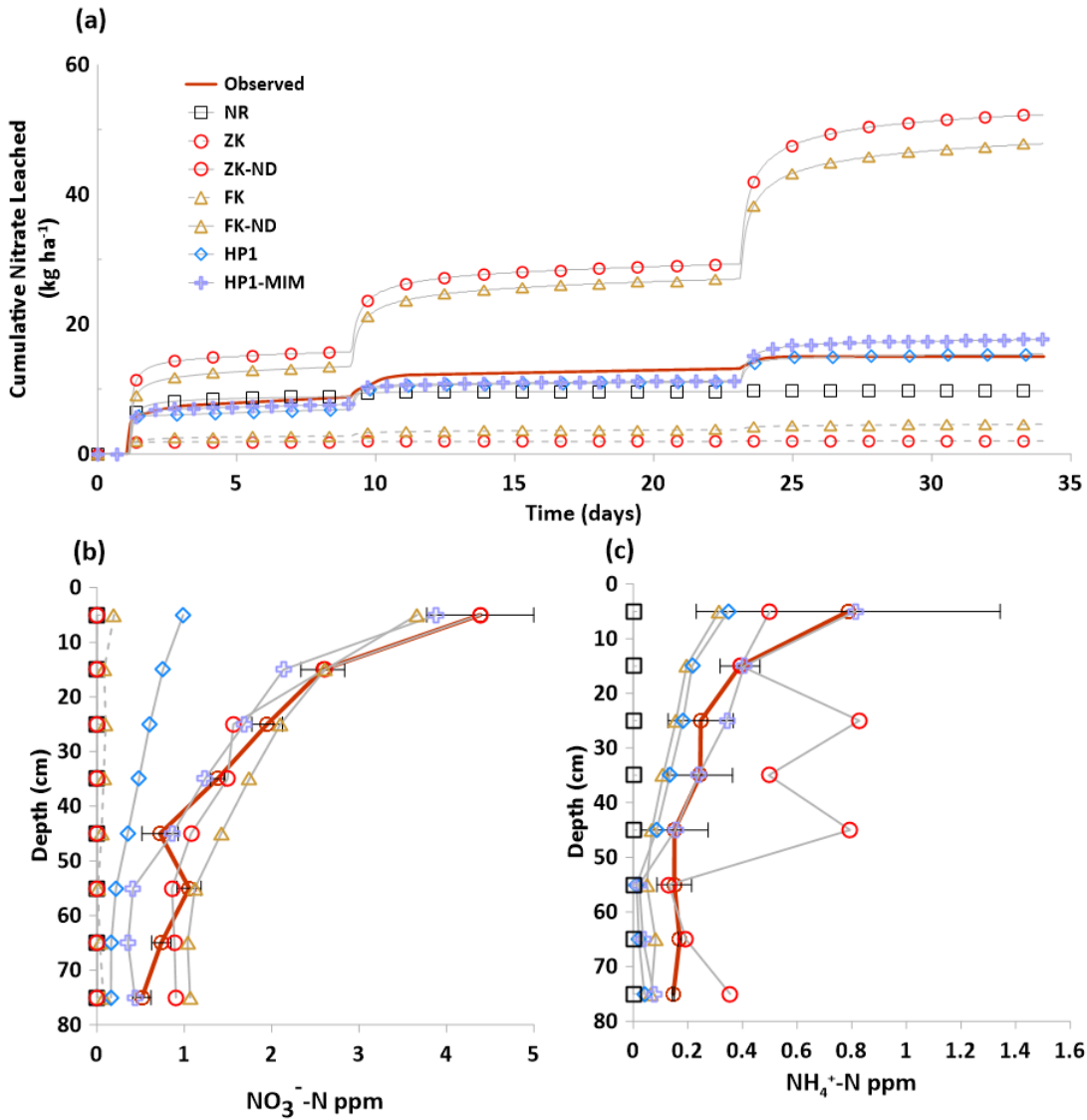


Figure 3.7: Comparison of selected N mass balance components simulated with the NR, ZK, FK, HP1, and HP1-MIM models for the fine sandy loam. (a) cumulative NO<sub>3</sub><sup>-</sup> leached at the bottom of model domain, (b) residual NO<sub>3</sub><sup>-</sup> in soil profile, (c) residual NH<sub>4</sub><sup>+</sup> in soil profile. -ND represents a model which does not incorporate denitrification in the biogeochemical processes.

In the sand the observed cumulative NO<sub>3</sub><sup>-</sup> amount leached after three water applications was 35.7 kg ha<sup>-1</sup> NO<sub>3</sub><sup>-</sup>-N, and residual NO<sub>3</sub><sup>-</sup>-N and NH<sub>4</sub><sup>+</sup>-N in the soil profiles were 4.2 (10cm) to 0.6 ppm (80cm) and 0.4 (10cm) to 0.2 ppm (80cm), respectively. Similar to the fine sandy loam, the NR model underestimates cumulative NO<sub>3</sub><sup>-</sup> leached (24.9 kg ha<sup>-1</sup> NO<sub>3</sub><sup>-</sup>-N), and

completely flushes the residual soil profile of  $\text{NO}_3^-$  (0-0.01 ppm  $\text{NO}_3^-$ -N). The ZK-ND model overestimates the cumulative  $\text{NO}_3^-$  leached ( $54.3 \text{ kg ha}^{-1} \text{ NO}_3^-$ -N), and overestimates the residual  $\text{NO}_3^-$  and  $\text{NH}_4^+$  soil profiles, 4.3 (10cm) to 1.3 ppm (80cm)  $\text{NO}_3^-$ -N and 1.1 (10cm) to 0.7 ppm (80cm)  $\text{NH}_4^+$ -N. When denitrification is included in the ZK model, we again see an underestimation of cumulative  $\text{NO}_3^-$  leached ( $26.8 \text{ kg ha}^{-1} \text{ NO}_3^-$ -N) and low concentrations of  $\text{NO}_3^-$  and  $\text{NH}_4^+$  in the soil profile, 1.3 (10cm) to 0 ppm  $\text{NO}_3^-$ -N (80cm) and 0.4 (10cm) to 0.04 ppm (80cm)  $\text{NH}_4^+$ -N. The FK model accurately represents the cumulative  $\text{NO}_3^-$  leached ( $35.7 \text{ kg ha}^{-1} \text{ NO}_3^-$ -N), overestimating the leaching during the first two water applications, and underestimating the leaching during the third. It underestimates the residual  $\text{NO}_3^-$  in the top 10 cm of the soil profile (1.6 ppm  $\text{NO}_3^-$ -N), and overestimates the 10 to 50 cm range, 2.0 (10cm) to 0.6 ppm (50cm)  $\text{NO}_3^-$ -N, while overestimating  $\text{NH}_4^+$ -N in the 0 to 20 cm range, 0.8 (0cm) to 0.4 ppm (20cm)  $\text{NH}_4^+$ -N. The HP1 model also accurately represents the cumulative  $\text{NO}_3^-$  leached ( $35.9 \text{ kg ha}^{-1} \text{ NO}_3^-$ -N). It underestimates the residual  $\text{NO}_3^-$  in the top 10 cm (1.5 ppm  $\text{NO}_3^-$ -N), but accurately represents the rest of the profile 1.0 (20cm) to 0.7 ppm  $\text{NO}_3^-$ -N (80cm). The residual  $\text{NH}_4^+$  profile shows some underestimation but is generally a good fit. The HP1-MIM model accurately represents the cumulative  $\text{NO}_3^-$  leaching ( $33.3 \text{ kg ha}^{-1} \text{ NO}_3^-$ -N). It slightly overestimates the residual  $\text{NO}_3^-$  in the soil profile 4.0 (10cm) to 1.3 ppm  $\text{NO}_3^-$ -N (80cm), but accurately represents the shape and directional trends of the residual soil profile  $\text{NO}_3^-$  observed after Ag-MAR water applications. The HP1-MIM model has a residual  $\text{NH}_4^+$  profile similar to the HP1 model, more accurately representing the 0 to 20 cm profile, but generally underestimating residual concentrations (Fig. 3.8).

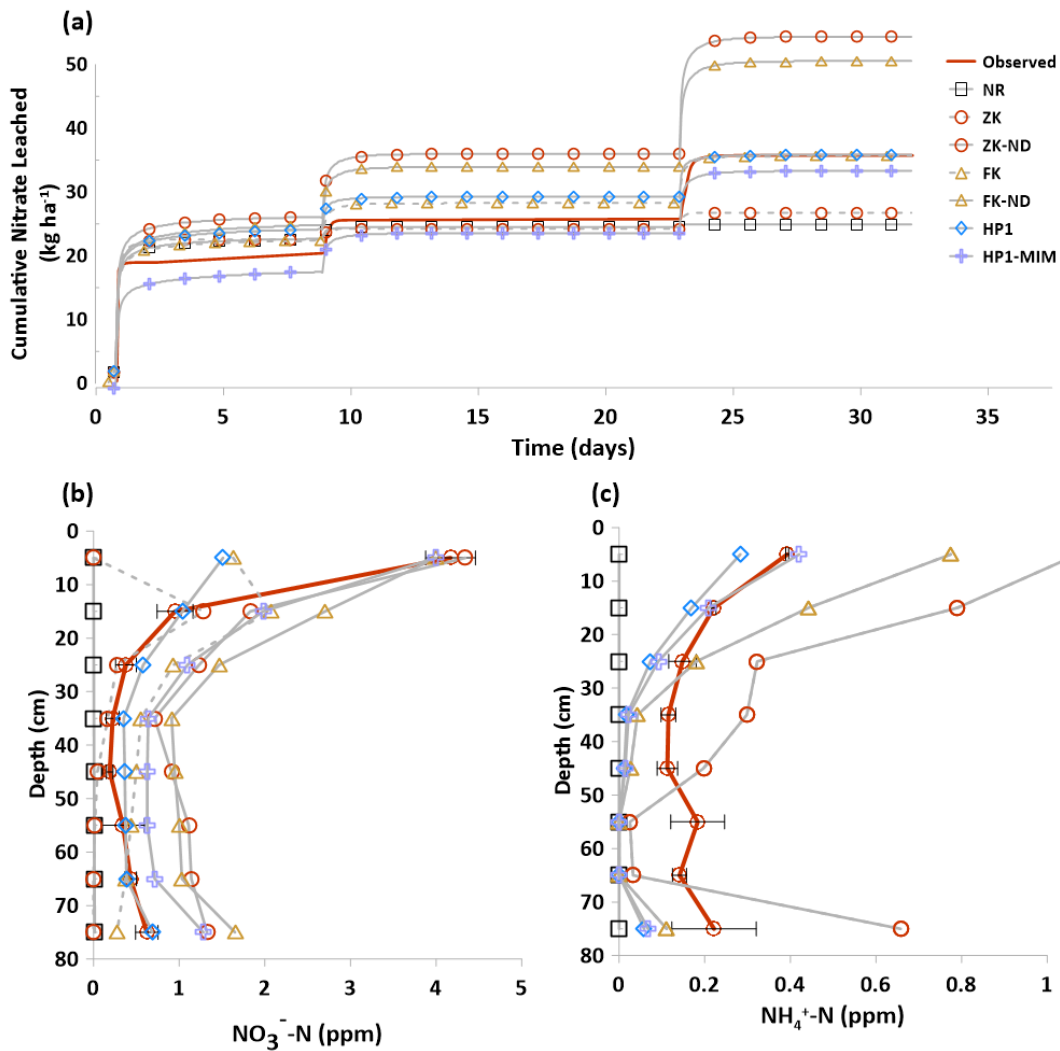


Figure 3.8: Comparison of selected N mass balance components simulated with the NR, ZK, FK, HP1, and HP1-MIM models for the sand. (a) cumulative NO<sub>3</sub><sup>-</sup> leached from the bottom of model domain, (b) residual NO<sub>3</sub><sup>-</sup> in soil profile, (c) residual NH<sub>4</sub><sup>+</sup> in soil profile. -ND represents a model which does not incorporate denitrification in the biogeochemical processes.

Comparing the total NO<sub>3</sub><sup>-</sup> mass balances between models indicates dominant biogeochemical processes and NO<sub>3</sub><sup>-</sup> leaching trends as a function of soil type and model scheme (Fig. 3.9 & 3.10). Due to the non-reactive nature of the NR model, the amount of NO<sub>3</sub><sup>-</sup> initially present (fine sandy loam: 10.0 kg ha<sup>-1</sup> N, sand: 25.8 kg ha<sup>-1</sup> N) in the model is approximately the amount of NO<sub>3</sub><sup>-</sup> leached from the model, across both soil types (fine sandy loam – NR: 9.7 kg ha<sup>-1</sup>

<sup>1</sup>, sand – NR: 24.9 kg ha<sup>-1</sup>). Generally, we see the ZK and FK models predict high amounts of mineralization (fine sandy loam – ZK: 66.5 kg ha<sup>-1</sup>, FK: 60.2 kg ha<sup>-1</sup> N, sand – ZK: 52.7 kg ha<sup>-1</sup>, FK: 47.1 kg ha<sup>-1</sup> N) and denitrification (fine sandy loam – ZK: 78.1 kg ha<sup>-1</sup>, FK: 64.2 kg ha<sup>-1</sup> N, sand – ZK: 49.7 kg ha<sup>-1</sup>, FK: 26.7 kg ha<sup>-1</sup> N). Across all soil types, the FK and ZK models predict higher amounts of mineralization and denitrification than the HP1 and HP1-MIM models. The FK-ND and ZK-ND models omit denitrification, resulting in the highest amounts of modeled NO<sub>3</sub><sup>-</sup> leaching, always resulting in an overestimation of the observed NO<sub>3</sub><sup>-</sup> leached. The HP1 and HP1-MIM models both accurately represent the NO<sub>3</sub><sup>-</sup> leaching trends observed, and estimate lower amounts of mineralization (fine sandy loam - HP1: 19.5 kg ha<sup>-1</sup>, HP1-MIM: 35.5 kg ha<sup>-1</sup> N, sand – HP1: 18.1 kg ha<sup>-1</sup>, HP1-MIM: 24.6 kg ha<sup>-1</sup>) and denitrification (fine sandy loam - HP1: 11.6 kg ha<sup>-1</sup>, HP1-MIM: 11.3 kg ha<sup>-1</sup>, sand – HP1: 1.4 kg ha<sup>-1</sup>, HP1-MIM: 0.7 kg ha<sup>-1</sup>) than the FK and ZK models. The HP1-MIM model estimates higher amounts of mineralization than the HP1 model, but similar amounts (within 1 kg ha<sup>-1</sup> N) of denitrification when compared in the same soil texture. When comparing across soil textures, the HP1 and HP1-MIM models show higher amounts of denitrification in the fine sandy loam than the sand soil, and slightly higher amounts of mineralization.

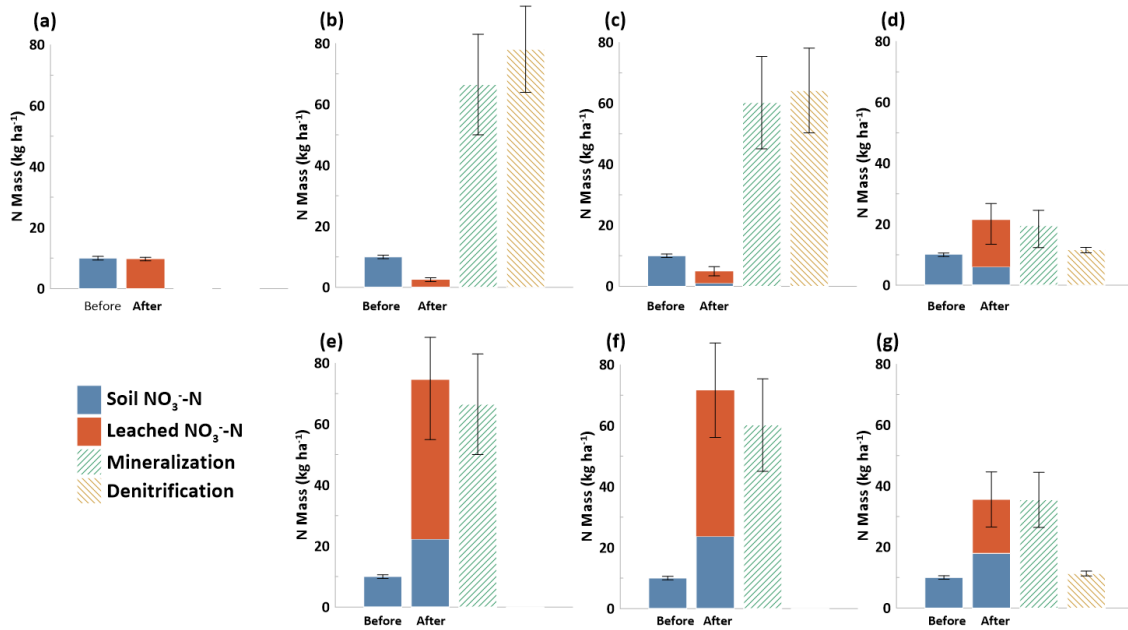


Figure 3.9: N mass balance for fine sandy loam with biogeochemical processes shown for models – (a) NR, (b) ZK, (c) FK, (d) HP1, (e) ZK-ND, (f) FK-ND, (g) HP1-MIM

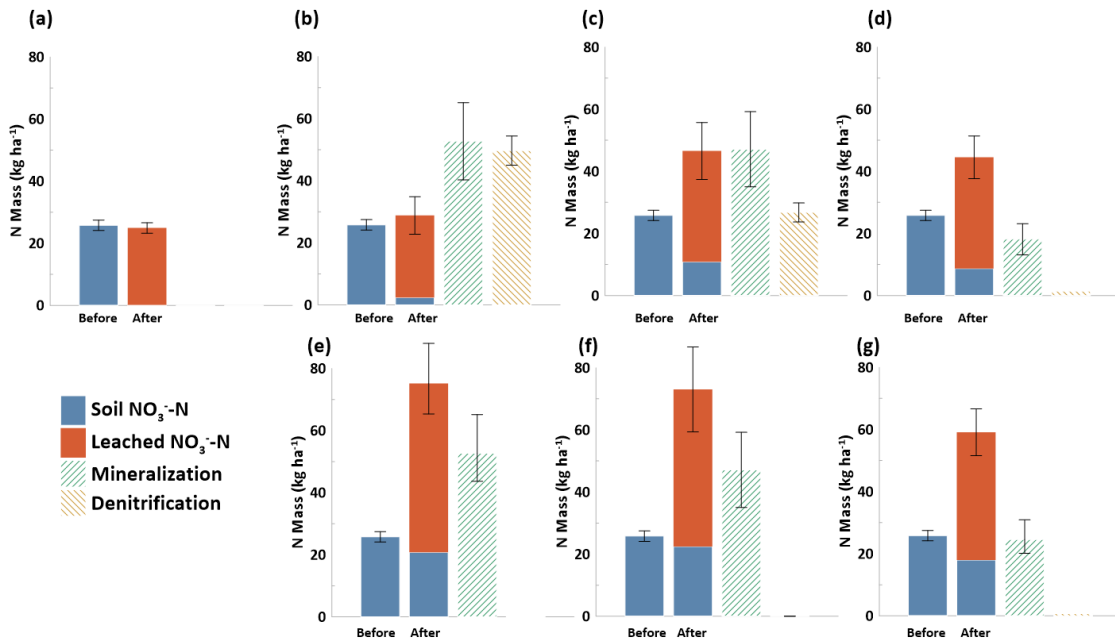


Figure 3.10: N mass balance for sand with biogeochemical processes shown for models – (a) NR, (b) ZK, (c) FK, (d) HP1, (e) ZK-ND, (f) FK-ND, (g) HP1-MIM.

## 3.5 DISCUSSION

### 3.5.1 Model Sensitivity Analysis and Calibration

A thorough exploration of model sensitivity is needed to be confident in the accuracy of model predictions and to ensure that model outcomes accurately reflect key processes of the system (van der Laan et al. 2014). In our application, accurate calibration of the hydraulic parameters is crucial to closely characterize the total amount of recharge passing through the soil profile and the associated timing and magnitude of the  $\text{NO}_3^-$  and  $\text{NH}_4^+$  breakthroughs. Thus, the sensitivity analysis presented above highlights distinct similarities and differences with regards to parameter importance and calibration when applying the HP1-MIM model across varying soil types.

On the hydrologic side of the HP1-MIM model,  $n$  is the most sensitive parameter, regardless of soil type. As an empirical parameter related to pore-size distribution,  $n$  impacts water retention characteristics, and has a strong control on soil drainage and the magnitude of cumulative discharge (Van Genuchten et al. 1985, Kool et al. 1985). The fine sandy loam shows a high sensitivity to  $K_s$ , as a result of longer transit times and a sensitivity to the breakthrough of water during water applications, compared to the sand which showed little sensitivity to its relatively high  $K_s$  value ( $23.6 \text{ cm hr}^{-1}$ ). The sand shows a high sensitivity to  $\theta_s$ , which impacts the size of the soil's pore volume and thus the magnitude of the observed cumulative discharge, rather than the breakthrough timing. Together these factors impact the fate and transport of  $\text{NO}_3^-$  in response to the total applied water for Ag-MAR, which has important implications for groundwater quality.

Accurate parameterization of the biogeochemical model parameters is also crucial to ensure  $\text{NO}_3^-$  leaching potential is adequately captured. While the hydraulic parameters have a

strong control on the initial timing and magnitude of solute transport during Ag-MAR water applications, the biogeochemical parameters impact the amount of  $\text{NO}_3^-$  available for leaching prior to each water application. Mineralization and subsequent nitrification can mobilize nitrogen previously held in organic-N pools, and can lead to leaching amounts greater than 100% of the  $\text{NO}_3^-$  measured in the soil profile prior to flooding (Murphy et al. 2021). For some systems it has been shown that denitrification may reduce the amount of  $\text{NO}_3^-$  available for leaching, decreasing the  $\text{NO}_3^-$  leaching potential of an Ag-MAR water application (Schmidt et al. 2011, Waterhouse et al. 2021). The biogeochemical sensitivity analysis presented in Section 4.2 highlights the importance of both the initial  $\text{NO}_3^-$  concentration in the soil, and the soil's mineralization rate on  $\text{NO}_3^-$  leaching potential under large irrigation events for both soil types. However, these two parameters differ in the timing of their impact on model uncertainty. The initial  $\text{NO}_3^-$  concentration in the soil profile affects the  $\text{NO}_3^-$  leaching potential of the first water application, but has little impact on subsequent water applications, as the majority (~70%, Murphy et al. 2021) of this  $\text{NO}_3^-$  pool is flushed during the first high-magnitude water application. Conversely, mineralization has little impact on the  $\text{NO}_3^-$  leaching potential during the first water application, but the model uncertainty compounds during each subsequent water application event, as mineralization is most influential during wet, low or no-flow periods between water applications (Fig. S3.3 & S3.4).

Denitrification potential varies strongly across soil types, showing a relatively high sensitivity for the fine sandy loam, and low sensitivity for the sand site. As we can see from the mass balance calculations (Fig. 3.10), the HP1 models for the sandy soil estimate low amounts of denitrification, as water content in the soil profile rarely stays above 70% PSF (percent pore space filled) for extended periods of time. The denitrification rates measured in the lab for the

fine sandy loam were higher than the sand (Supplementary Material, Table S3.1 & S3.2), and we see longer periods of time where the soil water content is sufficiently high for denitrification to occur (Fig. 3.9). The varying denitrification potential observed for both soils suggests unique opportunities for optimizing Ag-MAR best management practices, dependent on soil type. Some locations with high infiltration rates may be strong candidates for smaller but high-volume recharge sites, which helps the dilution of the initial spike in  $\text{NO}_3^-$  that occurs as water flushes residual  $\text{NO}_3^-$  from the vadose zone with subsequent water applications. Other locations with lower infiltration rates may be sites appropriate for water applications over large areas, where low  $K_{\text{sat}}$  soils and relatively quick buildup of low-oxygen conditions increase the denitrification potential thereby reducing the  $\text{NO}_3^-$  leaching risk. While the future development of Ag-MAR best management practices may require site-specific information, accurately modeling nitrogen cycling dynamics under varying soil textures can help inform basic soil and  $\text{NO}_3^-$  leaching suitability indices with regards to water quality concerns. To this end, applying the HP1-MIM model to test different soil textures, flooding scenarios and field data would provide greater understanding of biogeochemical dynamics occurring during Ag-MAR.

### **3.5.2 Conditionalization for Environmental Factors**

There are several key factors that are responsible for the HP1-MIM model to more accurately capture observed N cycling and loss processes under Ag-MAR compared to other modeling approaches. If we examine the  $\text{NO}_3^-$  mass balances (Fig. 3.9 & 3.10), we see an overestimation of mineralization in both the ZK and FK models, relative to the HP1 and HP1-MIM models. This overestimation is due to the inability of the ZK and FK models to account for the impact that environmental factors such as moisture and temperature play in biogeochemical

processes (Butterbach-Bahl & Dannenmann 2011, Munch & Velthof 2007, Paul et al. 2003, Miller & Geisseler 2018). In the HP1 models, the mineralization rate is dependent on a water content scaling factor, which ranges from 0.13 near residual water content to 0.92 at saturation. During Ag-MAR when water application has ceased there is little to no flow through the model domain but the soil is relatively moist (e.g. 0.1-0.2 VWC) for long periods of time. Under these conditions, mineralization is occurring, but the mineralization scaling factor is often only 0.28-0.64 of ideal laboratory-measured rates. Because the ZK and FK models cannot predict mineralization scaled to water content, they are often overestimating the mineralization rate during these soil drainage periods. We expect this effect to be magnified in field-scale modeling efforts. This is due to the fact that temperature, although incorporated in the HP1-model, does not play a large role in laboratory settings because laboratories often have a controlled temperature environment. Temperature, however, does play an important role for the conditionalization of mineralization at the field scale, especially when water applications of Ag-MAR are implemented during the winter months, when soil temperature may be sub-optimal (e.g. below 20°C) for most microbial processes. The mean soil temperature at our field sites at the time of soil collection was 13.8°C (Murphy et al. 2021), which would introduce a temperature scaling factor of 0.38 for mineralization (Miller & Geisseler 2018).

The opposite effect occurs with regards to the conditionalization of environmental factors controlling denitrification. If zero-order denitrification is included in the ZK model, with no additional proxy for oxic/anoxic conditions, a significant overestimation of denitrification occurs. This results all newly mineralized  $\text{NO}_3^-$  to be denitrified prior to leaching, leading to a subsequent underestimation of  $\text{NO}_3^-$  leaching during water applications. The incorporation of a proxy for the oxic/anoxic threshold (70% PSF) is a simplified assumption, but constrains

denitrification to time periods in the model that are more realistic for denitrification to occur (Linn & Doran 1984, Machefert & Dise 2004). Previous research has incorporated more complex representations of denitrification, specifically as a function of microbial activity. Ben-Moshe et al. (2021) for example represent denitrification with Monod kinetics, which accurately model DO consumption as a function of saturation and microbial activity. However, their model requires a large number of calibrated parameters (DF ~ 41), many of which cannot easily be independently measured in a lab or field setting. Future research should attempt to test the level of complexity needed in accurately capturing the oxic/anoxic threshold and other parameters controlling denitrification (e.g. micro-site denitrification) so that the number of model parameters can be reduced.

Several N cycle reactions were omitted from our study and HP1-MIM model for a variety of reasons. Nitrogen fixation, the process by which atmospheric N is converted to a plant available form, was not included based on the fact that no plants were grown during the period when water applications for Ag-MAR were conducted, and therefore microbial contributions were expected to be minimal (Graham & Vance 2000). Volatilization, the process by which urea is converted to  $\text{NH}_4^+$  and eventually lost as ammonia gas, was also not included, as the soils used in our field and column experiments did not contain recently applied fertilizers (i.e. fields were flooded about 6 months after last fertilizer application), or environmental conditions (hot, windy environment) conducive to volatilization (Hargrove 1988). Immobilization was not explicitly included, however, the mineralization incubation data used to calibrate the mineralization rates were net mineralization estimates, meaning immobilization was a process that factored into the rate estimates (Wade & Horwath 2016). We saw evidence of immobilization in several soil layers, where mineralization was relatively low, and in some cases even showed negative

mineralization rates indicating immobilization. Future model versions should strive to incorporate mineralization/immobilization dynamics, however, because they are often dependent on variables such as the C:N ratios of multiple organic matter pools and their associated lability such model versions would also have to include more detailed organic matter pools (Geisseler et al. 2019, Lazicki & Geisseler 2020).

### **3.5.3 Modeling Physical & Chemical Non-Equilibrium Dynamics**

As the results indicate, physical nonequilibrium processes were adopted into the HP1-MIM model in order to more accurately estimate both cumulative  $\text{NO}_3^-$  leached and the residual  $\text{NO}_3^-$  profile. The incorporation of a MIM soil phase allows for the characterization of physical processes which impact solute transport (Šimůnek & van Genuchten 2008). Dahan et al. (2009) identifies how MIM interactions can influence solute transport, where contaminants are stuck in “dead-end” pore spaces during an initial transport event (i.e. a water application), and how diffusion of solutes between MIM phases can cause a double-peaked breakthrough. The same general processes can impact the breakthrough of  $\text{NO}_3^-$  and the retention of residual  $\text{NO}_3^-$  in the soil profile. Prior to large water applications or Ag-MAR flooding, some fraction of  $\text{NO}_3^-$  may be contained within the immobile pore space, and is less susceptible to advection-dominated transport during the flooding (Liu et al. 2012, Ceriotti et al. 2019). Additionally, mineralization and other biogeochemical processes can occur within this immobile pore space, mainly transported into the mobile pore space through diffusion. HYDRUS-1D and other single porosity models don't allow for lateral flow or the development of preferential flow pathways based upon soil heterogeneity, as is possible in HYDRUS-2D/3D or other modeling approaches (Domínguez-Niño et al. 2020, Yetbarek et al. 2020). Since the magnitude of Ag-MAR flooding

is enough to fully saturate the profile, the majority of  $\text{NO}_3^-$  in the soil profile is transported at the beginning of the water application. This results in two inaccuracies in the HYDRUS-1D and HP1 models if mobile-immobile interactions were not explicitly enabled. First, it generally overestimates the amount of  $\text{NO}_3^-$  leached in a single water application event. Secondly, because the mobile  $\text{NO}_3^-$  is flushed to low concentrations in the soil profile after each water application, almost all of the  $\text{NO}_3^-$  measured in the residual profile at the end of the model run must have been mineralized in between the last water application and the end of the model run. Based upon mineralization rates, this is possible for the sand soil, as we see the HP1 model without MIM dynamics accurately capture the residual  $\text{NO}_3^-$  leaching trend in all soil layers (except for 0-10 cm). However, it is not accurately captured in the fine sandy loam, where the HP1 model without MIM dynamics significantly underestimates the  $\text{NO}_3^-$  in the residual soil profile. This indicates that while the uniform flow HP1 model may accurately represent some soil types, physical nonequilibrium must be considered in a complete model applied across multiple soil textures and water application or Ag-MAR scenarios. While the mobile-immobile characterization in this research is based around assumptions from solute breakthrough data, in the future it may be useful to characterize and calibrate the true porosity of the immobile pore space and implement a dual-porosity or dual-permeability model which accurately represents the hydrologic characteristics of mobile-immobile dynamics.

### **3.6 CONCLUSION**

Development of and comparison of an HP1-MIM model to non-reactive, zero-order and first-order kinetic HYDRUS transport models highlight the importance of conditionalizing physico-chemical processes and incorporating physical non-equilibrium dynamics when simulating  $\text{NO}_3^-$  transport in the vadose zone. Specifically, our results show that incorporating

moisture, temperature and oxic/anoxic thresholds when conditionalizing the magnitude and timing of mineralization and denitrification processes can result in increased model accuracy when simulating the effect of large irrigation events on  $\text{NO}_3^-$  leaching and N cycling. In addition, incorporation of mobile-immobile dynamics can improve model performance when simulating the residual  $\text{NO}_3^-$  present in the soil profile following water application events.

The results from a sensitivity analysis of model parameter influence on model outcomes increases our understanding of the relative importance of hydraulic and biogeochemical parameters and can be utilized to develop thorough field and laboratory experiments in the future. Lacking scaling factors for environmental conditions, the FK and ZK models predict higher rates of biogeochemical processes, compared to the HP1 and HP1-MIM models. The HP1 and HP1-MIM models accurately represent the  $\text{NO}_3^-$  leaching trends, estimating lower amounts of mineralization and denitrification than the FK and ZK models. The HP1-MIM model accurately constrains the biogeochemical processes dominating the nitrogen cycle under Ag-MAR across multiple soil types through the incorporation of important environmental conditions, and the collection of laboratory data providing soil-specific estimates of biogeochemical transformation rates. Going forward, additional N cycling processes may be incorporated into the model, including organic N pool ratios which impact mineralization/immobilization dynamics or organic pool lability and transport which impact biogeochemical rates and long-term soil health. Based on the model performance across soil textures, the HP1-MIM model is an appropriate tool to begin developing Ag-MAR best management practices and to examine how  $\text{NO}_3^-$  leaching may be minimized under large or Ag-MAR water application events.

### **Chapter 3 – A multi-scenario analysis examining the effect of flooding frequency and flooding magnitude on nitrate leaching under large water application events**

Nicholas P. Murphy<sup>1,\*</sup>, Helen E. Dahlke<sup>1</sup>

Affiliations: <sup>1</sup> Department of Land, Air and Water Resources, University of California, Davis, Davis, CA, 95616, USA. Corresponding author: [npmurphy@ucdavis.edu](mailto:npmurphy@ucdavis.edu)

#### Core Ideas:

- The multi-scenario analysis allows for the recommendation of site-specific best management practices to minimize nitrate leaching
- Differing soil textures exhibit different dominant biogeochemical processes
- The dilution effect may be leveraged to maximize groundwater recharge and decrease the potential for groundwater contamination

Abbreviations: Agricultural Managed Aquifer Recharge – Ag-MAR, best management practices – BMPs, groundwater sustainability plans – GSPs, groundwater sustainability agencies – GSAs,

## ABSTRACT

Best management practices with regards to  $\text{NO}_3^-$  leaching have been studied under traditional agricultural nutrient management and irrigation systems, but the management variables considered are often inapplicable to manage  $\text{NO}_3^-$  leaching under Ag-MAR, a practice where farm fields are flooded in the off-season for groundwater recharge. Using a previously developed HP1-MIM model and datasets from field experiments we evaluate the ability of the HP1-MIM model to simulate field-scale  $\text{NO}_3^-$  leaching and nitrogen (N) cycle dynamics under winter Ag-MAR. We observe higher contributions of newly mineralized inorganic-N to the total  $\text{NO}_3^-$  leached under a fine sandy loam soil (58 – 76%), compared to a sand soil (19 – 55%). The HP1-MIM model is able to satisfactorily simulate the residual  $\text{NO}_3^-$  in the soil profile following Ag-MAR and can estimate the mass of  $\text{NO}_3^-$  leached from the shallow vadose zone (100-cm) at both sites (fine sandy loam – 47 - 51  $\text{kg ha}^{-1} \text{NO}_3^-$ -N, sand – 42 - 98  $\text{kg ha}^{-1} \text{NO}_3^-$ -N). The calibrated HP1-MIM models were used to conduct a multi-scenario analysis, evaluating  $\text{NO}_3^-$  leaching and nitrogen cycling trends as a function of Ag-MAR management variables (flooding frequency, flooding magnitude) for varying soil textures (fine sandy loam, sand) and climate scenarios (dry year, wet year). This analysis shows that the fine sandy loam site has a high potential for denitrification, and may minimize  $\text{NO}_3^-$  leaching under high-magnitude, long-frequency water applications. The sand site has a low potential for denitrification and may minimize  $\text{NO}_3^-$  leaching by applying high-magnitude, short-frequency flooding applications. Both sites show significant potential for the dilution of  $\text{NO}_3^-$  in bulk recharge if flooding magnitude is increased >45 cm.

## 4.1 INTRODUCTION

Increased demand for water resources has led to the unsustainable use of groundwater resources in many regions worldwide (Kokinow et al. 2005). Continued unsustainable use of groundwater has resulted in undesirable effects, including the lowering of groundwater levels, the degradation of water quality, and land subsidence, to name a few (Zektser et al. 2005, Levy et al. 2021). In 2014, the Sustainable Groundwater Management Act was passed in California, requiring the development and implementation of groundwater sustainability plans (GSPs) within groundwater basins in order to prevent these undesirable effects, with the overarching goal of reaching sustainability by 2040. Over 120 groundwater basins have been ranked based upon the severity of their water resources issues, and Groundwater Sustainability Agencies (GSAs) have been established to manage them, responsible for implementing these GSPs. Agricultural Managed Aquifer Recharge (Ag-MAR) is a growing element of groundwater sustainability plans developed in many basins to offset groundwater pumping demands by flooding agricultural fields with excess surface water during wet years. Widespread implementation of Ag-MAR in California and other semi-arid regions is promising, since irrigation agriculture provides millions of hectares of viable land that can serve as spreading grounds for excess water (O'Geen et al. 2015). However, several logistical and scientific roadblocks (water rights, water conveyance infrastructure, crop flood tolerance, and more) stand in the way of widespread implementation. One of the largest concerns regarding widespread Ag-MAR implementation is the potential for groundwater contamination, specifically from legacy nitrate ( $\text{NO}_3^-$ ) stored in the vadose zone.

$\text{NO}_3^-$  leaching under agricultural fields is a widely researched topic, from both nutrient management and groundwater quality perspectives. At the regional scale, studies often estimate

$\text{NO}_3^-$  loading as a function of land use, using mass balance techniques, but neglect biogeochemical reactions, such as mineralization or denitrification (Ransom et al. 2018). At the field scale, research often focuses on the development of agricultural best management practices to reduce  $\text{NO}_3^-$  leaching often falls into two categories: the optimization of either nitrogen fertilization efficiency or irrigation efficiency.

Nitrogen fertilization efficiency aims to optimize the application timing, rate and method of fertilization prior to or during the cropping season (Gårdenäs et al. 2005, Hanson et al. 2006, Nyamangara et al. 2003). For example, Nyamangara et al. (2003) examined these dynamics on small farms in Zimbabwe, investigating the impact of manure versus mineral N fertilizer application rate and timing in a tropical sandy soil. This research study found that a combination of manure ( $12.5 \text{ Mg ha}^{-1}$ ) and mineral N (ammonium-nitrate -  $60 \text{ kg ha}^{-1}$ ) was the most beneficial combination for achieving satisfactory crop yields and minimizing N leaching losses, with the lowest N leaching occurring during sole manure treatments. Andraski et al. 2000 study the effects of cropping-manure systems and N application rates on  $\text{NO}_3^-$  leaching in corn fields in Wisconsin, identifying a direct relationship between  $\text{NO}_3^-$  leaching and the applying an excess of N, exceeding crop nutrient demands. In general, we see that a low fertilizer application efficiency results in higher amounts of  $\text{NO}_3^-$  leached in agricultural settings.

Irrigation efficiency examines the relationship between applied or pre-existing  $\text{NO}_3^-$  in the root zone, and the transport of  $\text{NO}_3^-$  out of the root zone due to irrigation events (Hergert et al. 1986, Mack et al. 2005, Vázquez et al. 2006). Mack et al. (2005), for example, examined  $\text{NO}_3^-$  leaching losses under a winter wheat-maize double cropping system in Beijing, China, comparing sprinkler and flood irrigation practices. They identified the irrigation regime as the main driver behind  $\text{NO}_3^-$  leaching losses, finding lower  $\text{NO}_3^-$  leaching under sprinkler irrigation

in comparison to conventional flood irrigation (5 kg ha<sup>-1</sup> NO<sub>3</sub><sup>-</sup>-N versus 25 kg ha<sup>-1</sup> NO<sub>3</sub><sup>-</sup>-N in the 1<sup>st</sup> year of study, 26 kg ha<sup>-1</sup> NO<sub>3</sub><sup>-</sup>-N versus 42 kg ha<sup>-1</sup> NO<sub>3</sub><sup>-</sup>-N in the 2<sup>nd</sup> year of study).

Best management practice (BMP) studies often optimize for both irrigation and fertilization efficiency, and their interactions (Ajdary et al. 2007, Gheysari et al. 2009, Diez et al. 2000, Phogat et al. 2014, Wen-Zhi et al. 2013). Unfortunately, research on the optimization of these variables cannot be directly translated into Ag-MAR best management practices, since the flooding of farm fields for groundwater recharge is preferably done outside the growing season on fallow fields or during crop dormancy, long after fertilization events have occurred. NO<sub>3</sub><sup>-</sup> leaching potential under Ag-MAR is therefore largely dependent on 1) the amount of legacy NO<sub>3</sub><sup>-</sup> in the shallow vadose zone, 2) the biogeochemical dynamics stimulated by the Ag-MAR flooding events, 3) the soil texture, and 4) the amount and frequency at which water is applied for recharge (Murphy et al. 2021, Murphy et al. In Prep). Many of the BMPs developed to increase fertilizer efficiency (split fertilizer applications, fertigation, timing of fertilization) may help reduce the amount of NO<sub>3</sub><sup>-</sup> leaching below the root zone during Ag-MAR (Diez et al. 2000), thus improving the initial viability of Ag-MAR at a site but will not be management variables that are implemented during an Ag-MAR flooding season. Best management practices related to irrigation efficiency often recommend decreasing the irrigation amount by applying water at a lower rate more frequently using sprinkler, drip or deficit irrigation methods that reduce recharge losses out of the root zone (Mack et al. 2005, Waddell et al. 2000). Using high efficiency irrigation methods for Ag-MAR would much reduce the amount of water that could potentially be recharged at a suitable site and therefore reduce beneficial outcomes for the groundwater system. Based on the existing body of NO<sub>3</sub><sup>-</sup> leaching studies, to our knowledge, there are no

research studies which employ a multi-scenario analysis to evaluate best management practices during Ag-MAR flooding that minimize  $\text{NO}_3^-$  leaching while maximizing groundwater recharge.

When considering best management practices that may impact the  $\text{NO}_3^-$  leaching potential during Ag-MAR, both physical and biogeochemical factors must be considered. Among the physical factors, best management practices may affect hydrologic processes including recharge rates, the timing and magnitude of solute transport, and physical non-equilibrium interactions such as mobile-immobile dynamics in the vadose zone. Biogeochemically, best management practices may affect environmental conditions such as moisture, temperature, dissolved oxygen, and redox conditions, which impact the timing and rates of important nitrogen cycling processes such as mineralization, denitrification and nitrification (Bremner et al. 1958, Cassman et al. 1980). Additionally, best management practices may be specific to the conditions of a particular Ag-MAR site. A sandy soil with high percolation rates may have different best management practices compared to a finer soil with relatively low infiltration. Additionally, a site with relatively high residual  $\text{NO}_3^-$  concentrations in the profile may require different best management practices than a site with low residual soil  $\text{NO}_3^-$  concentrations. As a result, this research acknowledges that some site-specific knowledge will be necessary to determine site-specific best management practices under Ag-MAR. This research aims to identify fundamental relationships between some of the major Ag-MAR management factors (i.e. flooding frequency, magnitude, duration, and timing) to determine their impact on nitrogen cycling processes and  $\text{NO}_3^-$  leaching under Ag-MAR.

In this study we specifically focus on two best management practices, which are easily varied under Ag-MAR, which are flooding frequency and flooding magnitude. Flooding frequency is the management of how often or at what time interval water is applied for recharge.

It has been shown to impact  $\text{NO}_3^-$  leaching potential, and the biogeochemical processes occurring under Ag-MAR (Murphy et al. 2021, Chapter 1). Specifically, shorter flooding frequencies between water applications have been shown to decrease the nitrogen mineralization potential occurring during wet, no-flow periods, resulting in less  $\text{NO}_3^-$  mineralized in the soil profile, and less  $\text{NO}_3^-$  available for leaching during subsequent flooding events (Murphy et al. 2021, Chapter 1). Flooding magnitude is the management strategy of how much water is applied during a single flooding event. It has the potential to initially increase  $\text{NO}_3^-$  leaching under Ag-MAR as a function of the first water application, as higher  $\text{NO}_3^-$  leaching amounts are often associated with higher irrigation inefficiency (i.e. higher amounts of water traveling through the soil profile) (Wang et al. 2010). However, the dilution effect has also been proposed as a possible Ag-MAR remediation strategy, whereby large water amounts are applied after the initial  $\text{NO}_3^-$  present in the soil profile has been flushed. This is hypothesized to cause a dilution in solute concentrations in the vadose zone and groundwater (Bachand et al. 2014). The relationship between flooding magnitude,  $\text{NO}_3^-$  leaching, biogeochemical processes, and the dilution effect is not yet thoroughly understood.

The focus of this research study builds on previous work which has evaluated the  $\text{NO}_3^-$  leaching potential under Ag-MAR using field and laboratory experiments, and developed a calibrated reactive transport model using a HYDRUS 1D dual-porosity, mobile-immobile zone model coupled to the USGS biogeochemical code PHREEQC (Murphy et al. 2021, Murphy et al. In Prep.). Using this model, hereby referred to as HP1-MIM model, we will perform a multi-scenario analysis examining the effect of flooding frequency, flooding magnitude, and their interactions, on  $\text{NO}_3^-$  leaching, dominant biogeochemical processes, and general implications for the viability of Ag-MAR on dedicated field sites, under varying soil textures and climate

scenarios. We hypothesize that the two soil textures examined (fine sandy loam and sand) will exhibit differing  $\text{NO}_3^-$  leaching trends in response to flooding frequency and flooding magnitude, resulting in distinct best management practices as a function of soil texture and residual soil  $\text{NO}_3^-$  content. We also hypothesize that differing climate scenarios will impact the rate of biogeochemical processes linked to soil profile saturation, such as mineralization and denitrification.

## **4.2 MATERIALS & METHODS**

### **4.2.1 Study Sites**

The multi-scenario analysis performed in this study, was modeled to evaluate water flow and reactive solute transport in the shallow vadose zone (100 cm) of two almond orchards in the Central Valley of California. During the 2015/16 winter field experiment, the fine sandy loam soil was flooded once a week with a total of 60 cm of water in four discrete flooding events of 15 cm of applied water each (Table 4.1). During the same winter, the sand soil was flooded with a total of 63 cm of water in three discrete flooding events of 15, 23 and 25 cm, respectively, spaced one to two weeks apart (Supplementary Information, Table S4.1).

The two sites have distinct soil textures, soil hydraulic properties and nitrogen cycling dynamics which are presented in detail in Murphy et al. (2021). One of the two sites is located south of Delhi, California, and is a rapidly draining sand (Delhi sand series, mixed, thermic, Typic Xeropsamments) with high infiltration rates ( $K_{\text{sat}} = 1.89 \text{ cm hr}^{-1}$ ). The second site is located southwest of Modesto, California, and is a moderately draining fine sandy loam derived from granitic alluvium (Dinuba series, coarse-loamy, mixed, active, thermic Typic Haploxeralfs) (Soil Series USDA). Soil cores (5 cm diameter) were collected at each site using a direct push drill method (DT-22 Geoprobe Systems, Salina, KS, USA) before and after Ag-MAR flooding

events, to a depth of 300 – 400 cm. Cores were analyzed for soil texture, pH, electrical conductivity, and soil chemistry, including nitrate-nitrogen ( $\text{NO}_3^-$ -N), ammonium-nitrogen ( $\text{NH}_4^+$ -N), total carbon (TC), and total nitrogen (TN). A detailed description of the experimental design, including field and laboratory datasets and methods, can be found in Murphy et al. (2021).

#### **4.2.2 Model Theory and Development**

The HP1-MIM model used in this study is a water flow and solute transport model comprised of HYDRUS-1D (Simunek et al. 1998) coupled to PHREEQC (Parkhurst et al. 1999). HYDRUS-1D calculates variably-saturated water flow in one dimension, while PHREEQC calculates relevant biogeochemical reactions, and their rates through time. Additionally, physical non-equilibrium dynamics are included in the form of a mobile-immobile (MIM) discretization. Previous research has developed calibrated HP1-MIM models for both the sand and fine sandy loam soils, using datasets collected through laboratory column experiments (Murphy et al. 2021). HYDRUS-1D simulates variably-saturated water flow through the soil profile by solving the 1D Richards Equation for vertical flow. PHREEQC simulates conditional, kinetic reactions including mineralization (the conversion of organic-N to  $\text{NH}_4^+$  through microbial decomposition), nitrification (the conversion of  $\text{NH}_4^+$  to  $\text{NO}_3^-$ ) and denitrification (conversion of  $\text{NO}_3^-$  to gaseous forms of N). Mineralization is represented as a first-order kinetic reaction, conditional to moisture content and temperature. Nitrification is represented as a first-order kinetic reaction, conditional to percent pore-space filled (%PSF), a proxy used to represent the oxic-anoxic boundary. Denitrification is represented as a zero-order kinetic reaction and is also conditional to %PSF. Biogeochemical parameters were either estimated using laboratory

incubation studies or calibrated during the model development. A detailed description of the model theory and development, model calibration, sensitivity analysis, and comparison to traditional  $\text{NO}_3^-$  leaching model schemes are presented in Murphy et al. In Prep (Chapter 2).

Table 4.1: Biogeochemical processes simulated with the HP1-MIM model and their conditionalization parameters.  $k_{\min}$  is the first order rate constant for mineralization,  $q$  is discharge,  $k_{\text{nit}}$  is the first order rate constant for nitrification,  $T$  is soil temperature,  $\omega$  is the mass transfer coefficient, and %PSF is the percent pore space filled with water.

Leaching	$f(q, [\text{NO}_3^-])$
Mobile Nitrification	$f(k_{\text{nit}}, [\text{NH}_4^+]_{\text{mob}}, \%PSF)$
Mobile Mineralization	$f(k_{\min}, [\text{Org-N}]_{\text{mob}}, \theta_{\text{mob}}, T)$
Immobile Nitrification	$f(k_{\text{nit}}, [\text{NH}_4^+]_{\text{imm}}, \%PSF)$
Immobile Mineralization	$f(k_{\min}, [\text{Org-N}]_{\text{imm}}, T)$
Denitrification	$f(k_{\text{denit}}, [\text{NO}_3^-], \%PSF)$
Mass transfer (mobile- immobile phase)	$f(\omega_{\text{mim}})$

### 4.2.3 Model Calibration and Validation

Because this study focuses on assessing field-scale best management practices, the hydrologic parameters of the HP1-MIM model were recalibrated using measured data from both Ag-MAR field sites, while biogeochemical parameters were calibrated with laboratory data from soil column experiments. Volumetric water content was measured with a GS-1 volumetric water content sensor (Decagon Inc.) every 10 min at 45 cm depth at both locations starting in December 2015, about 2-3 weeks prior to the recharge events. For both soil textures, the hydrologic calibration as obtained through the estimation of the van Genuchten parameters. The van Genuchten parameters were calibrated using volumetric water content data collected at the field sites at 45 cm depth.

In this study, we used the same biogeochemical parameters as Murphy et al. In Prep (Supplementary Information, Chapter 2, Tables S3.1 & S3.2). Nitrogen mineralization and denitrification kinetic rate parameters are based upon previous laboratory incubations, estimating kinetic rates under ideal conditions. Previous research has identified the importance of

environmental conditions in reactive N transport modeling (Murphy et al. In Prep (Chapter 2), Paul et al. 2003, Miller & Geissler 2018, Bateman & Baggs 2005). In the Murphy et al. In Prep (Chapter 2) study, which focused on simulating  $\text{NO}_3^-$  leaching and N cycling processes observed in controlled soil column experiments, experiments were conducted under constant environmental conditions (e.g. air temperature of  $23^\circ\text{C}$ ). In contrast, for the multi-scenario analysis conducted in this study, site-specific environmental data on soil temperature, precipitation, and soil moisture was incorporated in the HP1-MIM model to develop field realistic scaling factors for the conditionalization of biogeochemical processes.

All model runs simulated  $\text{NO}_3^-$  leaching and N cycling processes using observed precipitation and soil temperature data from energy balance stations near each field site. Hourly soil temperature and precipitation data were downloaded from the California Irrigation Management Information System (CIMIS) (CIMIS Station 71 & 206) for the time period of September – February, for both the 2015/16 and 2016/17 winter season. The 2015/16 winter, hereby referred to as ‘dry winter’, was historically dry, with a total precipitation at the field sites of 12.1 cm  $\text{H}_2\text{O}$  and 21.3 cm  $\text{H}_2\text{O}$  for the fine sandy loam and sand, respectively (Figure 4.1a & 4.2a). The average temperature during the 2015/16 winter season (Oct. – Feb.) was  $14.3^\circ\text{C}$  for the fine sandy loam and  $10.6^\circ\text{C}$  for the sand sites, respectively (Figure 4.1a & 4.2a). The 2016/17 winter season (Oct. – Feb.) was historically wet, hereby referred to a ‘wet winter’, with a total precipitation of 28.5 cm  $\text{H}_2\text{O}$  and 36.6 cm  $\text{H}_2\text{O}$ , for the fine sandy loam and sand sites, respectively (Figure 4.1b & 4.2b). The average air temperature during the 2016/17 winter was  $13.4^\circ\text{C}$  for the fine sandy loam, and  $12.7^\circ\text{C}$  for the sand site, respectively (Fig. 4.1b & 4.2b). The applied water across all model runs contains no  $\text{NO}_3^-$  in solution.

Biogeochemical model validation was performed using the RMSE (Willmott 1982) of simulated versus observed residual  $\text{NO}_3^-$  concentrations in the soil profile following the 2015/16 Ag-MAR flooding season.

#### **4.2.4 Multi-scenario Analysis**

A multi-scenario analysis was designed to evaluate the effect of Ag-MAR management variables (flooding frequency, flooding magnitude) on  $\text{NO}_3^-$  leaching potential and deep vadose zone recharge for the two soil textures (fine sandy loam, sand). The multi-scenario analysis contained two climate scenarios (dry winter, wet winter), 28 flooding frequency scenarios, and ten flooding magnitude scenarios. Flooding frequency, the time interval between water applications for Ag-MAR was varied between 1 and 28 days, increasing at 1-day increments. The ten flooding magnitude scenarios consisted of 5, 10, 15, 30, 45, 60, 75, 90, 105 and 120-cm water applications, in equivalent height of water applied within one flooding event. In all scenarios the number of flooding events was kept constant, consisting of four, equal-amount water applications that are spaced according to the flooding frequency set in a given scenario. The four flooding events directly mimic the flooding events that were tested at both field sites during the 2015/16 Ag-MAR season. In addition to the above listed scenarios, we also evaluated the interactions between flooding magnitude and flooding frequency at three separate intersections. Interactions were evaluated for all 28 flooding frequency scenarios at a flooding magnitude of 15 cm, 60 cm and 120 cm, and all flooding magnitude scenarios were evaluated at their intersection with the 7-day, 14-day and 21-day flooding frequencies.

Additionally, all multi-scenario modeling runs were run during a typical dry winter season (2015/16), and a typical wet winter season (2016/17). The total number of model runs across all combinations of flooding frequency, magnitude, soil texture, and climate scenarios

amounts to 456 unique scenarios, which allow a detailed evaluation of  $\text{NO}_3^-$  leaching potential and deep vadose zone recharge under varying Ag-MAR BMPs.

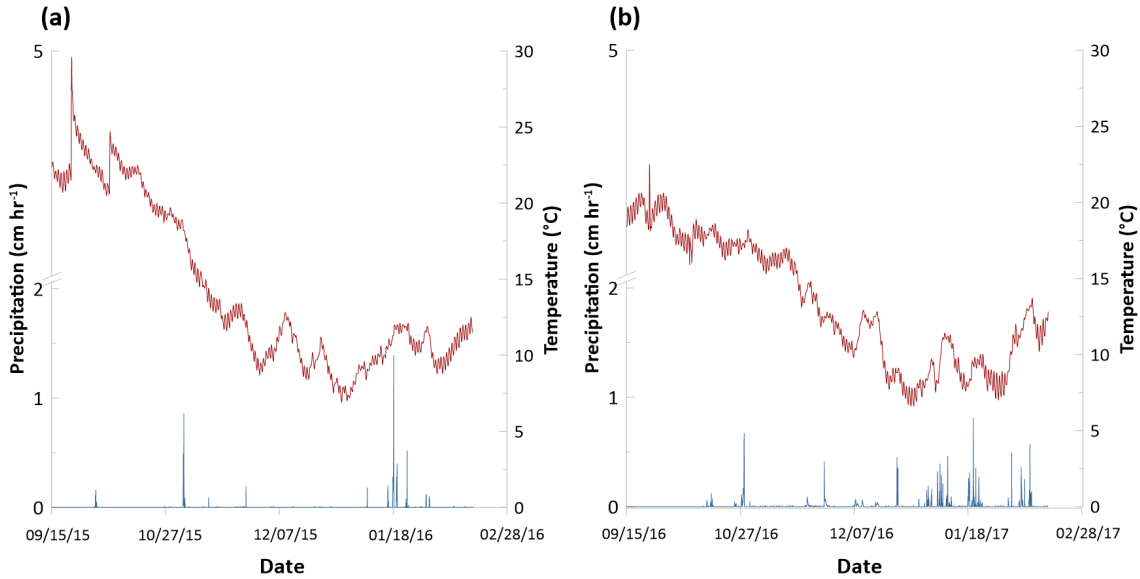


Figure 4.1: Soil temperature and precipitation data used for the fine sandy loam field site. Data used from CIMIS Station 71. (a) Soil temperature and precipitation from the 2015/16 season, representative of a dry winter. (b) Soil temperature and precipitation from the 2016/17 season, representative of a wet winter.

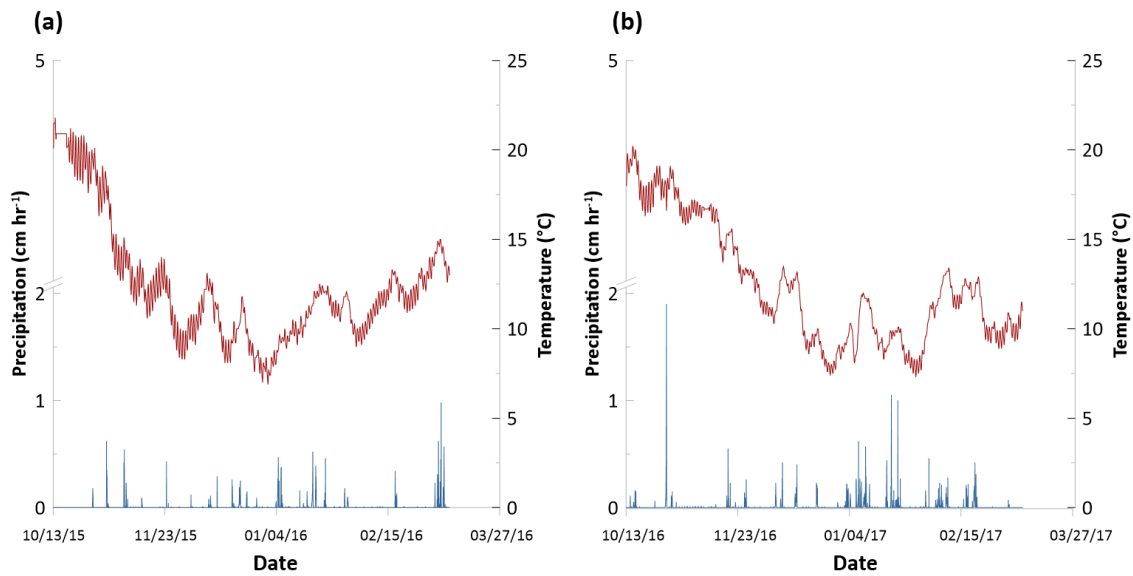


Figure 4.2: Soil temperature and precipitation data used for the sand field site. Data used from CIMIS Station 206. (a) Soil temperature and precipitation from the 2015/16 season, representative of a dry winter. (b) Soil temperature and precipitation from the 2016/17 season, representative of a wet winter.

## 4.3 RESULTS

### 4.3.1 Hydrologic Calibration

van-Genuchten parameters ( $\theta_r$ ,  $\theta_s$ ,  $\alpha$ ,  $n$ ,  $K_s$ ,  $l$ ) in the HP1-MIM models for the sand and fine sandy loam sites were calibrated using observed volumetric water content measured at 45 cm depths at both sites to minimize the residuals between the observed and simulated volumetric water content (Figure 4.3). As stated in the methods, using the same calibration technique presented in Murphy & Dahlke In Prep, field-observed volumetric water content measured at 45 cm depth was used to estimate van-Genuchten parameters for both the fine sandy loam and sand soils. Satisfactory model fits were found for both soils (sand -  $R^2 = 0.83$ , fine sandy loam -  $R^2 = 0.94$ ). RMSE for the simulated vs. observed volumetric water content in the fine sandy loam was  $0.010 \text{ cm}^3 \text{ cm}^{-3-1}$ , while the RMSE for the sand model was  $0.016 \text{ cm}^3 \text{ cm}^{-3-1}$ . Both models accurately capture the timing, magnitude, and recedence of all flooding events and significant precipitation events. Fig. 4.3 illustrates the HP1-MIM model hydrologic performance in comparison to observed field data during the Ag-MAR flooding season. The calibrated van Genuchten parameters used in the HP1-MIM for both soil textures are stated in Table 4.2. All other parameters were kept constant per the model development outlined in Murphy & Dahlke In Prep.

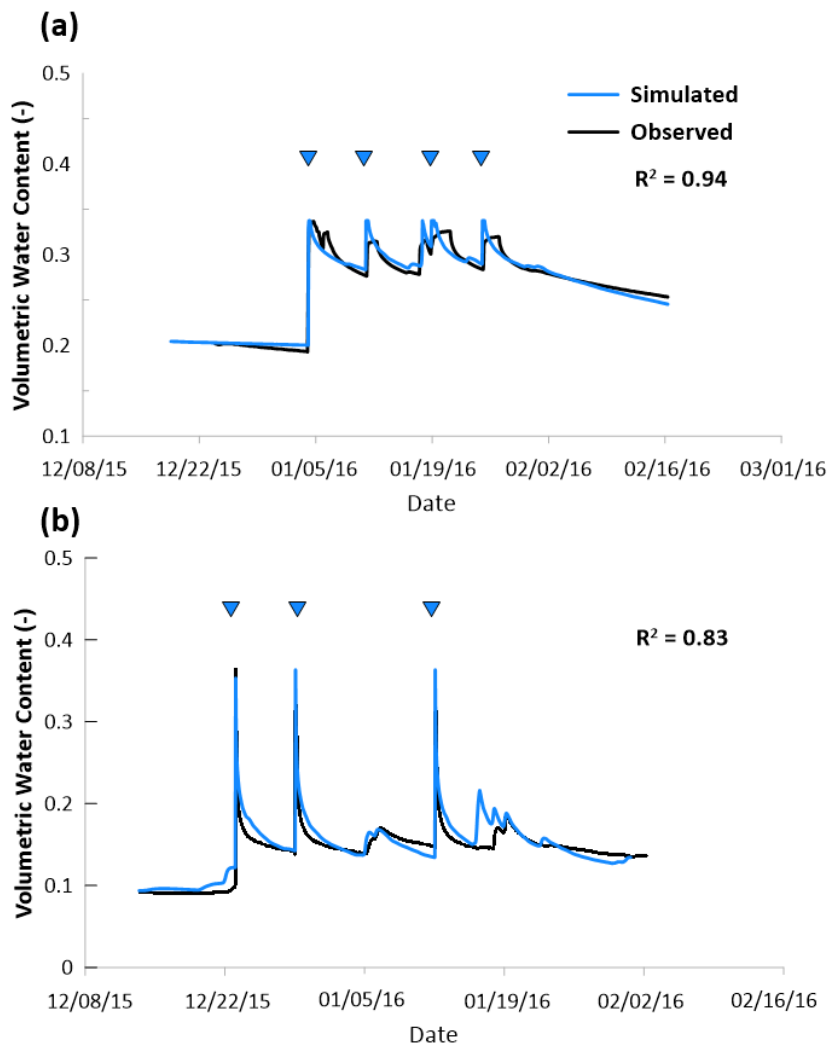


Figure 4.3: Hydrologic calibration metric for the (a) fine sandy loam and (b) sand soils. Comparison of modeled versus observed volumetric water content. Blue line represents modeled results. Black line represents observed field data. Blue triangles represent Ag-MAR flooding events.

Table 4.2: Calibrated van Genuchten parameters for the fine sandy loam and sand.

Layer	$\theta_r$ [-]	$\theta_s$ [-]	$\alpha$ [cm <sup>-1</sup> ]	n [-]	$K_s$ [cm hr <sup>-1</sup> ]	l [-]
<b>Fine sandy loam</b>						
<b>1 (0 - 80 cm)</b>	0.032	0.320	0.014	1.22	1.89	0.5
<b>Sand</b>						
<b>1 (0 - 80 cm)</b>	0.028	0.345	0.025	1.78	23.56	0.5

### 4.3.2 Biogeochemical Model Performance

As stated in the methods, calibration of biogeochemical parameters in the HP1-MIM models was not performed in this study and instead calibration parameters from the soil column modeling study conducted by Murphy & Dahlke In Prep. were used since these were derived for the same soils. However, despite using these calibration parameters, performance of the biogeochemical part of the HP1-MIM model was assessed by comparing the simulated residual soil NO<sub>3</sub><sup>-</sup> profile to the residual soil NO<sub>3</sub><sup>-</sup> measured in soil cores extracted from both field sites flooding for Ag-MAR was completed (Chapter 1, Fig. 2.1a). At the fine sandy loam site, model performance was evaluated for two soil cores collected in the flooded part of the orchard (Row 25, Tree 10: FSL-core 1 and Row 25, Tree 30: FSL-core 2, Chapter 1, Fig. 2.1a). The HP1-MIM model is capable of capturing the general magnitude and direction of the residual NO<sub>3</sub><sup>-</sup> trend in both cores. In both cores, we see an increase in residual NO<sub>3</sub><sup>-</sup> in the upper 10 cm following flooding events. While the model simulation underestimates this trend (6.42 ppm NO<sub>3</sub><sup>-</sup>-N predicted versus 8.4 ppm NO<sub>3</sub><sup>-</sup>-N observed at 10 cm (FSL-core 1), the direction and shape of the simulated 0-30 cm profile represents well the observed data. The 30-50 cm range shows a slight overestimation at 30 cm (3.4 ppm NO<sub>3</sub><sup>-</sup>-N simulated versus 1.1 ppm NO<sub>3</sub><sup>-</sup>-N observed, FSL-core 1), but is accurately modeled as depth increases to 50 cm. The 50-100 cm range is accurately

simulated in both cores, with the model uncertainty encompassing the observed residual  $\text{NO}_3^-$  load. The HP1-MIM model is able to accurately predict the general shape of the residual profile at the fine sandy loam site, even with varying shapes and trends in the initial concentrations of  $\text{NO}_3^-$  in the soil profile (i.e. 0.2 ppm  $\text{NO}_3^-$ -N initially at 10 cm depth in FSL-core 1, 4.1 ppm  $\text{NO}_3^-$ -N initially at 10 cm depth in FSL-core 2) (Figure 4.4). The RMSE of the HP1-MIM model for FSL-core 1 is 1.4 ppm  $\text{NO}_3^-$ -N, while the RMSE of the HP1-MIM model for FSL-core 2 is 1.7 ppm  $\text{NO}_3^-$ -N.

For the fine sandy loam, the HP1-MIM model predicts 47.5 kg ha<sup>-1</sup> (FSL-core 1) and 51.3 kg ha<sup>-1</sup> (FSL-core 2) of  $\text{NO}_3^-$ -N being leached from the model domain (100 cm profile), over the course of the simulated 2015/16 Ag-MAR flooding season (09/15/2015 - 02/16/2016). From the date when the before-flooding field cores were first collected (09/15/2015) to the date when the after-cores were collected following Ag-MAR flooding events (02/16/2016), an estimated 118.3 kg ha<sup>-1</sup> N of mineralization and 47.4 kg ha<sup>-1</sup> N of denitrification occurred in the soil profile of FSL-core 1, and an estimated 114.0 kg ha<sup>-1</sup> N of mineralization and 50.2 kg ha<sup>-1</sup> N of denitrification occurred in FSL-core 2. Of the  $\text{NO}_3^-$  that was leached below 100 cm depth during this period and as a result of Ag-MAR and recharge from precipitation events, the  $\text{NO}_3^-$  initially present in the soil profile at the start of the simulation period made up 23.8% and 41.6% for FSL-core 1 and FSL-core 2 locations, respectively, while 76.2% (FSL-core 1) and 58.4% (FSL-core 2) was newly mineralized  $\text{NO}_3^-$  following Ag-MAR flooding events or winter precipitation. The concentration of  $\text{NO}_3^-$  in the bulk recharge at the fine sandy loam field site were estimated to be 7.8 mg L<sup>-1</sup>  $\text{NO}_3^-$ -N (FSL-core 1) and 8.4 mg L<sup>-1</sup>  $\text{NO}_3^-$ -N (FSL-core 2), which is below the California maximum contaminant level (10 mg L<sup>-1</sup>  $\text{NO}_3^-$ -N) set by the California Environmental Protection Agency.

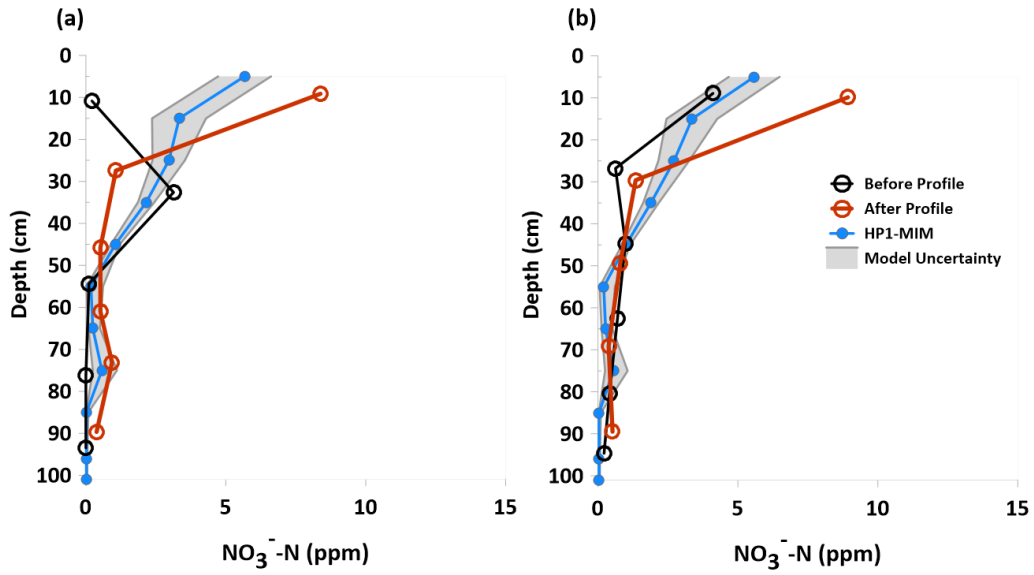


Figure 4.4: Model performance for the fine sandy loam field site. (a) residual  $\text{NO}_3^-$  in the soil profile at the end of model simulation for FSL-core 1, (b) residual  $\text{NO}_3^-$  in the soil profile at the end of model simulation for FSL-core 2. Model uncertainty represents the one standard deviation of error in the mineralization and denitrification kinetic rate parameters.

At the sand site three field cores were collected prior and after the Ag-MAR flooding (Row 9, Tree 2: S-core 1, Row 9, Tree 5: S-core 2, Row 9, Tree 8: S-core 3), (Chapter 1, Figure 2.1b), which were used for evaluating model performance for the sandy soil site. Generally, the HP1-MIM model accurately captures the magnitude and trend of the residual  $\text{NO}_3^-$  in the soil profile observed during the Ag-MAR flooding season across all three cores. Similar to the HP1-MIM model for the fine sandy loam, the sand site overestimates the amount of residual  $\text{NO}_3^-$  in the shallow soil profile (0-10 cm), with 2.1 ppm  $\text{NO}_3^-$ -N simulated and 0.8 ppm  $\text{NO}_3^-$ -N observed at 10 cm for S-core1. The rest of the soil profile is generally well simulated, with low  $\text{NO}_3^-$  concentrations in the residual profile post-flooding (<1 ppm  $\text{NO}_3^-$ -N). For all cores, the model simulations match the magnitude and trend of the observed residual soil data (Fig. 4.5). The

RMSE for the sand site was 0.6 ppm  $\text{NO}_3^-$ -N for S-core 1, 0.7 ppm  $\text{NO}_3^-$ -N for S-core 2, and 0.4 ppm  $\text{NO}_3^-$ -N for S-core 3.

The HP1-MIM model for the sand soil predicts 97.9 kg ha<sup>-1</sup>  $\text{NO}_3^-$ -N (S-core 1), 42.0 kg ha<sup>-1</sup>  $\text{NO}_3^-$ -N (S-core 2), and 61.2 kg ha<sup>-1</sup> of  $\text{NO}_3^-$ -N (S-core 3) being leached from the model domain (0-100 cm depth) over the course of the simulated 2015/16 Ag-MAR season (10/13/15 – 2/17/16). An estimated 35.9 kg ha<sup>-1</sup> N of mineralization and 0.7 kg ha<sup>-1</sup> N of denitrification occurred over the simulation period in each of the three cores. Of the  $\text{NO}_3^-$  that was leached below 100 cm depth towards the groundwater table, the initially present soil  $\text{NO}_3^-$  made up 80.6%, 45.2%, and 64.9% percent (S-core 1, S-core 2, S-core 3), while 19.4%, 54.8%, and 35.1% was newly mineralized following Ag-MAR flooding events or winter precipitation. The concentration of  $\text{NO}_3^-$  in the bulk recharge at the sand field site was estimated to be 12.7, 5.4, and 7.9 mg L<sup>-1</sup>  $\text{NO}_3^-$ -N at S-core 1, S-core 2, S-core 3, respectively, indicating that  $\text{NO}_3^-$ -N concentration in the bulk recharge transported through S-core 1 exceeded the California MCL, likely due to its high initial soil  $\text{NO}_3^-$  load (Fig. 4.5a).

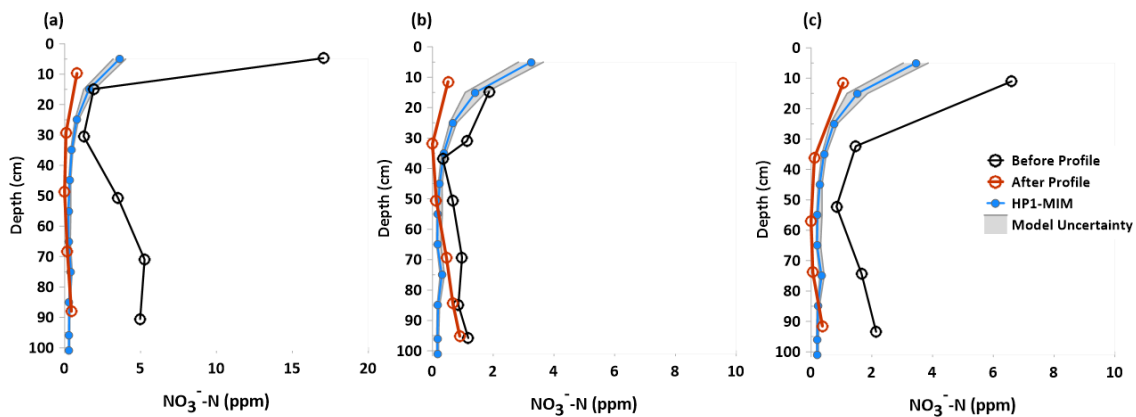


Figure 4.5: Model performance for the sand field site. (a) residual  $\text{NO}_3^-$  in the soil profile at the end of model simulation for core 1 (S-core1), (b) residual  $\text{NO}_3^-$  in the soil profile at the end of model simulation for core 2 (S-core2), (c) residual  $\text{NO}_3^-$  in the soil profile at the end of model simulation for core 3 (S-core 3). Model uncertainty represents one standard deviation error in mineralization and denitrification kinetic rate parameters.

### 4.3.3 Multi-Scenario Analysis

To determine Ag-MAR best management practices for different soil textures, results from the multi-scenario analysis were analyzed with respect to four model outputs: i)  $\text{NO}_3^-$  leached from the model domain (100 cm profile), ii) mass of residual  $\text{NO}_3^-$  in the soil profile, iii) mass of nitrogen mineralized, and iv) mass of nitrogen denitrified. These variables are examined for both the fine sandy loam and the sand soils, and evaluated under two climate scenarios consisting of a dry (2015/16) and wet (2016/17) winter season. For the initial conditions of the multi-scenario model runs, the initial concentration of  $\text{NO}_3^-$  in the soil profile was represented by FSL-core 1 for the fine sandy loam, and by S-core 2 for the sand. In the coming sub-sections we present the results from the interaction scenarios, starting with an analysis of all 28 flooding frequencies at a flooding magnitude of 15 cm (Fig. 4.6 & 4.7) for both the fine sandy loam and sand, followed by the analysis of a range of flooding magnitudes at their intersection with the 7-day flooding frequency (Fig. 4.8, 4.9). All other intersection scenarios of flooding frequencies at a flooding magnitude of 60 cm and 120 cm, and of all flooding magnitude scenarios at the intersection of the 14-day and 21-day flooding frequencies are presented in the Supplemental Information (Figures S4.2-4.9).

#### ***Flooding Frequency***

Variation in flooding frequency defines the time interval between the four, discrete water applications during the simulated Ag-MAR flooding season. The fine sandy loam shows differing trends regarding  $\text{NO}_3^-$  leaching potential, dependent on climate (Fig. 4.6). During the dry winter, we see a general decrease in  $\text{NO}_3^-$  leaching potential with increasing flooding frequency. The highest  $\text{NO}_3^-$  leaching potential is estimated to occur at a 1-day flooding

frequency, with an estimated  $56.9 \text{ kg ha}^{-1} \text{ NO}_3^- \text{-N}$  leached. As the flooding interval increases, we see  $\text{NO}_3^-$  leaching potential decrease, with the lowest  $\text{NO}_3^-$  leaching estimate at 24-day intervals ( $42.7 \text{ kg ha}^{-1} \text{ NO}_3^- \text{-N}$  leached) (Fig. 4.6a), followed by a slight increase in  $\text{NO}_3^-$  leached for the 25-day to 28-day frequency range. During the wet year, we see the amount of  $\text{NO}_3^-$  leached to plateau at around  $33\text{-}34 \text{ kg ha}^{-1} \text{ NO}_3^- \text{-N}$ , over the range of 4-day to 21-day flooding frequencies. As the flooding interval increases past 21 days, we see an increase in estimated  $\text{NO}_3^-$  leached, with a maximum of  $40.2 \text{ kg ha}^{-1} \text{ NO}_3^- \text{-N}$  at 26-day. The residual soil  $\text{NO}_3^-$  left behind in the soil after recharge events ranges between  $17 \text{ kg ha}^{-1} \text{ NO}_3^- \text{-N}$  and  $32 \text{ kg ha}^{-1} \text{ NO}_3^- \text{-N}$  for both climate scenarios (Fig. 4.6b). In the dry winter, the lowest residual  $\text{NO}_3^-$  is around  $17\text{-}18 \text{ kg ha}^{-1} \text{ NO}_3^- \text{-N}$  occurring in the 14 – 17-day and 26 – 28-day intervals. In the wet year, we see the lowest residual  $\text{NO}_3^-$  at flooding frequencies of around 6-11 day, before an increase is observed to  $\sim 30\text{-}32 \text{ kg ha}^{-1} \text{ NO}_3^- \text{-N}$  at 16-19-day frequencies. Unlike the other three variables, there is no clear directional trend or relationship between residual soil  $\text{NO}_3^-$  and flooding frequency (Fig. 4.6b). Mineralization increases with longer flooding frequencies (Fig. 4.6c). The lowest mineralization occurs for both climate scenarios at the highest flooding frequency (1-day), where  $109.5 \text{ kg ha}^{-1} \text{ N}$  and  $106.7 \text{ kg ha}^{-1} \text{ N}$  are mineralized for the dry and wet scenarios, respectively. The highest mineralization occurs for both climate scenarios at 28-day, when  $154.7 \text{ kg ha}^{-1} \text{ N}$  and  $144.9 \text{ kg ha}^{-1} \text{ N}$  are mineralized for the dry and wet scenarios, respectively (Fig. 4.6c). The amount of denitrification increases with longer flooding frequencies but exhibits a lesser degree of linearity compared to mineralization. In the dry year, there are several plateaus around 8-12-day, 16-18-day, and 25-28-day flooding frequencies, but we see an overall increase of denitrification with longer flooding frequencies, ranging from  $33.6 \text{ kg ha}^{-1} \text{ N}$  of denitrification at the 1-day frequency, to  $89.9 \text{ kg ha}^{-1}$  at the 26-day frequency. In the wet winter scenario, we see an increase

from 55.2 kg ha<sup>-1</sup> to 72.2 kg ha<sup>-1</sup> over the 1 to 19-day frequencies, and then a more rapid increase to 92.64 kg ha<sup>-1</sup> by the 28-day interval (Fig. 4.6d).

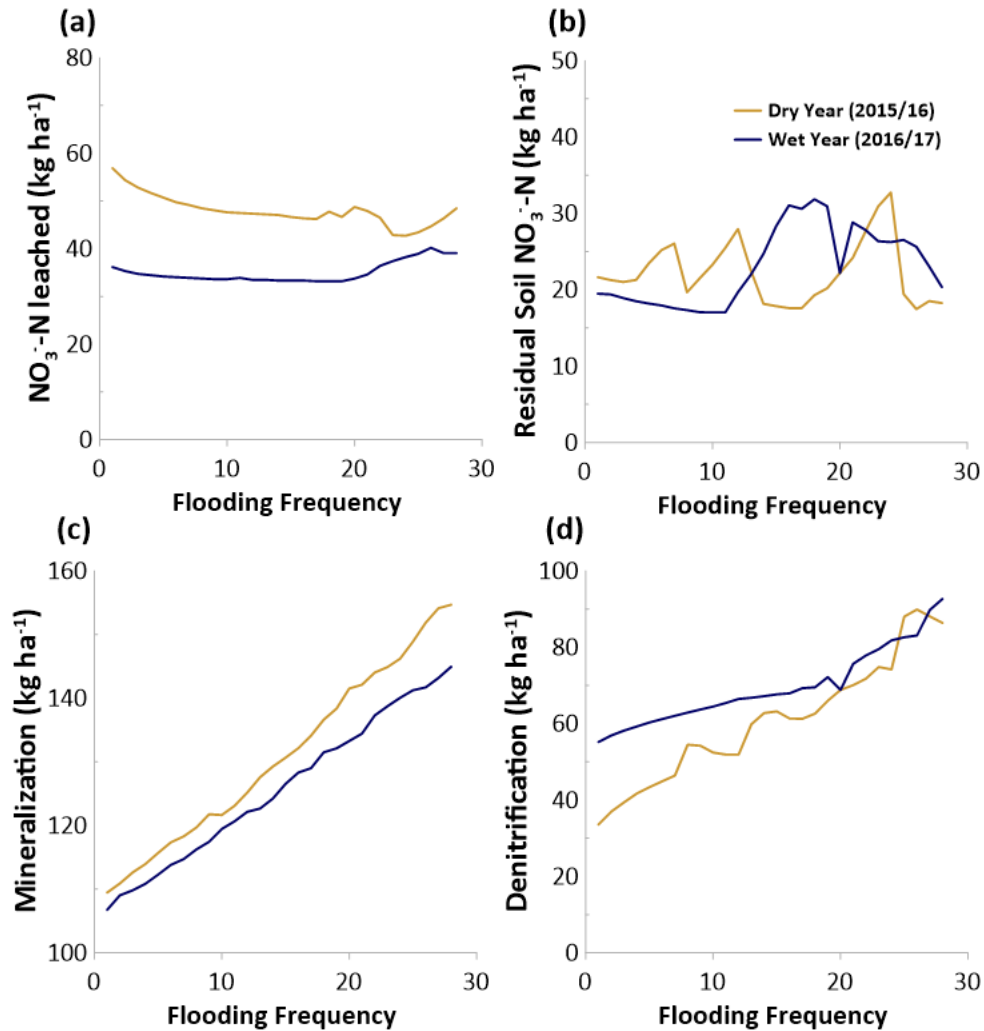


Figure 4.6: Flooding frequency scenarios for the fine sandy loam soil at 15 cm flooding magnitude. (a) sum of NO<sub>3</sub><sup>-</sup> leached from model domain during Ag-MAR flooding season, (b) residual NO<sub>3</sub><sup>-</sup> in soil profile following Ag-MAR flooding season, (c) amount of mineralization occurring during Ag-MAR flooding season, (d) amount of denitrification occurring during Ag-MAR flooding season, as a function of flooding frequency.

The impact of flooding frequency in the sand soil exhibits differing behavior in some of the model outputs in comparison to the fine sandy loam soil. The amount of NO<sub>3</sub><sup>-</sup> leached

increases with longer flooding frequencies, with the lowest amount observed at the 1-day frequency ( $83.8 \text{ kg ha}^{-1} \text{ NO}_3^- \text{-N}$  – dry winter,  $92.0 \text{ kg ha}^{-1} \text{ NO}_3^- \text{-N}$  - wet winter) and the highest  $\text{NO}_3^-$  amount leached at the 28-day frequency ( $112.5 \text{ kg ha}^{-1} \text{ NO}_3^- \text{-N}$  – dry winter,  $113.0 \text{ kg ha}^{-1} \text{ NO}_3^- \text{-N}$  – wet winter) (Figure 4.7a). The dry winter scenario shows a decrease in residual  $\text{NO}_3^-$  with longer flooding frequencies, with the highest residual  $\text{NO}_3^-$  ( $18.4 \text{ kg ha}^{-1} \text{ NO}_3^- \text{-N}$ ) observed at 1-day, decreasing to  $12.9 \text{ kg ha}^{-1} \text{ NO}_3^- \text{-N}$  at 22-day, before showing a slight increase to  $14.9 \text{ kg ha}^{-1}$  at 28-day. The wet winter scenario shows a residual soil  $\text{NO}_3^-$  mass of  $\sim 10\text{-}11 \text{ kg ha}^{-1} \text{ NO}_3^- \text{-N}$  from 1-day to 23-day frequencies, before increasing to  $14.2 \text{ kg ha}^{-1} \text{ NO}_3^- \text{-N}$  at 28-day (Fig. 4.7b). Mineralization increases with longer flooding frequencies for both the dry and wet scenarios, with the lowest mineralization occurring at 1-day ( $31.1 \text{ kg ha}^{-1} \text{ N}$  – dry winter,  $33.4 \text{ kg ha}^{-1} \text{ N}$  – wet winter), and the highest occurring at 28-day ( $52.7 \text{ kg ha}^{-1} \text{ N}$  – dry winter,  $52.91 \text{ kg ha}^{-1} \text{ N}$  – wet winter) (Fig. 4.7c). Denitrification is relatively constant across flooding frequencies, for both the dry and wet winter ( $0.67\text{--}0.91 \text{ kg ha}^{-1} \text{ N}$  – dry winter,  $1.2\text{--}1.3 \text{ kg ha}^{-1} \text{ N}$  - wet winter).

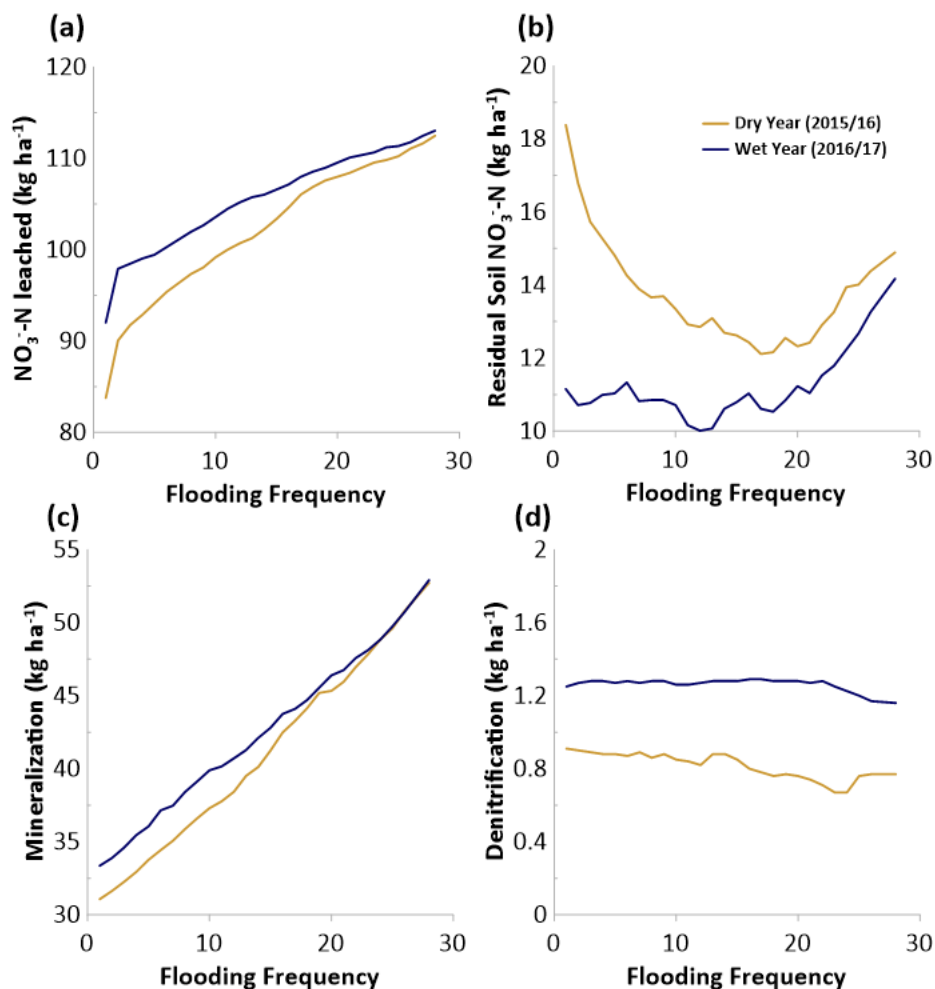


Figure 4.7: Flooding frequency scenarios for the sand soil at 15 cm flooding magnitude. (a) sum of  $\text{NO}_3^-$  leached from model domain during Ag-MAR flooding season, (b) residual  $\text{NO}_3^-$  in soil profile following Ag-MAR flooding season, (c) amount of mineralization occurring during Ag-MAR flooding season, (d) amount of denitrification occurring during Ag-MAR flooding season, as a function of flooding frequency.

### ***Flooding Magnitude***

Variation in flooding magnitude defines the amount of water applied during each of the four, discrete water applications simulated for the Ag-MAR flooding season. For both the fine sandy loam and sand soil, we generally see only a narrow range in conditions over which flooding magnitude drastically impacts the four model outputs of interest, before reaching a plateau, and showing low or no sensitivity to further increases in flooding magnitude.

For the fine sandy loam, we see an increase in  $\text{NO}_3^-$  leached as flooding magnitude increases from 5 cm to 45 cm (Fig. 4.8a), in both the dry and wet winter scenarios ( $14.9 \text{ kg ha}^{-1} \text{ NO}_3^- \text{-N}$  at 5 cm,  $62.3 \text{ kg ha}^{-1} \text{ NO}_3^- \text{-N}$  at 45 cm – dry winter,  $17.8 \text{ kg ha}^{-1} \text{ NO}_3^- \text{-N}$  at 5 cm,  $37.4 \text{ kg ha}^{-1} \text{ NO}_3^- \text{-N}$  at 45 cm, wet winter). With further increases in flooding magnitude above 45 cm, we see little change in  $\text{NO}_3^-$  leached (Fig. 4.8a). The residual soil  $\text{NO}_3^-$  decreases with increased flooding magnitude in the dry winter ( $30.3 \text{ kg ha}^{-1} \text{ NO}_3^- \text{-N}$  at 5 cm,  $22.3 \text{ kg ha}^{-1} \text{ NO}_3^- \text{-N}$  at 120 cm), but remains relatively constant at  $\sim 17 \text{ kg ha}^{-1} \text{ NO}_3^- \text{-N}$  across all flooding magnitudes in the wet winter scenario (Fig. 4.8b). Mineralization shows the same trend in both the dry and wet winter, decreasing slightly from 5 cm to 45 cm, before plateauing as flooding magnitude increases further ( $\sim 116 \text{ kg ha}^{-1} \text{ N}$  – dry winter,  $\sim 113 \text{ kg ha}^{-1} \text{ N}$  – wet winter) (Fig. 4.8c). Denitrification decreases in both the dry and wet winter. In the dry winter, we see a decrease from 5 cm to 45 cm ( $80.9 \text{ kg ha}^{-1} \text{ N}$  – 5cm,  $32.3 \text{ kg ha}^{-1} \text{ N}$  – 45 cm), before plateauing. The wet scenario shows the same directional trend, but plateaus at  $58.5 \text{ kg ha}^{-1} \text{ N}$  above 30 cm flooding magnitude (Fig. 4.8d).

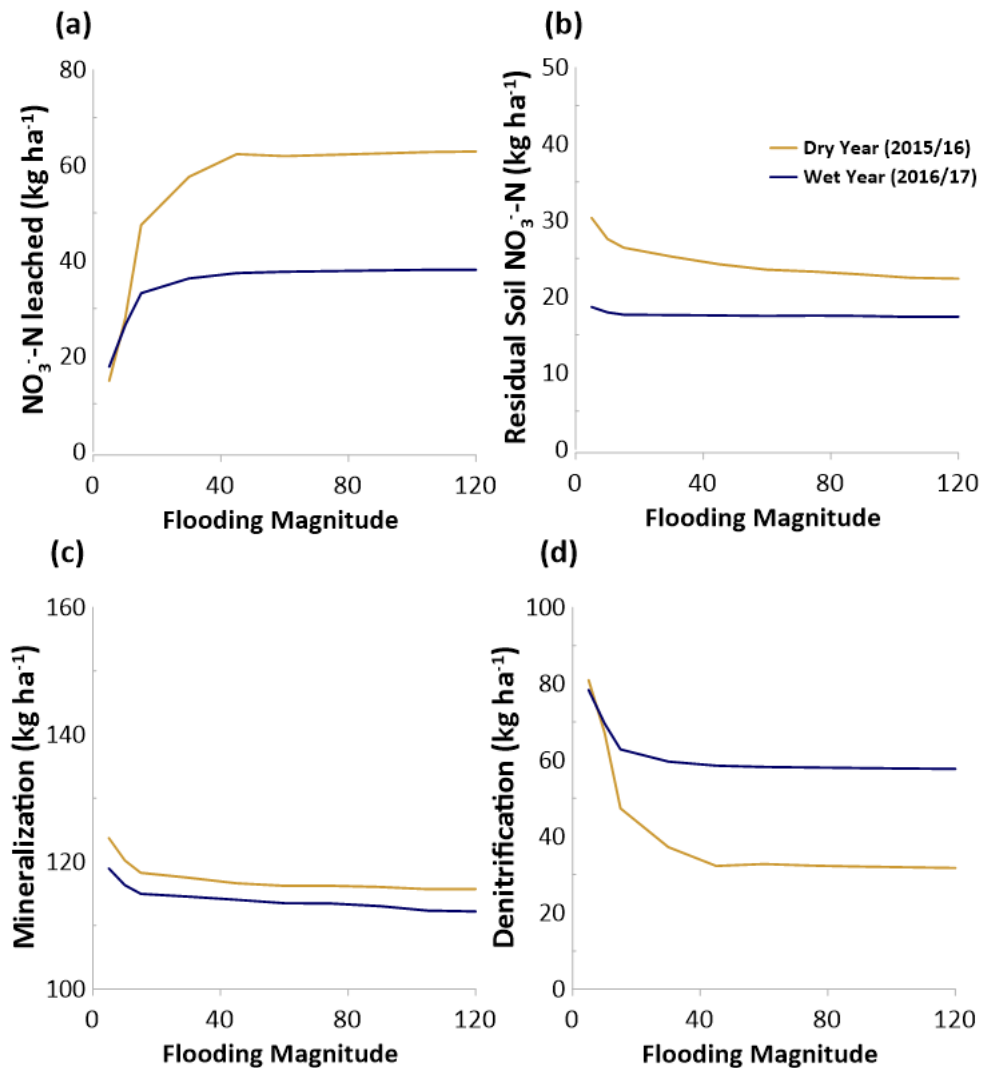


Figure 4.8: Flooding magnitude scenarios for the fine sandy loam soil at the 7-day flooding frequency. (a) sum of  $\text{NO}_3^-$  leached from model domain during Ag-MAR flooding season, (b) residual  $\text{NO}_3^-$  in soil profile following Ag-MAR flooding season, (c) amount of mineralization occurring during Ag-MAR flooding season, (d) amount of denitrification occurring during Ag-MAR flooding season, as a function of flooding magnitude.

For the sand soil, we see the same trend in  $\text{NO}_3^-$  leached during the dry scenario, as in the fine sandy loam, an increase in  $\text{NO}_3^-$  leached from 5 cm to 30-cm ( $97.2 \text{ kg ha}^{-1} \text{ NO}_3^- \text{-N} - 5 \text{ cm}$ ,  $103.64 \text{ kg ha}^{-1} \text{ NO}_3^- \text{-N} - 30\text{-cm}$ ). During the wet scenario, we see a plateau across all flooding magnitudes, around  $103 \text{ kg ha}^{-1} \text{ NO}_3^- \text{-N}$  (Fig. 4.9a). The residual soil  $\text{NO}_3^-$  in the dry scenario decreases from 5 cm to 30-cm, at which it plateaus ( $19.88 \text{ kg ha}^{-1} \text{ NO}_3^- \text{-N} - 5 \text{ cm}$ ,  $11.08 \text{ kg ha}^{-1}$

NO<sub>3</sub><sup>-</sup>-N 30-cm). The wet scenario shows a slight decrease from 14.76 kg ha<sup>-1</sup> NO<sub>3</sub><sup>-</sup>-N at 5 cm and then plateaus to ~12 kg ha<sup>-1</sup> NO<sub>3</sub><sup>-</sup>-N (Fig. 4.9b). Flooding magnitude has a low impact of mineralization, with a slight decrease from 5 cm to 120-cm across both the dry and wet scenarios (Dry: 41.8 kg ha<sup>-1</sup> N – 5 cm, 39.4 kg ha<sup>-1</sup> N– 120-cm, Wet: 43.1 kg ha<sup>-1</sup> N – 5 cm, 40.6 kg ha<sup>-1</sup> N – 120 cm) (Fig. 4.9c). Denitrification is relatively constant across climate scenarios, with low amounts occurring at 5 cm (0.4 kg ha<sup>-1</sup> N), increasing to and plateauing at 40-cm (~ 1.4 kg ha<sup>-1</sup> N) (Fig. 4.9d).

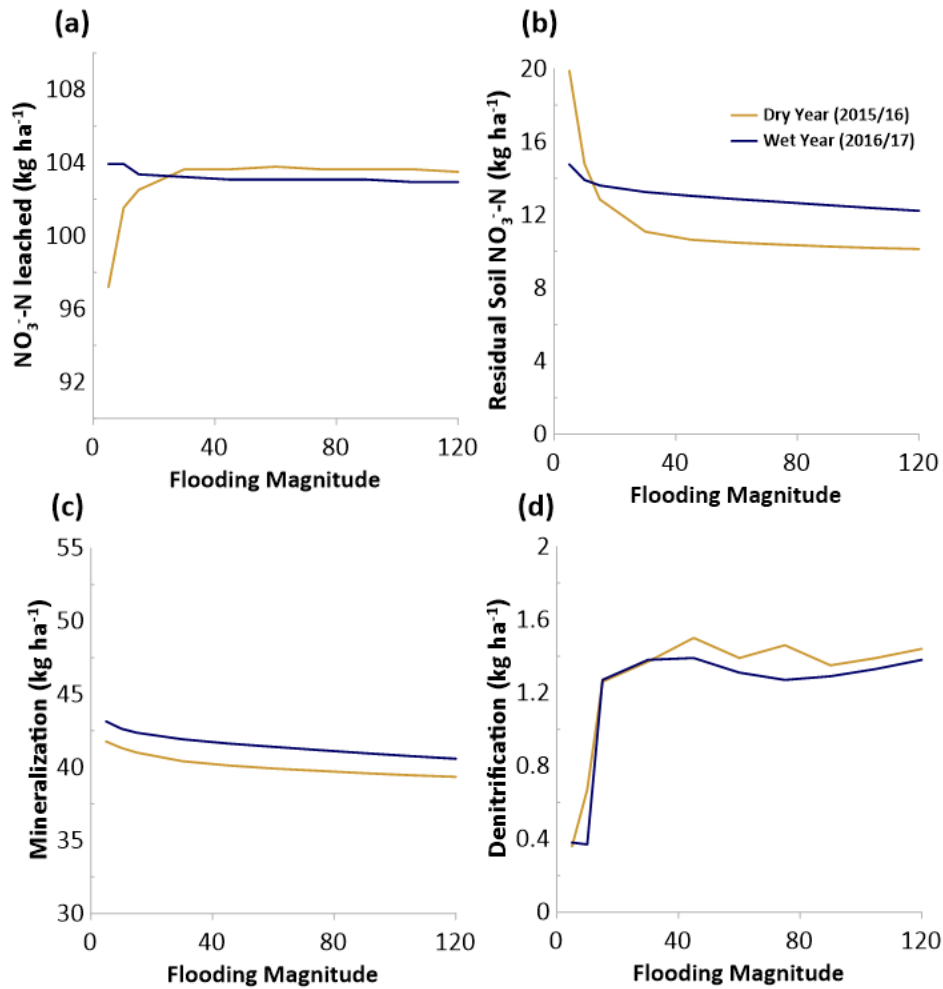


Figure 4.9: Flooding magnitude scenarios for the sand soil at the 7-day flooding frequency. (a) sum of  $\text{NO}_3^-$  leached from model domain during Ag-MAR flooding season, (b) residual  $\text{NO}_3^-$  in soil profile following Ag-MAR flooding season, (c) amount of mineralization occurring during Ag-MAR flooding season, (d) amount of denitrification occurring during Ag-MAR flooding season, as a function of flooding magnitude.

For both soil textures, we plotted  $\text{NO}_3^-$  concentration in the bulk recharge as a function of both flooding frequency and flooding magnitude (Fig. 4.10 & 4.11). These plots show distinct differences between the soil textures with respect to flooding frequency, and similarities with respect to flooding magnitude. For the fine sandy loam, the concentration of  $\text{NO}_3^-$  in the bulk recharge is highest at short flooding frequencies and decreases with longer flooding frequencies (Fig. 4.10). In contrast, the sand shows an increase in  $\text{NO}_3^-$  concentration in the bulk recharge with longer flooding frequencies, which is most pronounced at low flooding magnitudes. Both soil textures show a significant response to flooding magnitude, where increased flooding magnitude decreases the  $\text{NO}_3^-$  concentration in the bulk recharge, across both soil textures, and all flooding frequencies.

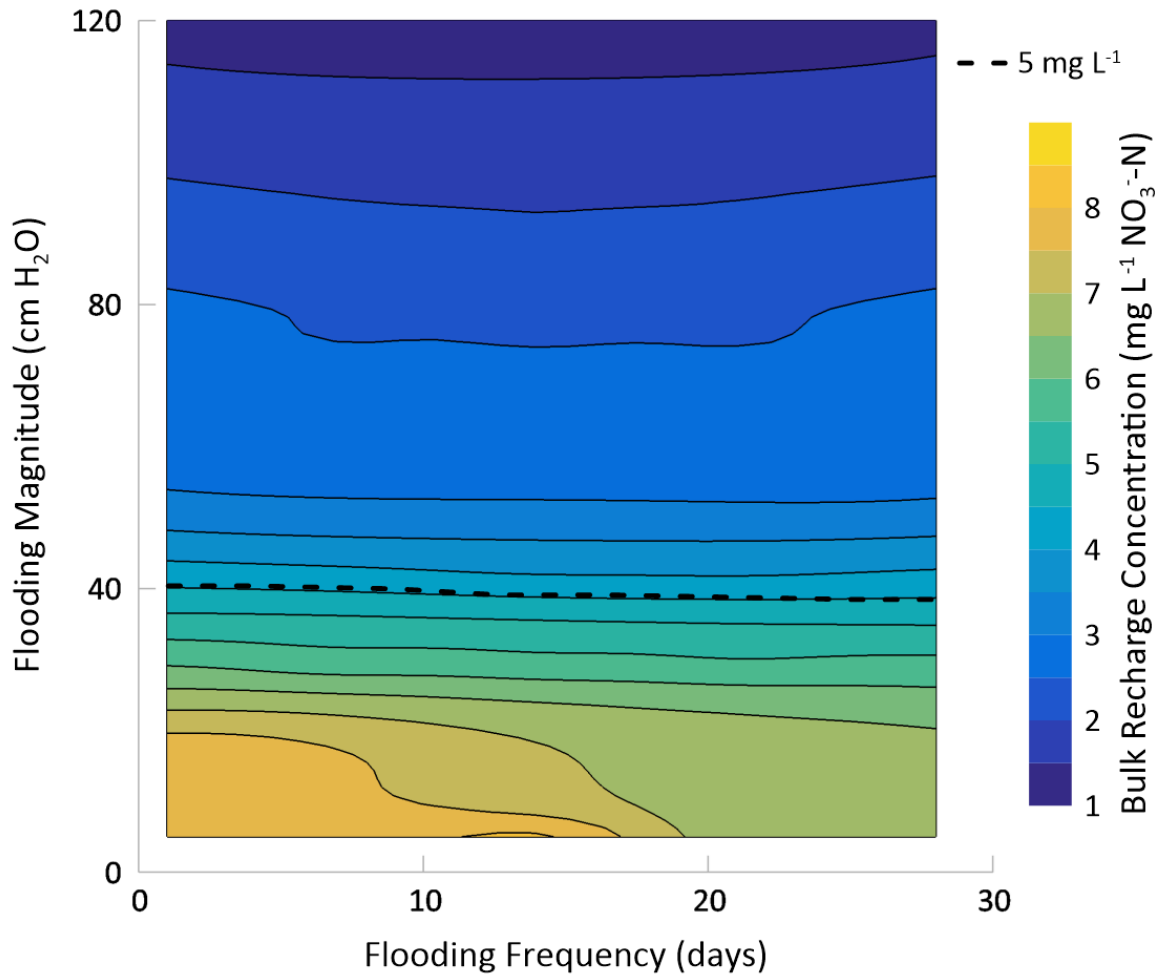


Figure 4.10: Concentration of  $\text{NO}_3^-$  in the bulk applied recharge during an Ag-MAR season, as a function of flooding magnitude and flooding frequency for the fine sandy loam site. The thick dashed line represents the  $5 \text{ mg L}^{-1} \text{NO}_3^- \text{-N}$  concentration threshold.

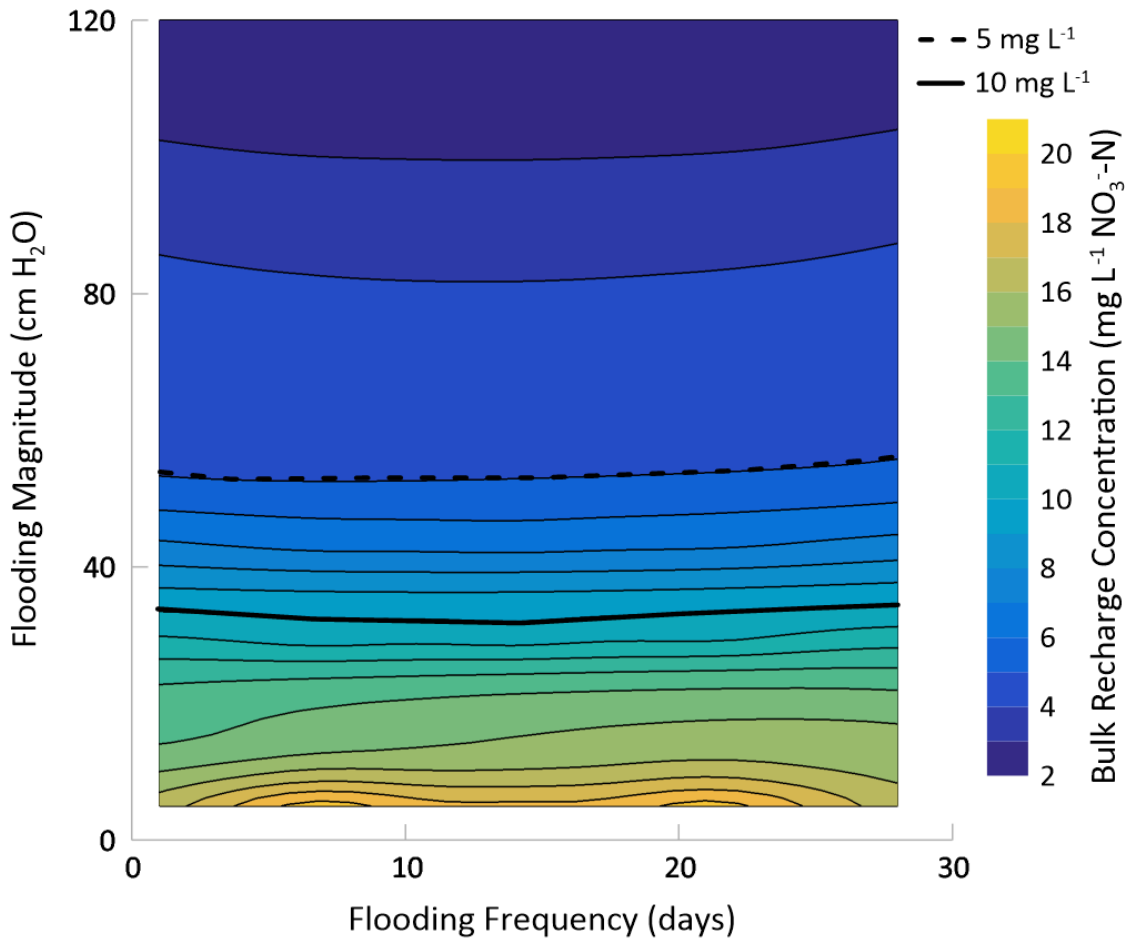


Figure 4.11: Concentration of  $\text{NO}_3^-$  in the bulk applied recharge during an Ag-MAR season, as a function of flooding magnitude and flooding frequency for the sand site. The thick black line represents the  $10 \text{ mg L}^{-1} \text{ NO}_3^- \text{-N}$  concentration threshold and the dashed line represents the  $5 \text{ mg L}^{-1} \text{ NO}_3^- \text{-N}$  concentration threshold.

## 4.4 DISCUSSION

### 4.4.1 Multi-Scenario Analysis – Ag-MAR Best Management Practices

This research demonstrates that varying Ag-MAR best management practices can have tangible influence on the amount of  $\text{NO}_3^-$  leached from the shallow vadose zone, the amount of  $\text{NO}_3^-$  remaining in the soil profile following an Ag-MAR season, and the dominant

biogeochemical processes occurring under Ag-MAR. Our results clearly highlight that different soil textures require soil-specific Ag-MAR best management practices and overall climate (e.g. wet vs dry) observed during the winter season. Specifically, our results show, that soil texture, residual soil  $\text{NO}_3^-$ , as well as N mineralization and denitrification potential of a site create complex interactions between physical and biogeochemical processes impacting the effect that Ag-MAR will have on  $\text{NO}_3^-$  leaching and N cycling processes post-flooding for groundwater recharge.

#### *4.4.1.1 Flooding Frequency*

The impact of flooding frequency on Ag-MAR, and the management implications it presents varies across soil texture. The fine sandy loam investigated in this study indicates that  $\text{NO}_3^-$  leaching and N cycling processes are dominated by the denitrification potential of the soil. Nitrogen mineralization occurs prior to, and in between Ag-MAR flooding events, but the lower saturated hydraulic conductivity of the soil profile creates a favorable environment for denitrification that removes a large portion of the  $\text{NO}_3^-$  from the soil profile before it can be leached below the shallow vadose zone (100 cm). The denitrification occurring over the course of the flooding season (33 – 86 kg ha<sup>-1</sup> N – dry winter, 55 – 145 kg ha<sup>-1</sup> N – wet winter) is within the wide range that previous literature review has observed for the yearly rates of denitrification in N fertilized, irrigated soils (49 – 239 kg ha<sup>-1</sup> N) (Barton et al. 1999). Favorable conditions for denitrification persisted at the fine sandy loam field site for extended periods after each water application for Ag-MAR. However, we observe that shorter flooding frequencies actually decrease the amount of denitrification occurring at a field site, by introducing rapid wetting events which transport  $\text{NO}_3^-$  out of the model domain before large amounts of denitrification can occur.

The sand investigated in this study indicates a system dominated by N mineralization, and rapid transport of  $\text{NO}_3^-$  below the shallow vadose zone with the applied recharge. Low amounts of denitrification are observed at the sand site, as the high saturated hydraulic conductivity of the soil profile results in the leaching of  $\text{NO}_3^-$  and a general substrate depletion prior to reaching conditions favorable to denitrification. This results in a positive feedback between  $\text{NO}_3^-$  leached and longer flooding frequencies, since longer flooding frequencies allow for more N mineralization to occur, which increases the amount nitrification between Ag-MAR events. The sharp increase in  $\text{NO}_3^-$  leaching observed between increases in short flooding frequencies (1 day – 2 day, Fig. 4.7a) is most likely related to the mobile-immobile interactions in the HP1-MIM model. During rapid water applications, the bulk of recharge is applied in a short period of events, which does not allow for large amounts of diffusion to occur between the mobile-immobile phases of the domain, which decreases the  $\text{NO}_3^-$  leaching potential. Under longer flooding frequencies ( $> 2$  days), there is sufficient time between flooding events for diffusion to occur, and the  $\text{NO}_3^-$  leaching potential is less driven by physical nonequilibrium transport dynamics, and more by the potential for biogeochemical processes such as mineralization.

#### *4.4.1.2 Flooding Magnitude*

Our results indicate that flooding magnitude mainly influences  $\text{NO}_3^-$  leaching and N cycling processes in the low value range, when small amounts of water are applied, irrespective of soil texture or flooding frequency. In the fine sandy loam, we see this pattern occur across all four model outputs we investigated ( $\text{NO}_3^-$  leached, residual soil  $\text{NO}_3^-$ , mineralization and denitrification), with the highest rate of change occurring during the shift from 5 cm to 15 cm of

water applied and plateauing at approximately 45 cm and above in all cases. As the amount of water applied per flooding event is increased from 5 cm to 45 cm, we see an increase of more than 40 kg ha<sup>-1</sup> of NO<sub>3</sub><sup>-</sup> leached. This is clearly indicating a transport-based mechanism, dependent on whether the flooding magnitude is high enough to promote complete flushing of residual NO<sub>3</sub><sup>-</sup> from the soil profile, or if residual NO<sub>3</sub><sup>-</sup> is still present post-flooding, to be denitrified during the time periods between water applications. This mechanism is further supported by the relationship between flooding magnitude and denitrification, where the highest amounts of denitrification occurred at 5 cm and 10 cm flooding magnitudes, before plateauing at 45 cm. Mineralization shows a relatively weak response to flooding magnitude. The slight changes in mineralization observed (Fig. 4.8 & 4.9) are mainly a function of increased DON transport deeper into the soil profile under higher flooding magnitudes. This is because mineralization rates are highest in the top 10 cm of the soil profile (Murphy et al 2021), hence, with transport of organic substrates deeper into the model domain with increasing flooding magnitude, we see decreased rates of N mineralization as a function of declining substrate availability.

In the sand, we see similar directional trends as observed in the fine sandy loam, with a few notable exceptions. The constant plateau of NO<sub>3</sub><sup>-</sup> leached during the wet year (~103 kg ha<sup>-1</sup> NO<sub>3</sub><sup>-</sup>-N, Fig. 4.9a), indicates a relative insensitivity to flooding magnitude. The amount of denitrification occurring in the sand shows an opposite directional trend to the fine sandy loam, increasing slightly over the 5 cm to 45 cm interval. However, the absolute increase is small compared to the fine sandy loam (1 kg ha<sup>-1</sup> N – sand) vs. >20 kg ha<sup>-1</sup> N – fine sandy loam), that it is effectively negligible, due to the negligible role denitrification plays at the sand site.

Across both sites, we see the same threshold behavior, with the majority of output variation occurring between 5 cm and 30 or 45 cm of water applied. Model outputs of interest tend to plateau after flooding magnitude exceeds 45 cm. This behavior indicates a relative insensitivity of  $\text{NO}_3^-$  leaching and N cycling to flooding magnitudes greater than 45 cm. This highlights the viability of implementing higher magnitude flooding events (permitting crop flood tolerance, water availability, water conveyance and application capacity, and other non-water quality related roadblocks) in order to increase the dilution effect of an Ag-MAR site, decreasing the  $\text{NO}_3^-$  leaching potential.

#### *4.4.1.3 Climate*

Our results show that a wet or dry climate (i.e. high or low soil moisture) can influence and shift the amount of  $\text{NO}_3^-$  leaching and N cycling that occurs prior and after an Ag-MAR event. In our study, the fine sandy loam exhibits lower  $\text{NO}_3^-$  leaching during the wet year, as a function of both flooding frequency and flooding magnitude. This is due to a combination of increased denitrification and decreased N mineralization. We see increased denitrification as the soil profile during the wet year is near-saturation for longer periods of time, promoting conditions more favorable to denitrification than during the dry year. The decreased N mineralization is somewhat unexpected, as generally we associate wetter soils with higher amounts. However, we see a significant soil temperature difference between the dry and wet years, especially during the first month of the model simulation (dry year – 22.6°C, wet year – 18.8°C), preceding the first flooding event. This offsets the impact of wetter soils, and results in slightly more N mineralization occurring during the dry years, indicating the complex relationship between environmental variables and biogeochemical processes. The sand shows an opposite trend, where the wet year encourages more N mineralization, nitrification and  $\text{NO}_3^-$

leaching, as frequent precipitation events maintain a higher soil moisture but oxic conditions, which favor N mineralization. The soil temperatures are similar across the wet and dry winters at the sand site, however, due to the higher soil moisture content prevailing during the wet winter we see increased N mineralization during the low flooding frequency scenarios. There is a convergence at high flooding frequencies in both  $\text{NO}_3^-$  leaching and N mineralization, which may indicate a decreased sensitivity to the relationship between these factors and climate at high flooding frequencies.

The amount of precipitation occurring during the winter season exhibits a strong control on residual  $\text{NO}_3^-$  in the soil profile. Precipitation events occurring directly before a flooding event can stimulate increased amount of denitrification in the profile (Supplemental Materials, Fig. S4.1). Additionally, precipitation occurring after the final water application for Ag-MAR event encourages low amounts of  $\text{NO}_3^-$  transport and may be responsible for much of the variation observed in the residual  $\text{NO}_3^-$  profiles in the flooding frequency analysis. As flooding frequency increases, the time period that the model simulates increases, and we see higher amounts of interaction with late-season precipitation events. This may result in the natural precipitation driving deeper  $\text{NO}_3^-$  leaching in soils which have been flooded more frequently and have not fully drained. Overall, incorporating local climate data adds complexity to the HP1-MIM model, on both the physical and biogeochemical sides of the model. The interaction of local precipitation and temperature can impact the  $\text{NO}_3^-$  leaching potential of a site and interact with Ag-MAR BMPs in multiple ways.

#### **4.4.2 Overarching Ag-MAR Considerations**

The multi-scenario analysis presented in this research indicates that different soil texture and climate scenarios can produce distinct responses to Ag-MAR management practices.

Consequently, the recommendations for Ag-MAR BMPs designed to minimize  $\text{NO}_3^-$  leaching from the vadose zone, while maximizing groundwater recharge, will vary based upon physical and biogeochemical characteristics of an Ag-MAR site. While we can make some general recommendations based upon the observed results from the fine sandy loam and sand site, some amount of hydrologic characterization, and comparison to similar Ag-MAR sites should be done during the planning and development of a new Ag-MAR site.

The fine sandy loam site in our study is characterized by lower infiltration rates ( $K_{\text{sat}} = 1.9 \text{ cm hr}^{-1}$ ), resulting in a higher prevalence of saturated conditions during the winter months, specifically in the periods in between Ag-MAR flooding events. As a result, we see a slower transport of  $\text{NO}_3^-$  from the shallow vadose zone, and more favorable conditions for denitrification to occur in between flooding events, which may decrease the mass of  $\text{NO}_3^-$  leaching during an Ag-MAR water application. The multi-scenario analysis indicates further that longer flooding frequencies may encourage denitrification and decrease  $\text{NO}_3^-$  leaching. This results in Ag-MAR management scenarios which must balance the potential for denitrification to be used as a  $\text{NO}_3^-$  remediation technique in conjunction with other Ag-MAR management considerations (i.e. crop tolerance to flooding, water availability). One approach would be to apply relatively large magnitude water applications ( $>45 \text{ cm}$ ), at relatively long flooding frequencies. Another management factor worth considering is the plot size of the Ag-MAR site, over which water is applied. In the case of the fine sandy loam, it may be beneficial to spread water over relatively large surface areas, in an attempt to maximize denitrification occurring during the applied recharge.

The sand site is characterized by high infiltration rates ( $K_{\text{sat}} = 23.6 \text{ cm hr}^{-1}$ ), which drains rapidly following flooding events, and does not exhibit environmental conditions conducive to

large amounts of denitrification. Thus, targeting denitrification to offset  $\text{NO}_3^-$  leaching is not a viable Ag-MAR management strategy at this type of field site. Instead,  $\text{NO}_3^-$  leaching at the sand site is more strongly controlled by the initial mass of residual  $\text{NO}_3^-$  present in the soil profile prior to Ag-MAR. We see this in the breakdown of the percent of initial soil  $\text{NO}_3^-$  that is contributing to the total amount of  $\text{NO}_3^-$  leached, which was much higher at the sand site compared to the fine sandy loam, which had a lower initial soil  $\text{NO}_3^-$  and higher newly nitrified  $\text{NO}_3^-$  fraction. Sites similar to the sand field site presented in this study should prioritize maximizing the potential dilution effect by applying large amounts of water as is feasible, over relatively small surface areas of land. As a result, a high initial soil  $\text{NO}_3^-$  amount will result in a high-concentration pulse of  $\text{NO}_3^-$  being pushed towards the groundwater table with the initial water applications, but subsequent water applications for Ag-MAR can offset the bulk recharge concentration of  $\text{NO}_3^-$ . Bulk recharge concentrations may be estimated from a thorough understanding of the  $\text{NO}_3^-$  concentrations in the soil profile prior to flooding, paired with estimates of the amount of mineralization expected to occur over the course of an Ag-MAR flooding season, and the total amount of applied water.

#### **4.4.3 Model Calibration & Validation**

Although the soil textures simulated in this study are the same as the soils calibrated by Murphy & Dahlke In Prep in their previous HP1-MIM model development, the fine sandy loam required additional calibration with field data, while the sand did not. This is most likely due to the presence of a hardpan we observed in the field just below the simulated domain (>100 cm). The volumetric water content data collected at the fine sandy loam field site reflects the presence of this hardpan, which manifests itself in decreased infiltration and drainage rates of the soil profile. The recalibration of the fine sandy loam identifies the need for monitoring of hydrologic

conditions when calibrating and validating a reactive transport model. The presence of the hardpan below the soil profile, while not directly represented in the model, slows Ag-MAR recharge rates, and encourage conditions more conducive to denitrification in comparison to the soil column experiment simulated by Murphy & Dahlke In Prep, which allowed free drainage of pore water from the 80 cm soil column. In contrast, the sand site continued to show rapid infiltration rates and drainage from the shallow vadose zone, irrespective whether the soil was flooded in the field or in the laboratory during the soil column experiment. The observed volumetric water content data was well represented by the HP1-MIM model when using parameters calibrated from previous laboratory experiments, exhibiting that there was minimal influence from any confining layers potentially present deeper in the vadose zone.

Biogeochemically, the HP1-MIM model is able to accurately represent the shape and dominant trend of the residual  $\text{NO}_3^-$  in the soil profile following field-scale Ag-MAR events, across both soil textures. While there is some error in the exact estimation of  $\text{NO}_3^-$  concentrations (specifically in the top 10-cm range, where high rates of microbial activity and N mineralization are observed (Murphy et al. 1998)), the HP1-MIM model, which was not calibrated on the biogeochemical side, simulates reasonable estimations of residual soil  $\text{NO}_3^-$  concentrations, in multiple field locations with varying initial amounts. Additionally, it accurately represents the dominant biogeochemical trends that differ between the fine sandy loam and sands sites. For the fine sandy loam, we see the interaction between N mineralization and denitrification, where high amounts of N mineralization occurring during wet low-flow periods are offset by denitrification during the Ag-MAR flooding events. For the sand, we see a N mineralization-dominated setting, where very little denitrification occurs, due to the rapid drainage of the shallow vadose zone following an Ag-MAR event. The bulk of the N mineralization occurs slowly, when the soils are

relatively well drained, but still moist. In both soils, we see N mineralization occurring over the course of the simulated Ag-MAR season (109 – 154 kg ha<sup>-1</sup> N – fine sandy loam, 31 - 53 kg ha<sup>-1</sup> N – sand). These amounts are comparable to annual estimates of N mineralization occurring on traditionally cultivated agricultural land (76 – 123 kg ha<sup>-1</sup> N in the top 30-cm (Geisseler et al. 2019)), which calls into question whether increased N mineralization during an Ag-MAR season will impact rates over the rest of the year. Based on this study, it is unclear if N mineralization potential significantly decreases organic substrate availability or transports quantities of labile organic matter out of the shallow vadose zone (Borken et al. 2009), two mechanisms which could potentially decrease N mineralization potential in the following growing seasons and in subsequent Ag-MAR flooding seasons.

One notable trend observed in our study is the relatively similar residual NO<sub>3</sub><sup>-</sup> profile across all cores at each field site following the Ag-MAR season. The cores at the fine sandy loam site range from 8.4 to 8.9 ppm NO<sub>3</sub><sup>-</sup>-N for the top 0-10 cm, before decreasing to ~0.5 ppm NO<sub>3</sub><sup>-</sup>-N at 100 cm depth. The cores at the sand field site range from 0.51 to 1.06 ppm NO<sub>3</sub><sup>-</sup>-N from 0-10 cm, decreasing to ~0.4 ppm NO<sub>3</sub><sup>-</sup>-N at 100 depth. This is in juxtaposition to their initial state, which varied widely from 17.0 ppm NO<sub>3</sub><sup>-</sup>-N at 10 cm depth (S-core 1) to 1.86 ppm NO<sub>3</sub><sup>-</sup>-N at 10 cm depth (S-core 2). It is possible that the flushing and subsequent N mineralization in the shallow vadose zone encourages some amount of soil homogenization, decreasing the heterogeneity of NO<sub>3</sub><sup>-</sup> distributions commonly found at the field-scale. The spatial heterogeneity of soil nutrients is hypothesized to be impacted by land use (Fraterrigo et al. 2005), which has implications regarding our understanding of soil heterogeneity and microbial activity, specifically with respect to nutrient management plans following an Ag-MAR flooding season, and should be investigated further.

## 4.5 CONCLUSION

Using a HP1-MIM reactive transport model calibrated with field-data allowed investigation of different Ag-MAR management practices and their effect on  $\text{NO}_3^-$  leaching and N cycling processes in different soil textures. In this study, we conducted a multi-scenario analysis to specifically evaluate different flooding frequency and flooding magnitude scenarios on the  $\text{NO}_3^-$  leaching potential of a fine sandy loam and a sandy Ag-MAR site. Our results allow for the development of some recommendations regarding general Ag-MAR BMPs, but further research should be dedicated to increasing our knowledge of solute transport dynamics under Ag-MAR.

In this study, we see distinct differences in recommended management strategies, dependent on soil texture. We observe that the fine sandy loam site has a high potential for denitrification, and may minimize  $\text{NO}_3^-$  leaching under high-magnitude, low-frequency water applications, over a relatively large surface area. We observe that the sand site has a low potential for denitrification and may minimize  $\text{NO}_3^-$  leaching by maximizing the dilution effect, if high magnitude water applications are made at short-frequency over a relatively small surface area. Both field sites should attempt to leverage the dilution effect, however, feasibility of this management practice will depend on crop tolerance to flooding, water availability, and water conveyance infrastructure able to deliver large amounts of water. If only low magnitude events are possible, some amount of  $\text{NO}_3^-$  leaching is observed, which can be estimated with an understanding of its residual content in the soil profile prior to flooding, and an understanding of the N mineralization and denitrification rates that the Ag-MAR soil is able to achieve. Overall, this study shows that with proper management, minimizing  $\text{NO}_3^-$  leaching while maximizing groundwater recharge over the course of an Ag-MAR season is possible, and is encouraging for the general viability of Ag-MAR as an effective managed aquifer recharge technique.

**APPENDIX 1: SUPPLEMENTARY INFO FOR CHAPTER 1**

Table S2.1: Cores taken at each field site before and after AgMAR experiments.

<b>Site</b>	<b>Winter season</b>	<b># of cores in Control Plot</b>	<b># of cores in Flood Plot</b>	<b>Date collected</b>
<b>Sand</b>	2015/2016	5	3	Before cores: 11/23/15 After cores: 02/17/16
<b>Fine sandy loam</b>	2015/2016	6	3	Before cores: 09/15/15 After cores: 02/16/16
<b>Sand</b>	2016/2017	2	3	Before cores: 12/13/16 After cores: 03/02/17
<b>Fine sandy loam</b>	2016/2017	2	2	Before cores: 12/13/16 After cores: 03/02/17

Table S2.2: Water application schedule for AgMAR at fine sandy loam and sand field sites.

<b>Fine sandy loam</b>		<b>Sand</b>	
<b>Date</b>	<b>Applied Water (cm)</b>	<b>Date</b>	<b>Applied Water (cm)</b>
1/4/16	15	12/23/15	15
1/11/16	15	12/29/15	23
1/19/16	15	1/12/16	25
1/25/16	15		
1/9/17	15	1/3/17	37
1/16/17	15	1/19/17	15
1/23/17	15	1/26/17	15
2/1/17	15		

Table S2.3: Soil water balance and estimated deep percolation from AgMAR for the Sand and Fine sandy loam almond orchards for 2015-2017.

	Precipitation	Applied Water	Total Deep Percolation	Deep Percolation from Rainfall	Deep Percolation of Applied Water		Loss of Applied Water to Soil Storage	
	cm	cm	cm	cm	cm	%	cm	%
<b>Sand (Oct-Mar) 2015/2016</b>	32.8	66.4	73.9	12.2	61.7	93%	4.7	7%
<b>Sand (Oct-Mar) 2016/2017</b>	44.3	65.5	83.9	18.9	65.0	99%	0.5	1%
<b>Fine sandy loam (Nov-Mar) 2015/2016</b>	25.2	60.9	55.6	6.5	49.2	81%	11.8	19%
<b>Fine sandy loam (Oct-Mar) 2016/2017</b>	31.6	60.9	71.0	12.1	58.8	96%	2.1	4%

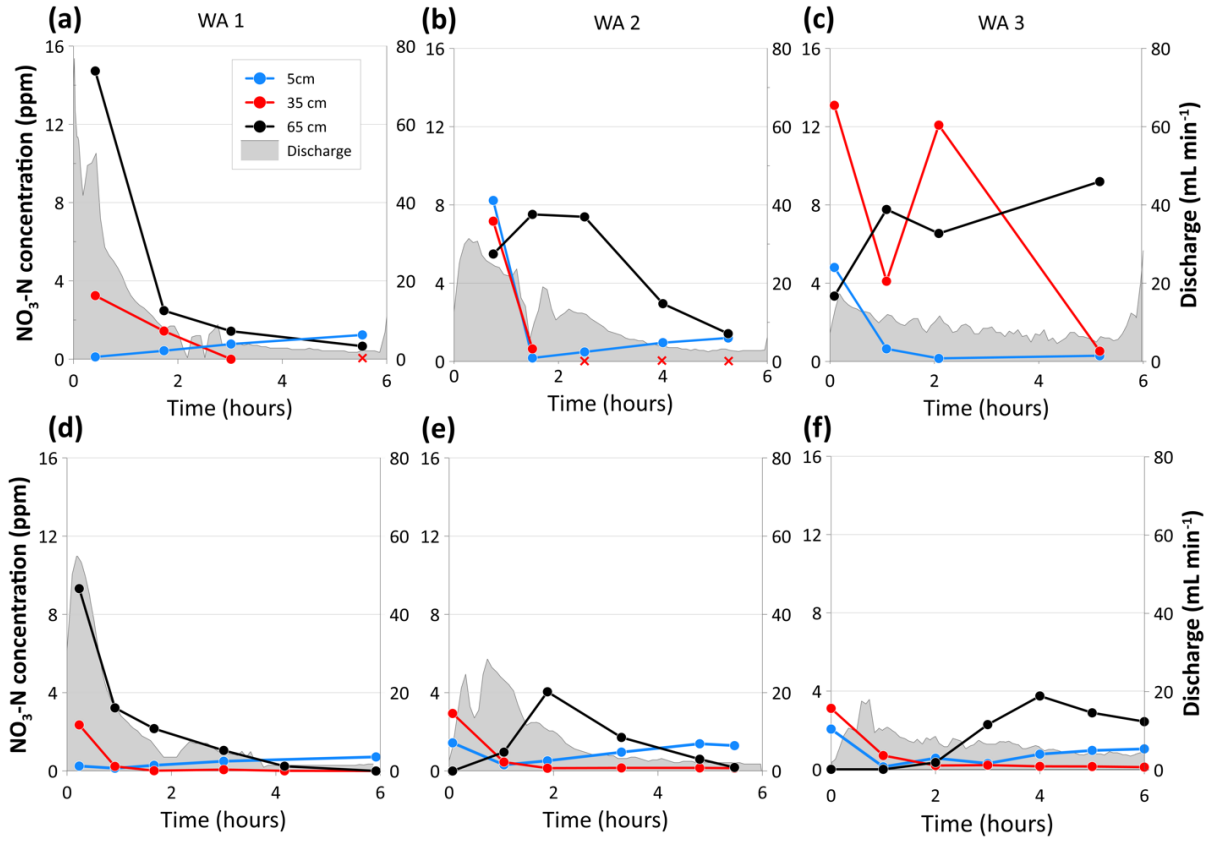


Figure S2.1: Sand pore water trends during the first 6 hours of the low frequency (a), (b), and (c), and high frequency (d), (e) and (f) water applications. Red and blue crosses indicate missing samples due to low soil water content.

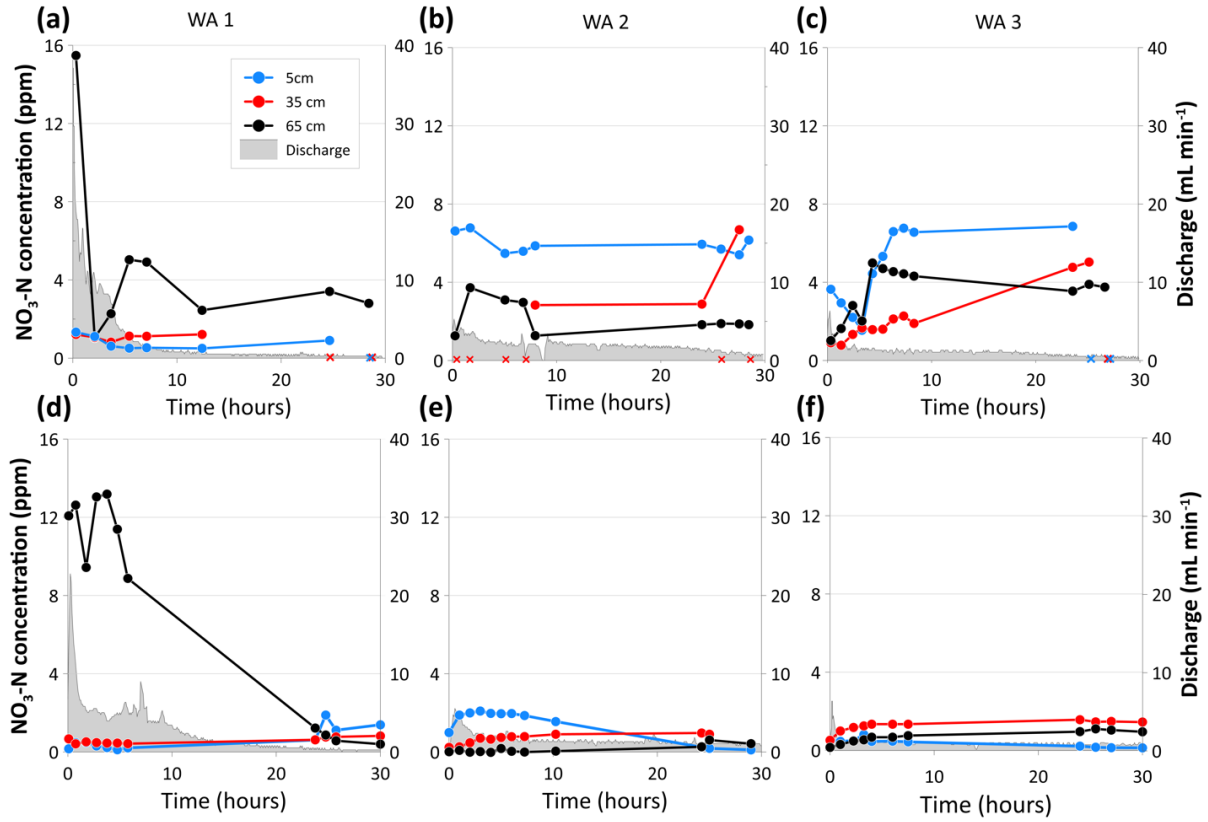


Figure S2: Fine sandy loam pore water trends during the first 30 hours of the low frequency (a), (b), and (c), and high frequency (d), (e) and (f) water applications. Red and blue crosses indicate missing samples due to low soil water content.

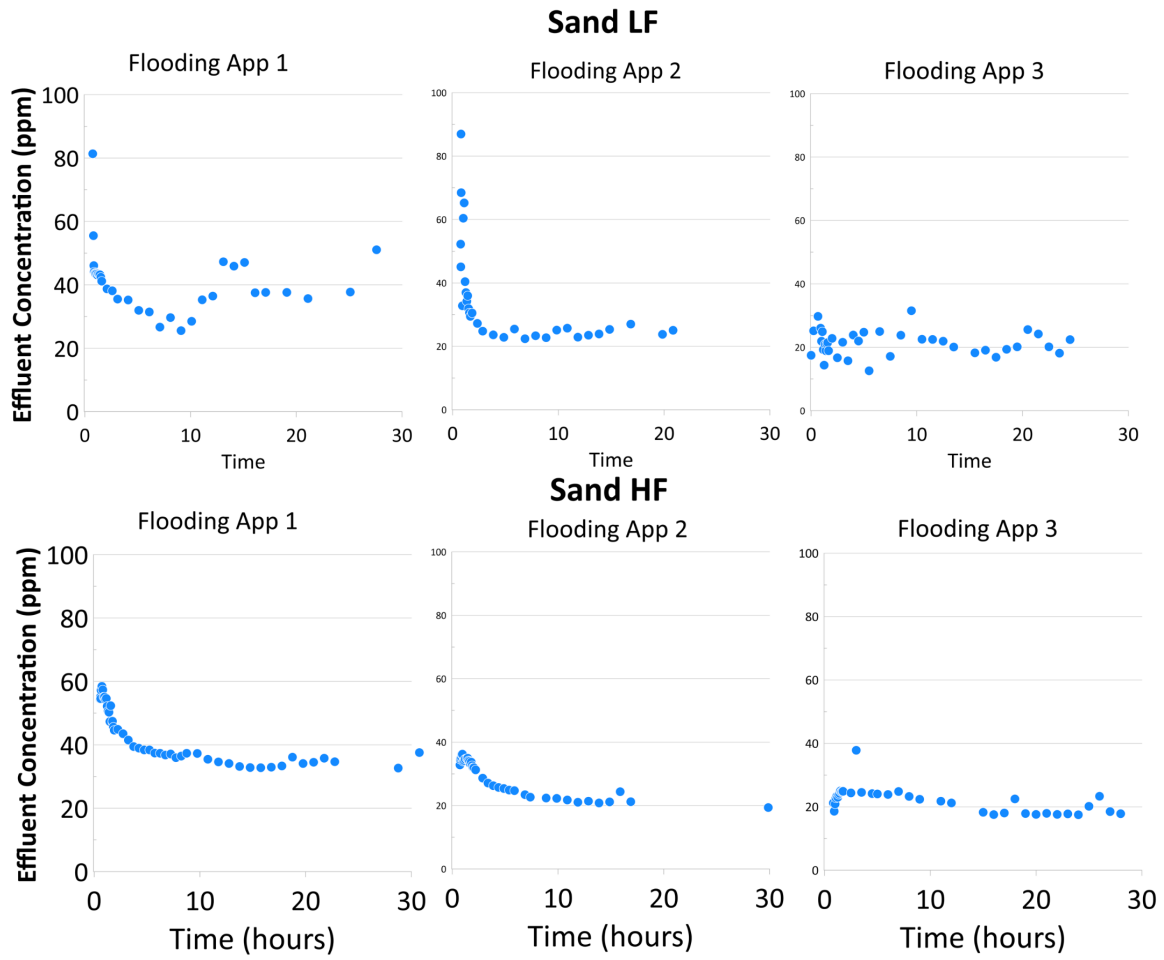


Figure S2.3: Effluent DOC concentrations [ppm] in the sand.

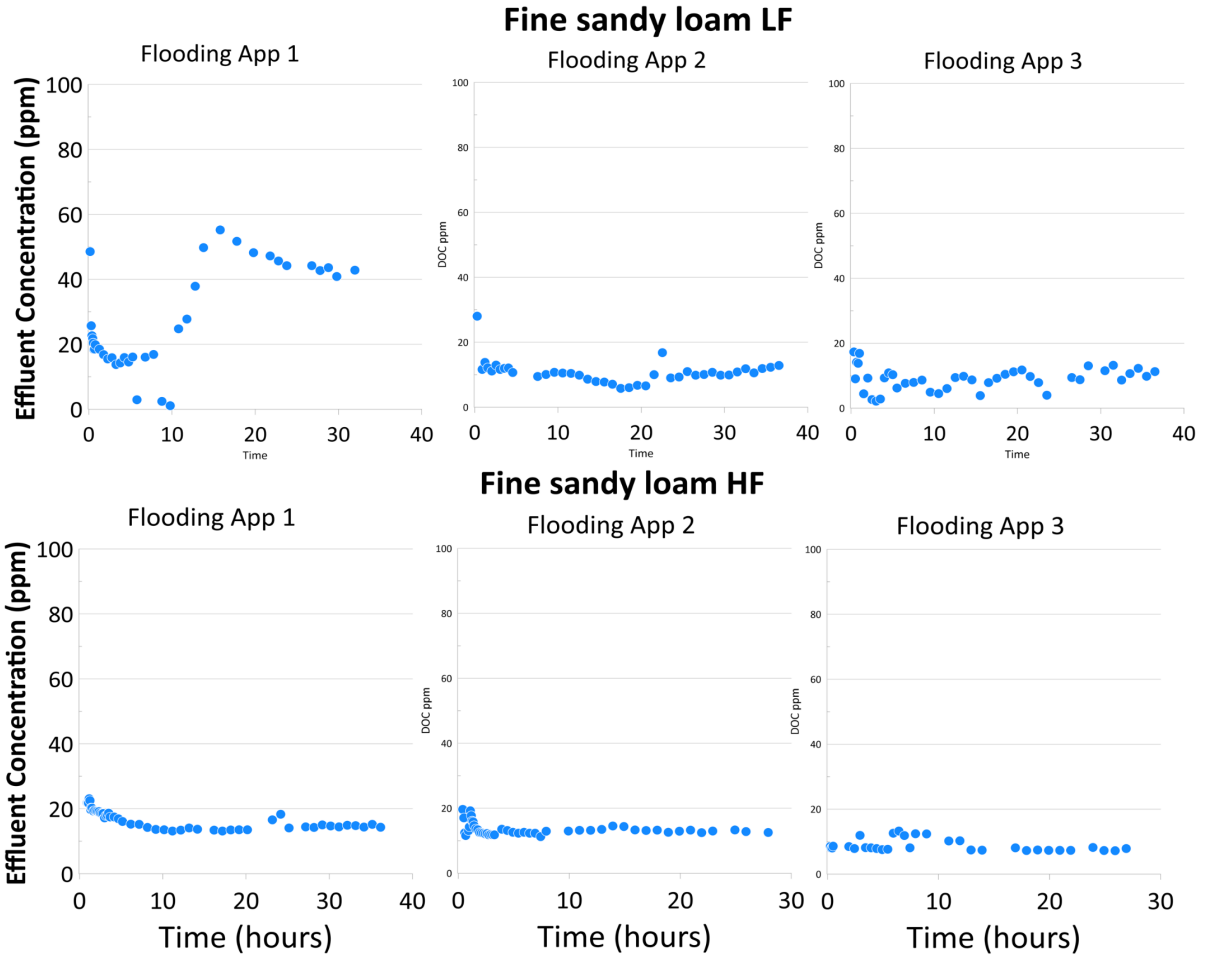


Figure S2.4: Effluent DOC concentration [ppm] in the fine sandy loam.

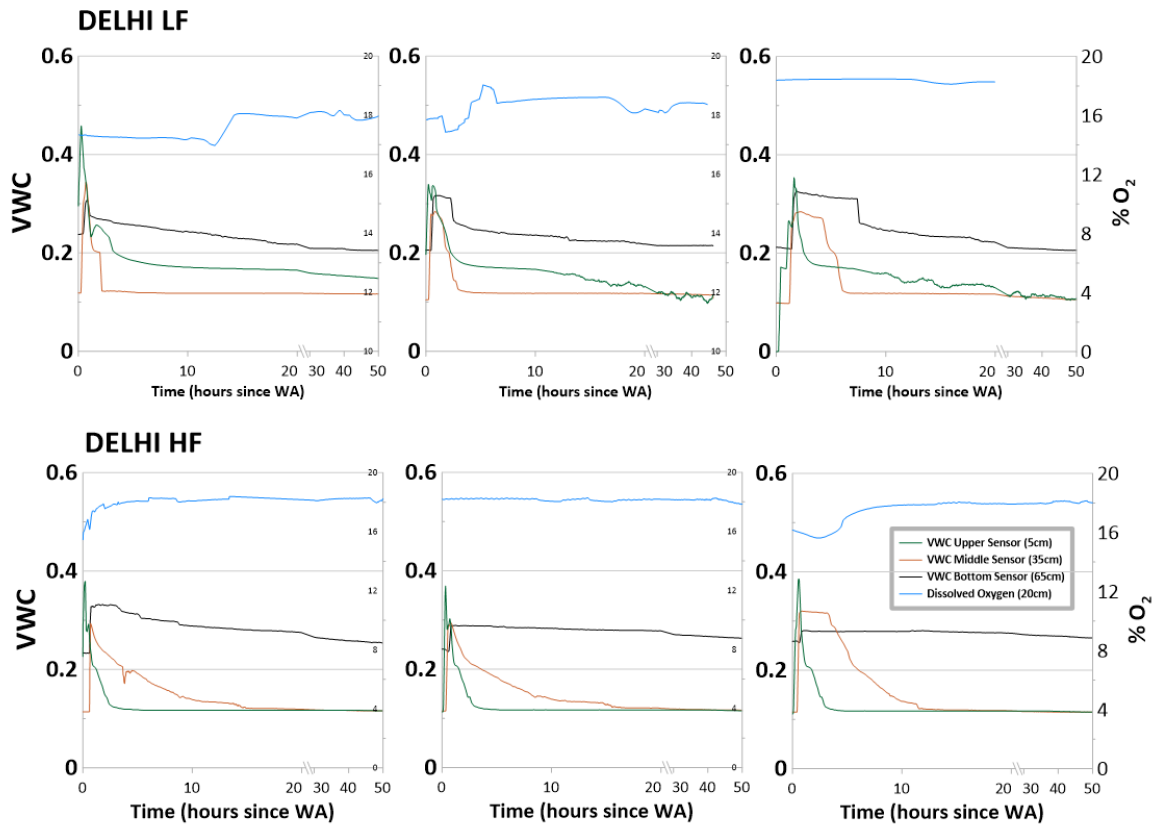


Figure S2.5: Volumetric water content (VWC) [ $\text{cm}^3/\text{cm}^3$ ] and dissolved oxygen ( $\text{O}_2$ ) [%] in the sand.

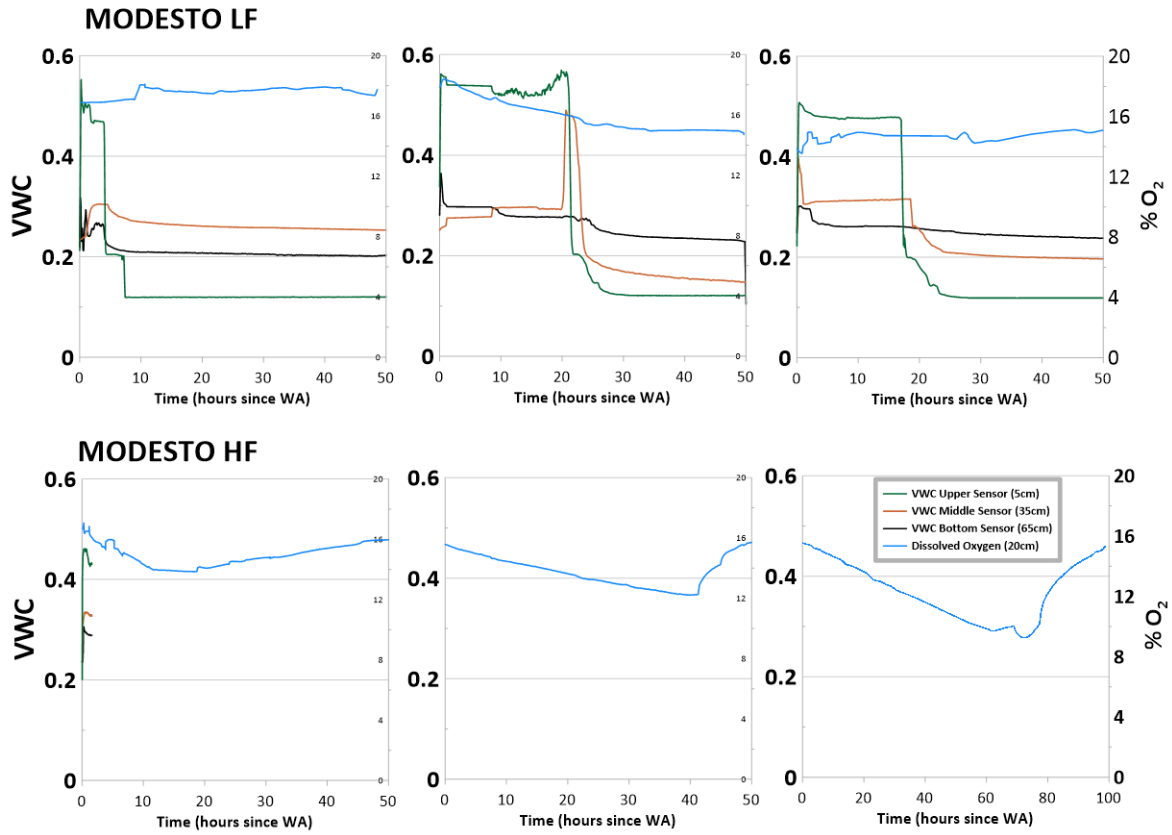


Figure S2.6: Volumetric water content (VWC) [cm<sup>3</sup>/cm<sup>3</sup>] and dissolved oxygen (O<sub>2</sub>) [%] in the fine sandy loam. (Note – Data logger error resulted in Modesto HF VWC data loss.)

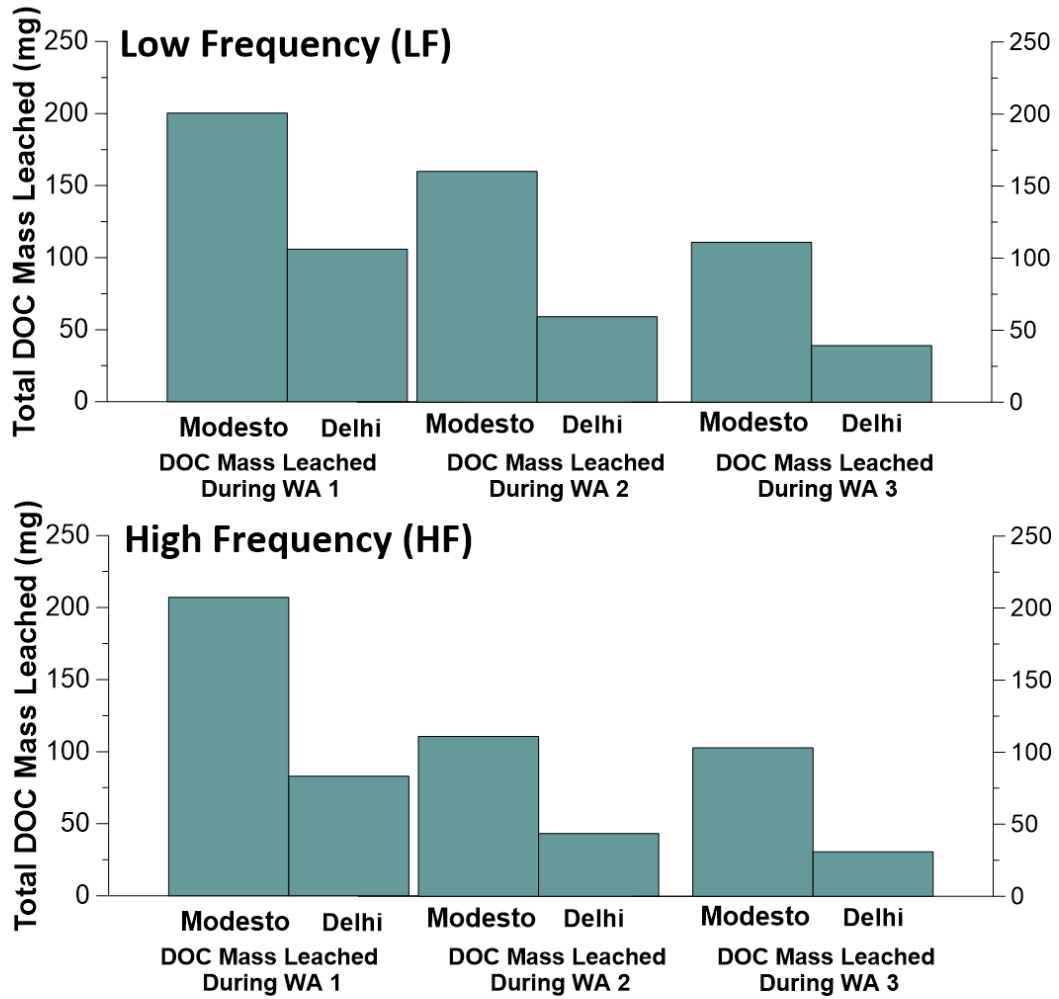


Figure S2.7: Mass balance for DOC [mg] leached from column during AgMAR experiments.

Table S2.4: Timing of peak chemical concentrations in soil column effluent. WA denotes water application.

	Fine sandy loam LF			Sand HF		
Time to peak	NO <sub>3</sub> -N	NH <sub>4</sub> -N	DOC	NO <sub>3</sub> -N	NH <sub>4</sub> -N	DOC
WA 1	0:53:00	0:45:00	0:45:00	0:39:00	0:34:00	0:44:00
WA 2	3:51:00	0:49:00	0:48:00	5:23:00	0:58:00	0:58:00
WA 3	8:29:00	-	00:39:00 & 9:29:00	15:00:00	1:00:00	1:30:00
	Fine sandy loam LF			Sand HF		
	NO <sub>3</sub> -N	NH <sub>4</sub> -N	DOC	NO <sub>3</sub> -N	NH <sub>4</sub> -N	DOC
WA 1	1:17:00	0:10:00	0:10:00	4:10:00	0:15:00	1:10:00
* secondary peak at	29:47:00	-	15:47:00	1:05:00	-	0:24:00
Water Application 2	1:03:00	-	0:18:00			1:05:00
Water Application 3	0:21:00	-	0:21:00	50:55:00	-	6:25:00

Table S2.5: Time until 90% of the applied water and residual soil nitrate load have left the system.

	<b>Sand LF</b>		<b>Sand HF</b>	
	Applied water	Nitrate Load Transport	Applied water	Nitrate Load Transport
<b>WA 1</b>	10:36:00	1:56:00	10:56:00	1:53:00
<b>WA 2</b>	8:49:00	8:38:00	16:35:00	13:43:00
<b>WA 3</b>	16:12:00	14:31:00	21:48:00	31:26:00
	<b>Fine sandy loam LF</b>		<b>Fine sandy loam HF</b>	
	Applied Flow	Nitrate Load Transport	Applied Flow	Nitrate Load Transport
<b>WA 1</b>	23:48:00	28:22:00	20:38:00	13:55:00
<b>WA 2</b>	30:25:00	30:44:00	34:00:00	4:56:00
<b>WA 3</b>	29:15:00	21:36:00	66:05:00	73:26:00

Table S2.6: Upper, average, and lower bound estimates of total carbon mass transport [%] in soil column effluent. Upper and lower bounds are based upon one standard deviation of soil TC data. Upper and lower bounds were calculated using the total DOC effluent mass divided by the upper and lower bounds of one standard deviation change of total TC mass measured in the soil profile.

	<b>Lower Bound %TC leached</b>	<b>Average %TC Leached</b>	<b>Upper Bound %TC leached</b>
<b>Sand LF</b>	0.184	0.259	0.435
<b>Fine sandy loam LF</b>	0.072	0.083	0.101
<b>Sand HF</b>	0.164	0.231	0.389
<b>Fine sandy loam HF</b>	0.056	0.066	0.078

Table S2.7: Water Holding Capacity – Sand and Fine sandy loam

<b>Sand</b>	
<b>Depth (cm)</b>	<b>Water holding capacity (cm<sup>3</sup>/cm<sup>3</sup>)</b>
0 – 10	0.402
10 – 20	0.373
20 – 30	0.338
30 – 40	0.314
40 – 50	0.300
50 – 60	0.329
60 – 70	0.363
70 – 80	0.338
<b>Fine sandy loam</b>	
<b>Depth (cm)</b>	<b>Water holding capacity (cm<sup>3</sup>/cm<sup>3</sup>)</b>
0 – 10	0.415
10 – 20	0.450
20 – 30	0.419
30 – 40	0.407
40 – 50	0.367
50 – 60	0.382
60 – 70	0.388
70 – 80	0.357

APPENDIX 2: SUPPLEMENTARY INFO FOR CHAPTER 2

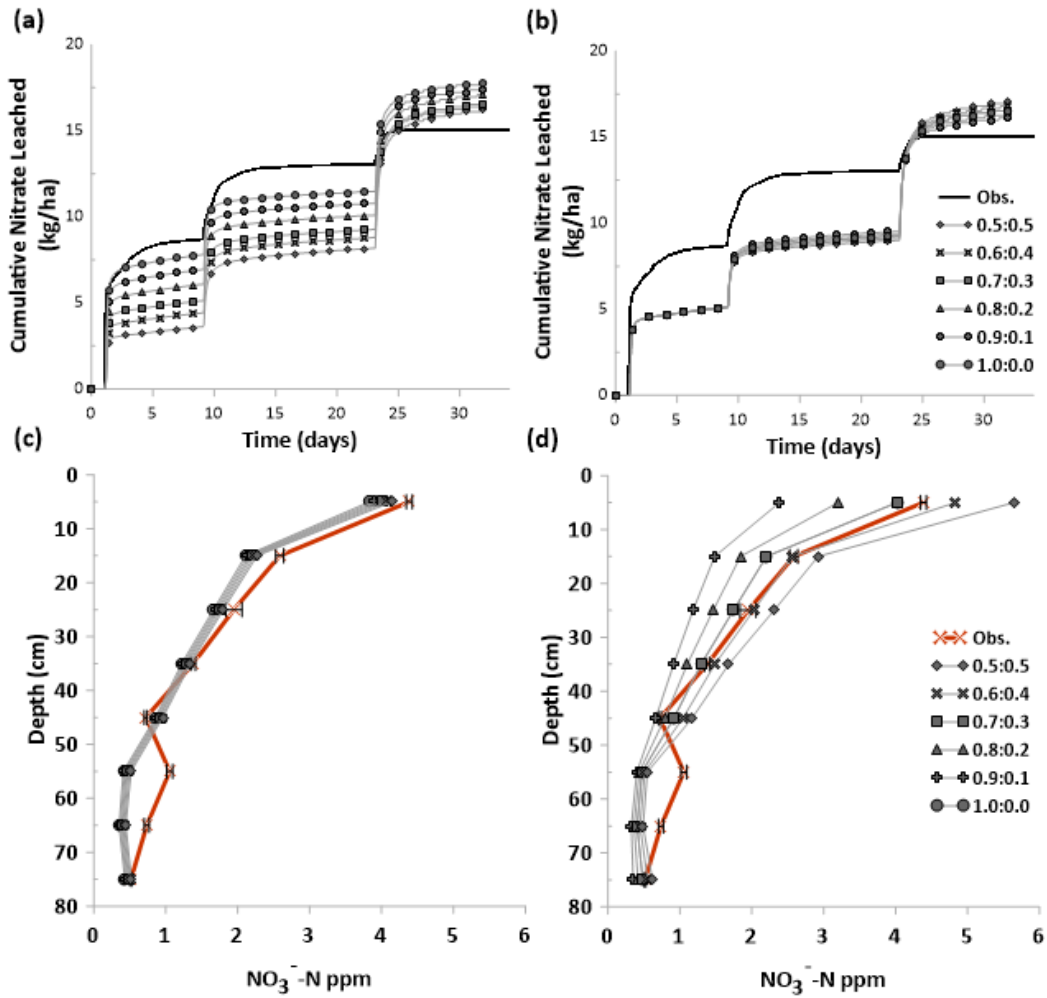


Figure S3.1: MIM splits for fine sandy loam. (a) and (c) represent  $r$  distribution of initially present NO<sub>3</sub><sup>-</sup> in the mobile-immobile pore space. (b) and (d) represent  $r_{kin}$  of kinetic distribution of mineralization and nitrification occurring in the mobile-immobile pore space

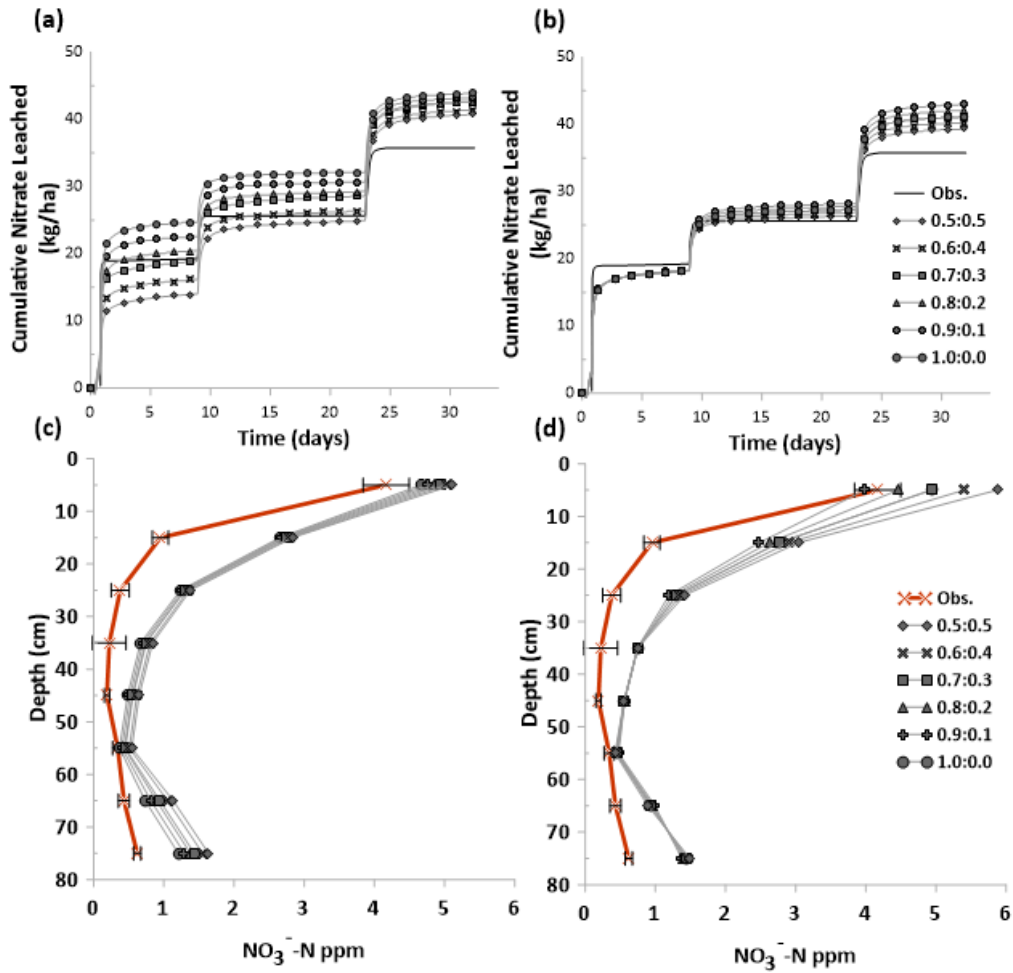


Figure S3.2: MIM Splits for sand. (a) and (c) represent  $r$  distribution of initially present  $\text{NO}_3^-$  in the mobile-immobile pore space. (b) and (d) represent  $r_{kin}$  of kinetic distribution of mineralization and nitrification occurring in the mobile-immobile pore space

Table S3.1: Biogeochemical parameters for the HP1-MIM model – fine sandy loam.

Parameter	Process	Units	Value	Reference
$k_{min}$	Mineralization	$\text{min}^{-1}$	0 – 10cm: 4.69E-07	Laboratory incubation measurements (Murphy et al. 2021)
			10 – 20cm: 2.76E-07	
			20 – 30cm: 2.68E-07	
			30 – 40cm: 2.40E-07	
			40 – 50cm: 1.81E-07	
			50 – 60cm: 2.88E-08	
			60 – 70cm: 5.53E-08	
			70 – 80cm: 1.23E-07	

$k_{nit}$	Nitrification	min <sup>-1</sup>	0 – 80cm: 2.00E-04	McLaren, 1976; Jemison et al. 1994
$k_{denit}$	Denitrification	mol dm <sup>-3</sup> min <sup>-1</sup>	0 – 10cm: 5.38E-07 10 – 20cm: 2.21E-07 20 – 30cm: 1.14E-07 30 – 40cm: 7.72E-08 40 – 50cm: 3.07E-08 50 – 60cm: 2.85E-08 60 – 70cm: 2.69E-08 70 – 80cm: 2.76E-08	Laboratory incubation measurements
$r$	Initial NO <sub>3</sub> <sup>-</sup> distribution ratio (immobile- mobile)	-	0.0:1.0	
$r_{kin}$	Kinetic reaction distribution ratio (immobile- mobile)		0.3:0.7	

Table S2: Biogeochemical parameters for the HP1-MIM model – sand.

Parameter	Process	Units	Value	Reference
$k_{min}$	Mineralization	min <sup>-1</sup>	0 – 10cm: 8.14E-07 10 – 20cm: 6.69E-07 20 – 30cm: 5.17E-07 30 – 40cm: 2.23E-07 40 – 50cm: 1.88E-07 50 – 60cm: 0.00 60 – 70cm: 0.00 70 – 80cm: 1.23E-07	Laboratory incubation measurements (Murphy et al. 2021)
$k_{nit}$	Nitrification	min <sup>-1</sup>	0 – 80cm: 4E-04	McLaren, 1976; Jemison et al. 1994
$k_{denit}$	Denitrification	mol dm <sup>-3</sup> min <sup>-1</sup>	0 – 10cm: 8.40E-08 10 – 20cm: 3.62E-09 20 – 30cm: 5.96E-09 30 – 40cm: 1.06E-09 40 – 50cm: 1.27E-09 50 – 60cm: 1.84E-09 60 – 70cm: 5.95E-09	Laboratory incubation measurements

			70 – 80cm: 4.83E-08	
$r$	Initial NO <sub>3</sub> <sup>-</sup> distribution ratio (immobile-mobile)	-	0.3:0.7	
$r_{kin}$	Kinetic reaction distribution ratio (immobile-mobile)	-	0.3:0.7	
$\omega_{mim}$	Mass transfer coefficient	min <sup>-1</sup>	1E-06	Rukh et al. 2018

Table S3.3: NO<sub>3</sub><sup>-</sup> Mass Balance Load for Model Comparison for fine sandy loam

<b>Model</b>	<b>Initial NO<sub>3</sub><sup>-</sup>-N Mass (kg ha<sup>-1</sup>)</b>	<b>Residual NO<sub>3</sub><sup>-</sup>-N Mass (kg ha<sup>-1</sup>)</b>	<b>Mass of NO<sub>3</sub><sup>-</sup>-N Leached (kg ha<sup>-1</sup>)</b>	<b>Net Mineralization (kg ha<sup>-1</sup> N)</b>	<b>Net Denitrification (kg ha<sup>-1</sup> N)</b>
HP1-MIM	10.01	17.96	17.64	35.49	11.30
HP1	10.01	6.01	15.41	19.50	11.64
FK	10.01	1.00	3.92	60.21	64.21
FK-ND	10.01	24.19	44.25	60.21	0
ZK	10.01	0	2.50	66.51	78.08
ZK-ND	10.01	22.31	52.24	66.51	0
NR	10.01	0.00	9.70	0	0

Table S3.4: N Mass Balance Load for Model Comparison for sand.

<b>Model</b>	<b>Initial NO<sub>3</sub><sup>-</sup>-N Mass (kg ha<sup>-1</sup>)</b>	<b>Residual NO<sub>3</sub><sup>-</sup>-N Mass (kg ha<sup>-1</sup>)</b>	<b>Mass of NO<sub>3</sub><sup>-</sup>-N Leached (kg ha<sup>-1</sup>)</b>	<b>Net Mineralization (kg ha<sup>-1</sup> N)</b>	<b>Net Denitrification (kg ha<sup>-1</sup> N)</b>
--------------	---	--	--	--	---

HP1-MIM	25.79	17.94	33.33	24.56	0.74
HP1	25.79	8.66	35.86	18.11	1.41
FK	25.79	10.86	35.72	47.10	26.74
FK-ND	25.79	18.26	50.56	47.10	0
ZK	25.79	2.35	26.47	52.69	49.66
ZK-ND	25.79	20.79	54.34	52.69	0
NR	25.79	0	24.93	0	0

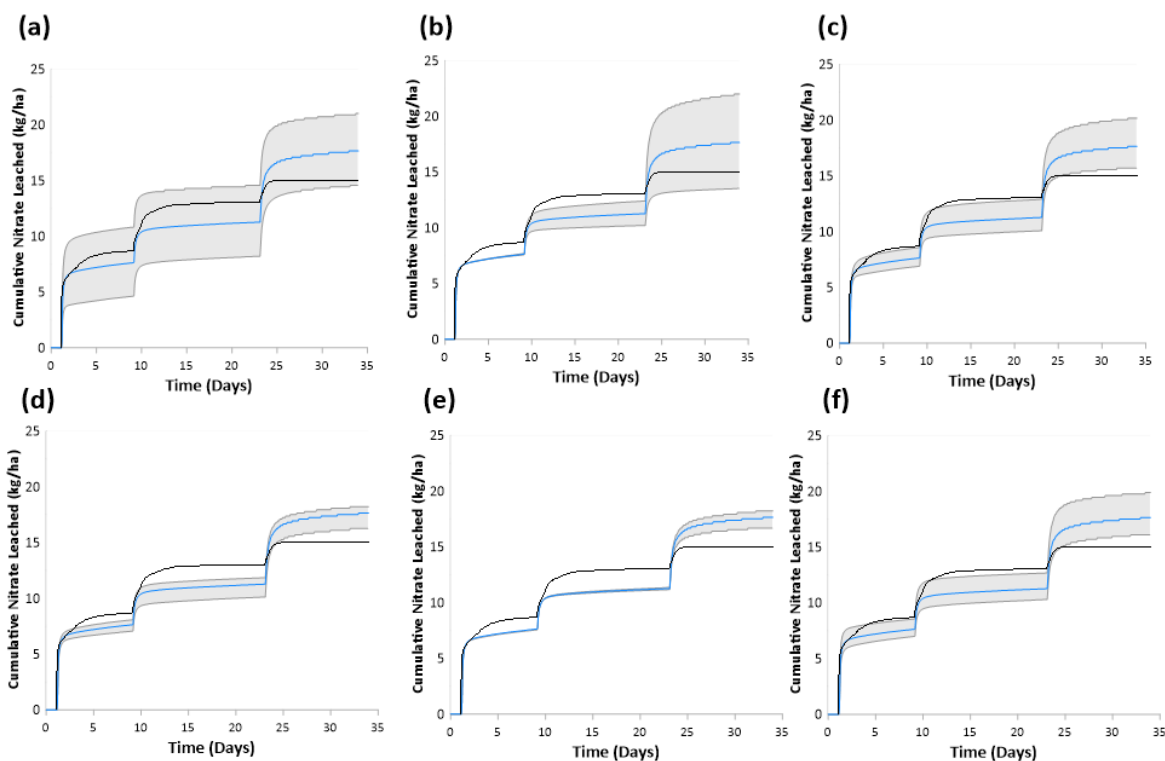


Figure S3.3: Local sensitivity analysis of biogeochemical parameters for the fine sandy loam soil. Grey bars represent the uncertainty associated with a 40% increase and decrease in – (a) initially present  $\text{NO}_3^-$  in soil profile, (b) mineralization rate constant  $k_{\text{min}}$ , (c) denitrification rate constant  $k_{\text{denit}}$ , (d) nitrification rate constant  $k_{\text{nit}}$ , (e) mass transfer coefficient  $\omega_{\text{mim}}$ , (f) longitudinal dispersivity,  $D_L$

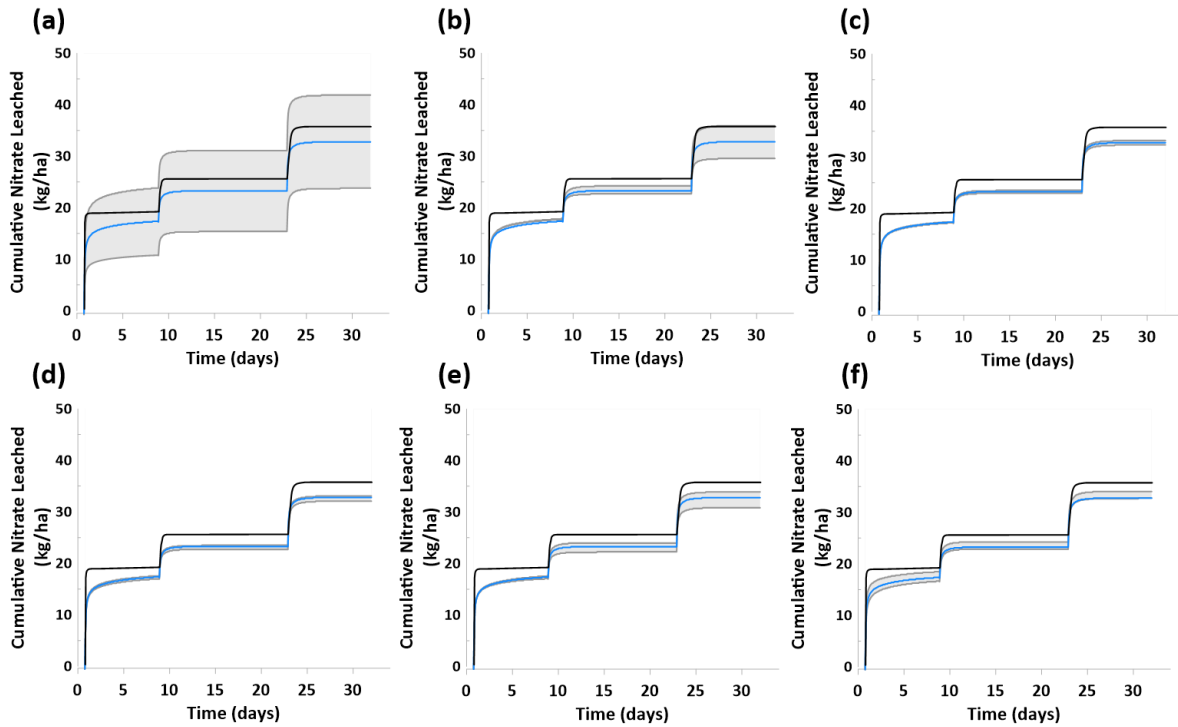


Figure S3.4: Local sensitivity analysis of biogeochemical parameters for the sand soil. Grey bars represent the uncertainty associated with a 40% increase and decrease in – (a) initially present  $\text{NO}_3^-$  in soil profile, (b) mineralization rate constant  $k_{\text{min}}$ , (c) denitrification rate constant  $k_{\text{denit}}$ , (d) nitrification rate constant  $k_{\text{nit}}$ , (e) mass transfer coefficient  $\omega_{\text{mim}}$ , (f) longitudinal dispersivity,  $D_L$

Appendix 3: Supplementary Information for Chapter 3

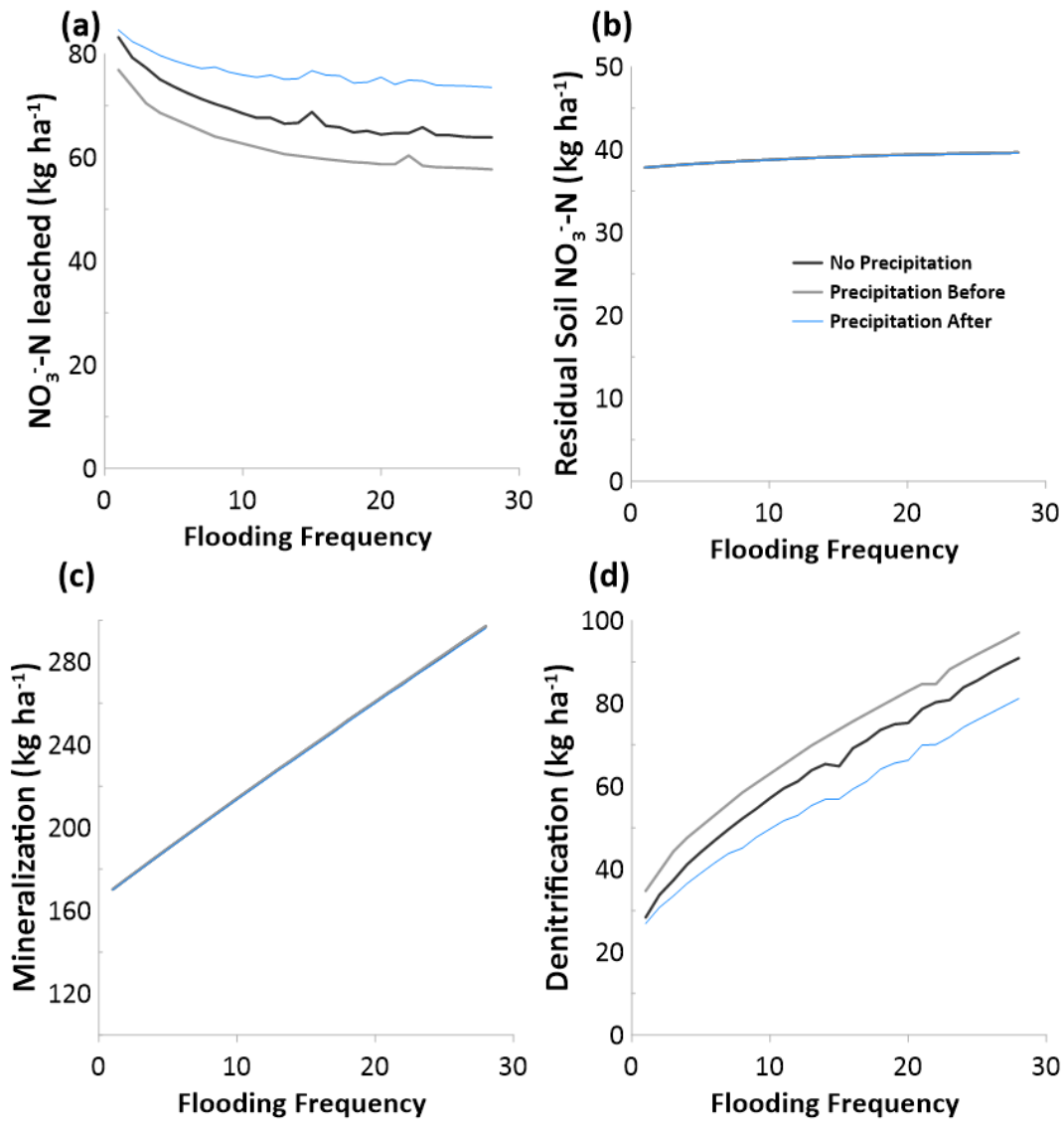


Fig. S4.1: Impact of precipitation on denitrification. Black line represents modeling scenarios where no precipitation or temperature is included. Grey line represents a 5cm precipitation event, spaced 12 hours prior to each flooding application. Blue line represents a 5cm precipitation event, spaced 12 hour after each flooding application.

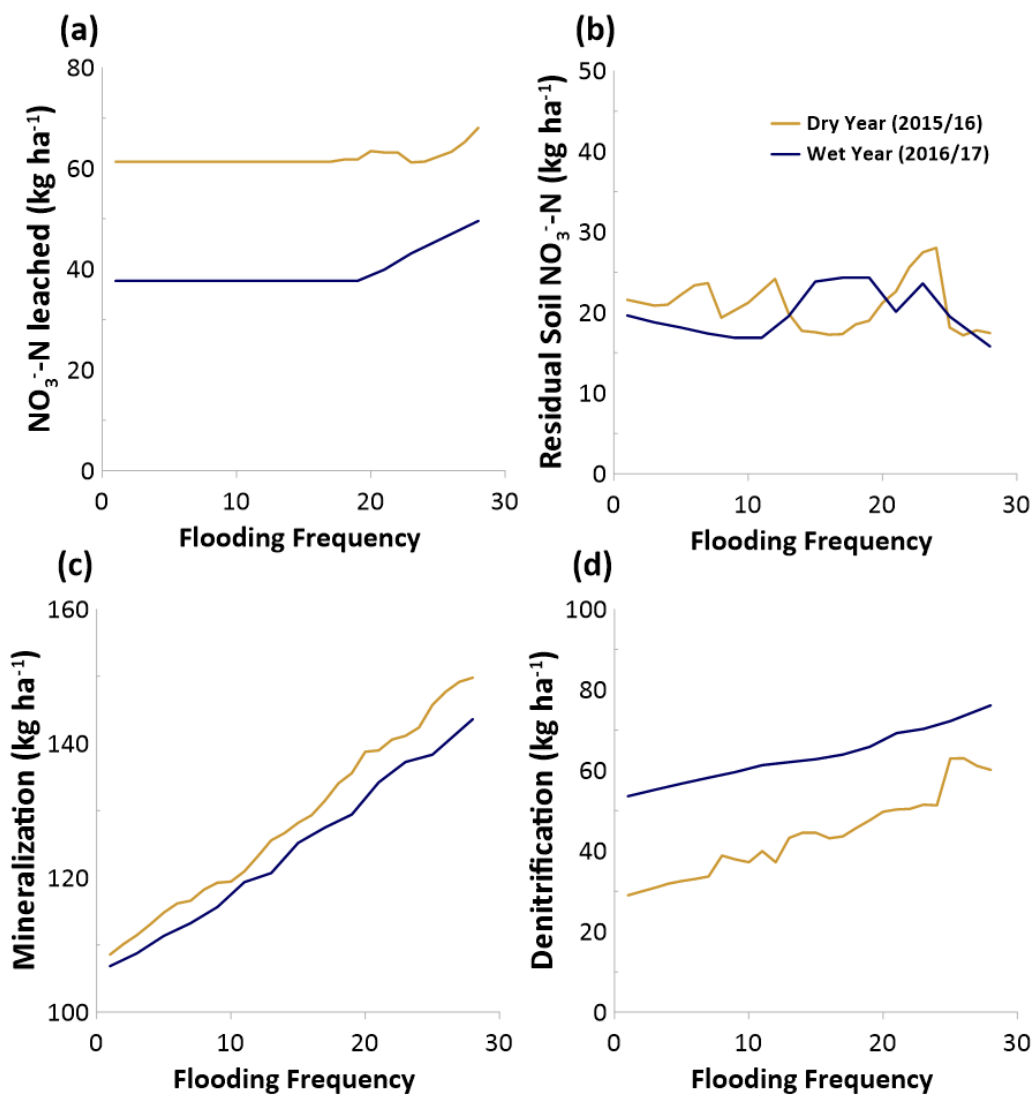


Fig. S4.2: Flooding frequency scenarios for the fine sandy loam soil at 60 cm flooding magnitude. (a) sum of  $\text{NO}_3^-$  leached from model domain during Ag-MAR flooding season, (b) residual  $\text{NO}_3^-$  in soil profile following Ag-MAR flooding season, (c) amount of mineralization occurring during Ag-MAR flooding season, (d) amount of denitrification occurring during Ag-MAR flooding season, as a function of flooding frequency.

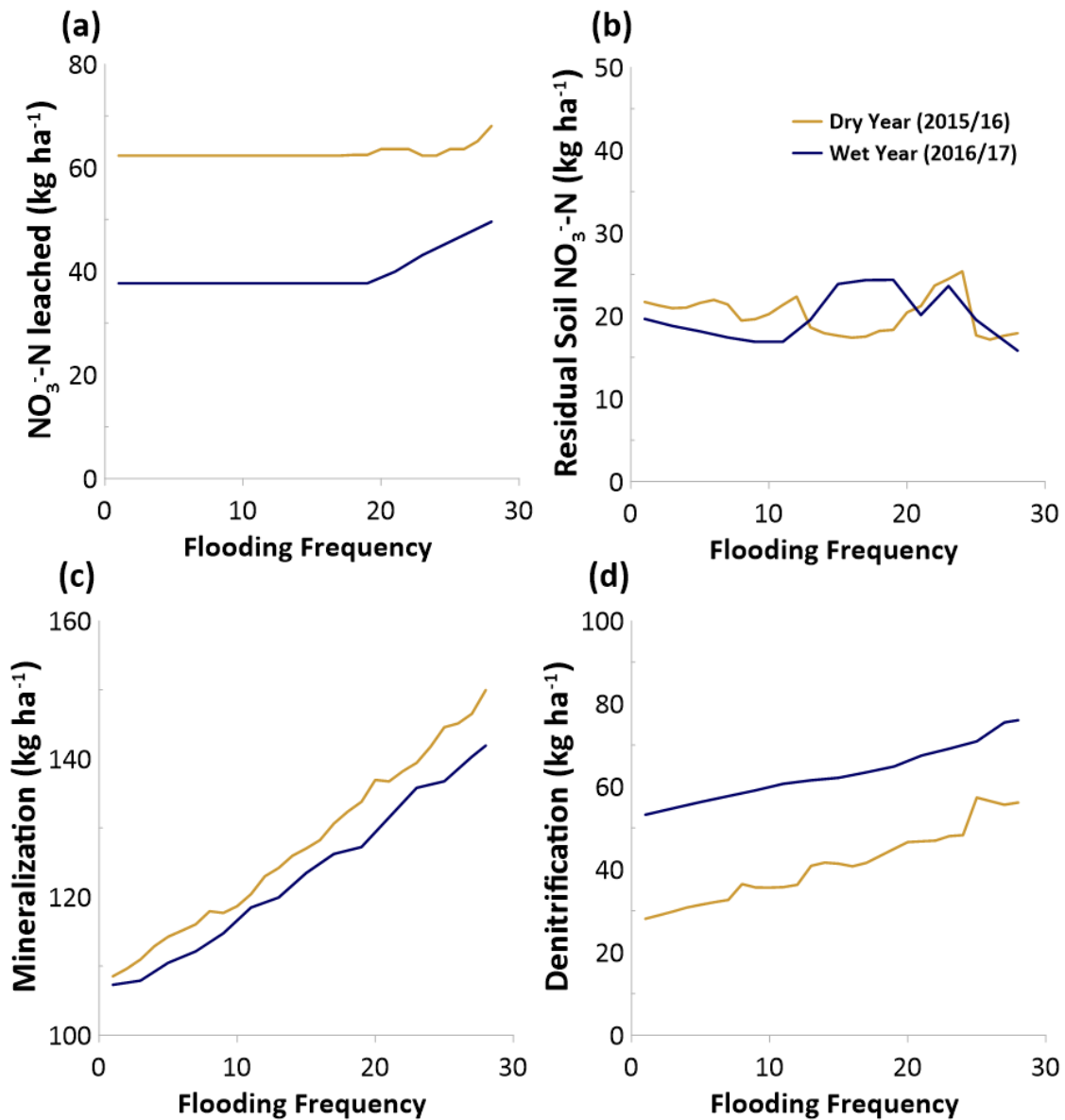


Fig. S4.3: Flooding frequency scenarios for the fine sandy loam soil at 120 cm flooding magnitude. (a) sum of NO<sub>3</sub><sup>-</sup> leached from model domain during Ag-MAR flooding season, (b) residual NO<sub>3</sub><sup>-</sup> in soil profile following Ag-MAR flooding season, (c) amount of mineralization occurring during Ag-MAR flooding season, (d) amount of denitrification occurring during Ag-MAR flooding season, as a function of flooding frequency.

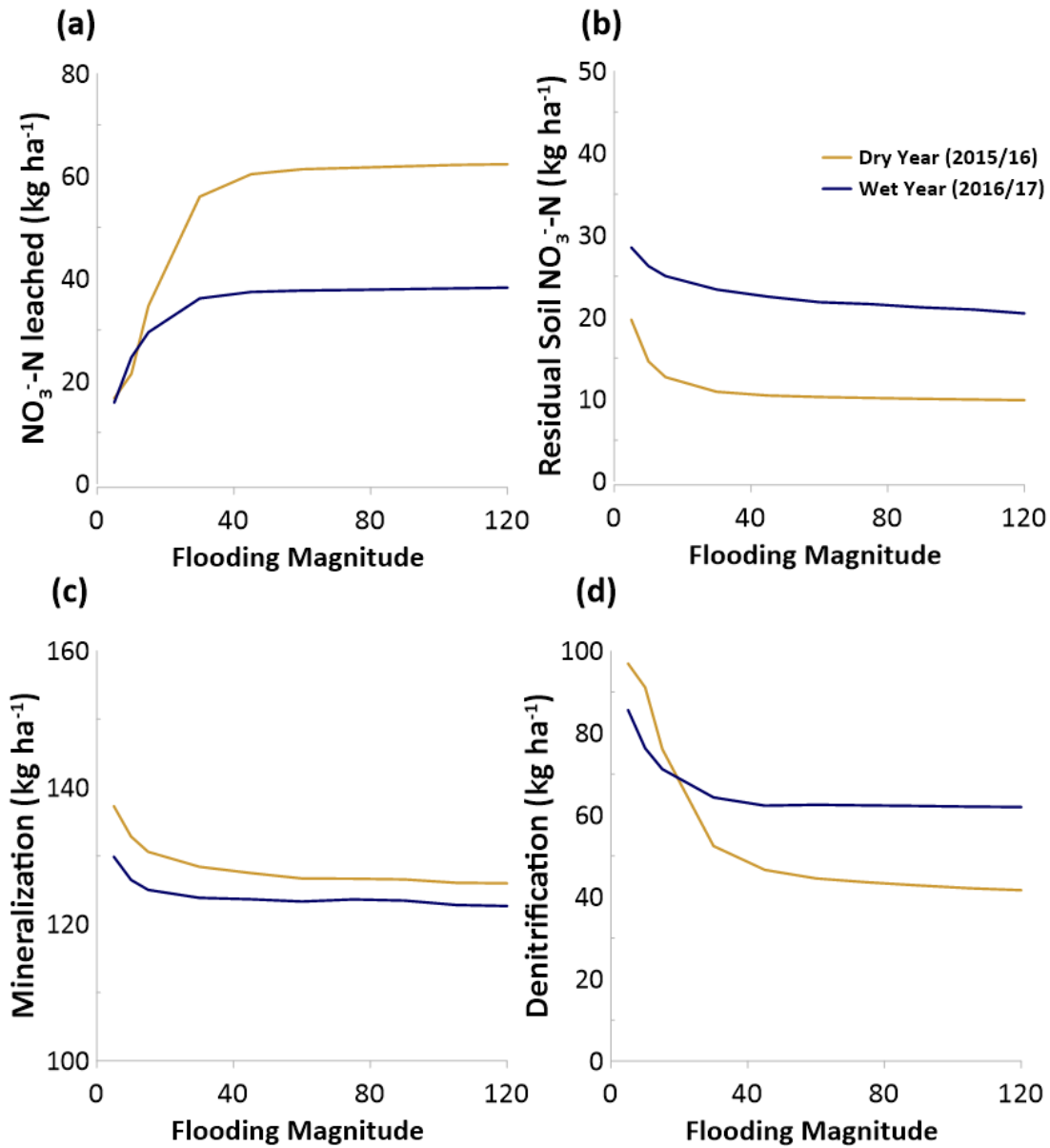


Fig. S4.4: Flooding magnitude scenarios for the fine sandy loam soil at the 14-day flooding frequency. (a) sum of NO<sub>3</sub><sup>-</sup> leached from model domain during Ag-MAR flooding season, (b) residual NO<sub>3</sub><sup>-</sup> in soil profile following Ag-MAR flooding season, (c) amount of mineralization occurring during Ag-MAR flooding season, (d) amount of denitrification occurring during Ag-MAR flooding season, as a function of flooding magnitude.

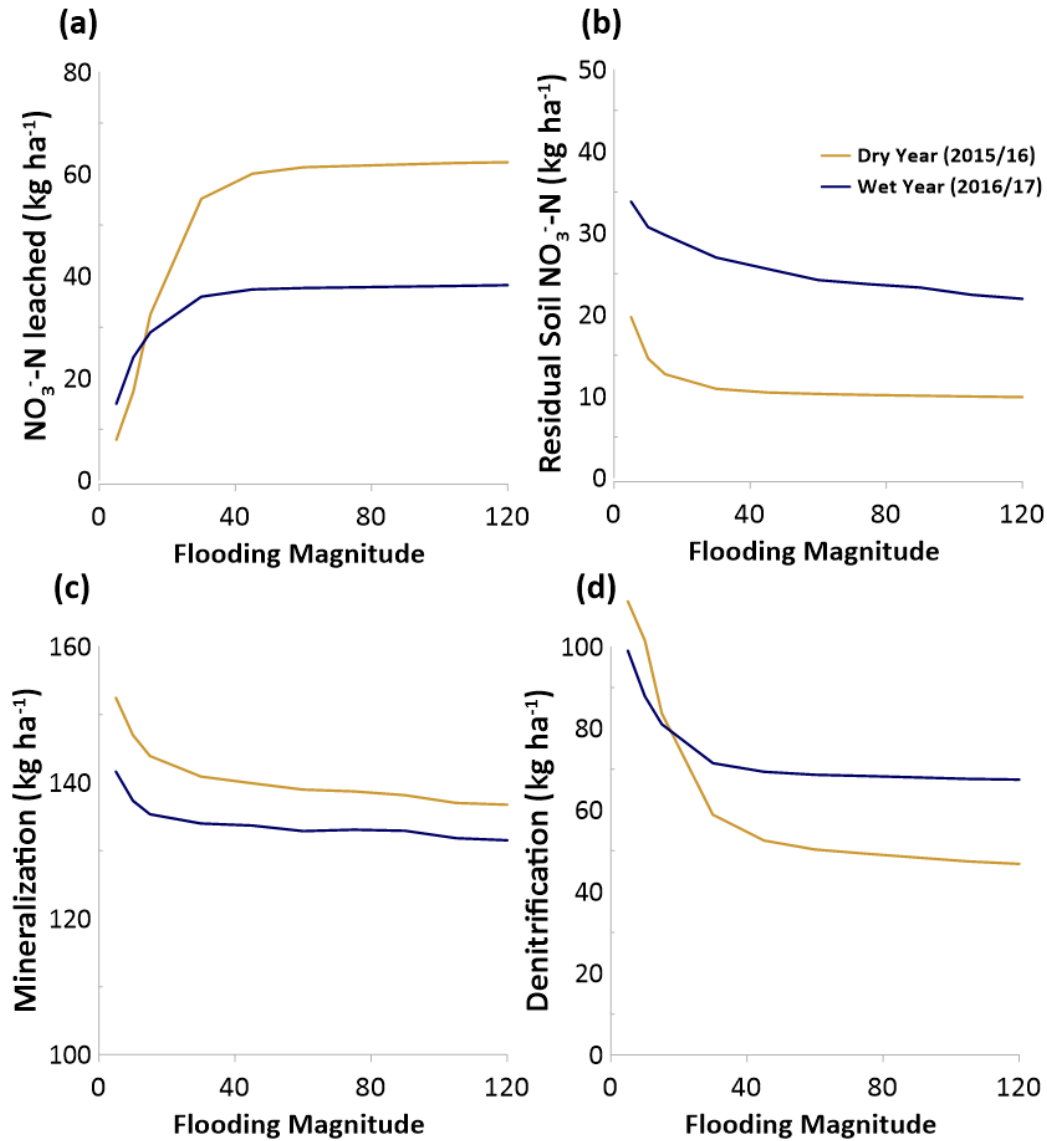


Fig. S4.5: Flooding magnitude scenarios for the fine sandy loam soil at the 21-day flooding frequency. (a) sum of NO<sub>3</sub><sup>-</sup> leached from model domain during Ag-MAR flooding season, (b) residual NO<sub>3</sub><sup>-</sup> in soil profile following Ag-MAR flooding season, (c) amount of mineralization occurring during Ag-MAR flooding season, (d) amount of denitrification occurring during Ag-MAR flooding season, as a function of flooding magnitude.

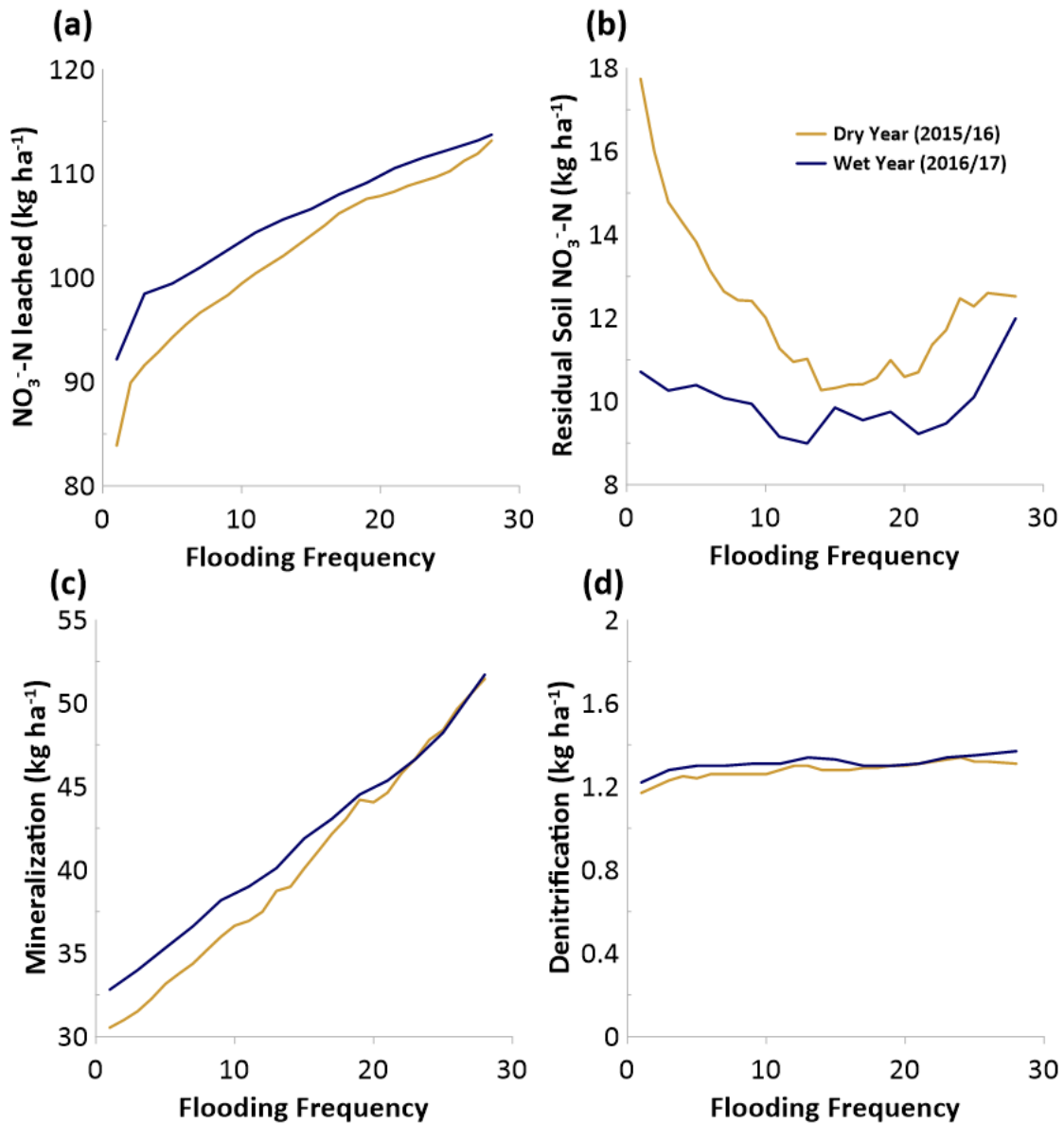


Fig. S4.6: Flooding frequency scenarios for the sand soil at 60 cm flooding magnitude. (a) sum of  $\text{NO}_3^-$  leached from model domain during Ag-MAR flooding season, (b) residual  $\text{NO}_3^-$  in soil profile following Ag-MAR flooding season, (c) amount of mineralization occurring during Ag-MAR flooding season, (d) amount of denitrification occurring during Ag-MAR flooding season, as a function of flooding frequency.

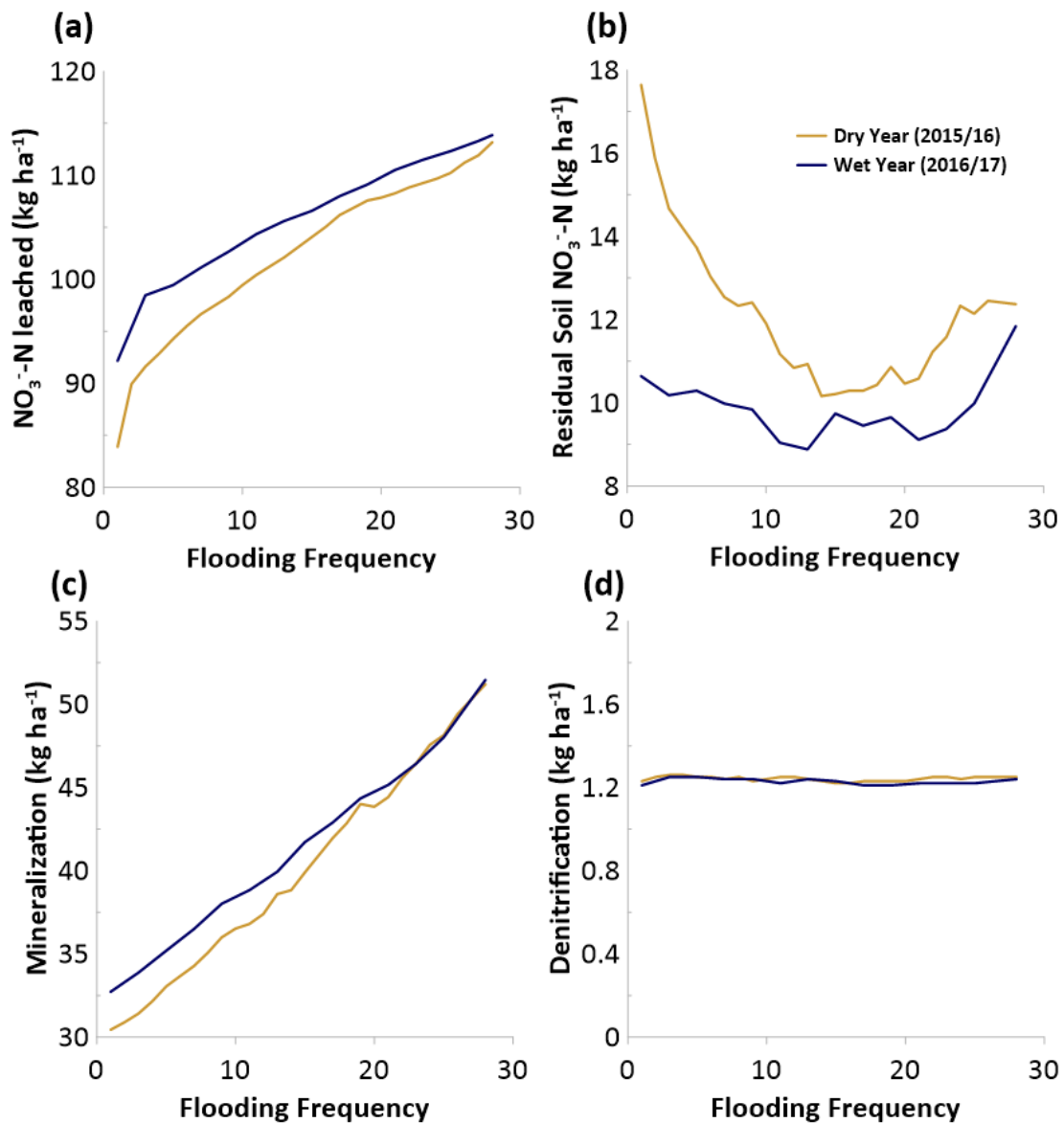


Fig. S4.7: Flooding frequency scenarios for the sand soil at 120 cm flooding magnitude. (a) sum of  $\text{NO}_3^-$  leached from model domain during Ag-MAR flooding season, (b) residual  $\text{NO}_3^-$  in soil profile following Ag-MAR flooding season, (c) amount of mineralization occurring during Ag-MAR flooding season, (d) amount of denitrification occurring during Ag-MAR flooding season, as a function of flooding frequency.

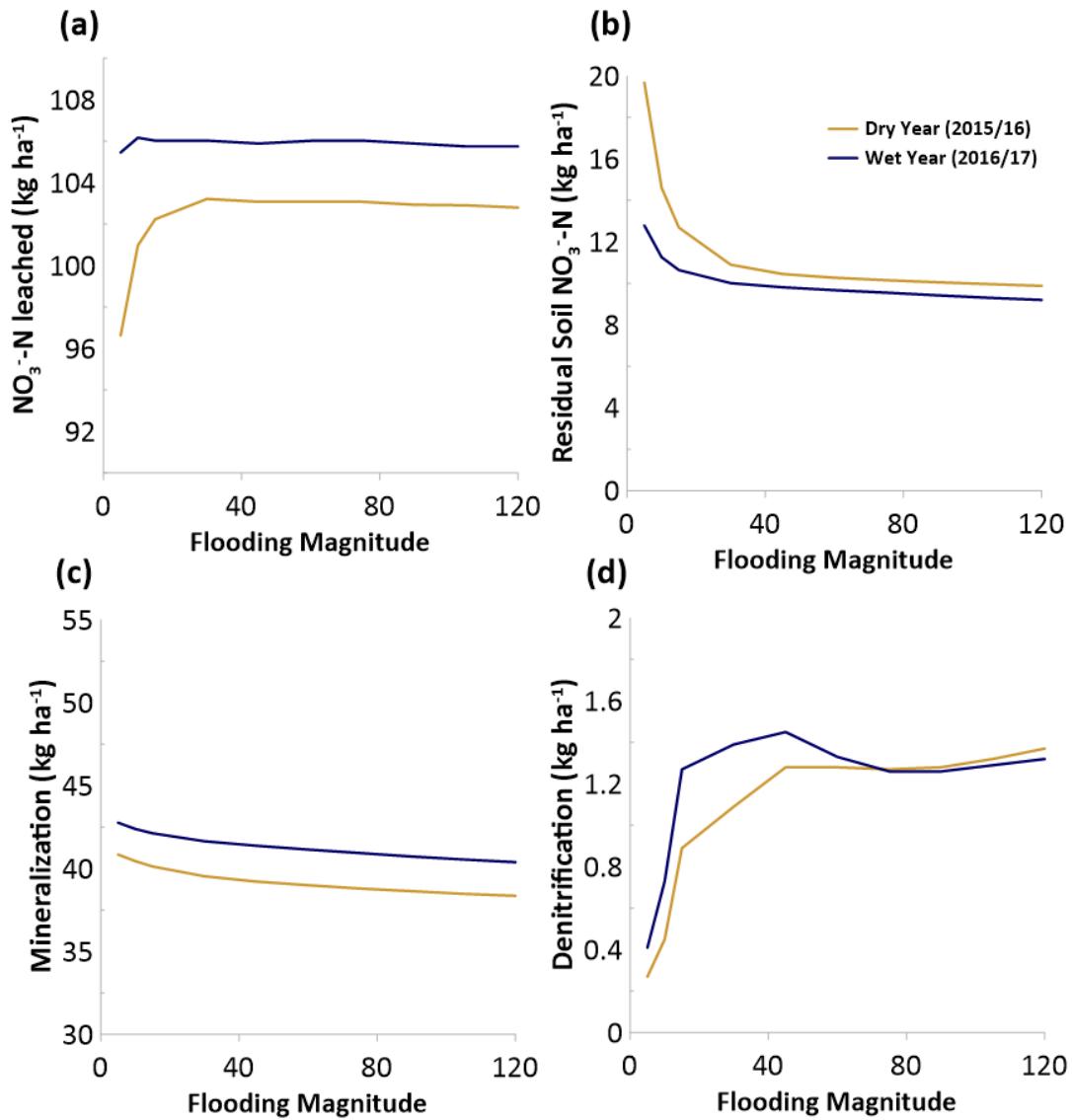


Fig. S4.8: Flooding magnitude scenarios for the sand soil at the 14-day flooding frequency. (a) sum of  $\text{NO}_3^-$  leached from model domain during Ag-MAR flooding season, (b) residual  $\text{NO}_3^-$  in soil profile following Ag-MAR flooding season, (c) amount of mineralization occurring during Ag-MAR flooding season, (d) amount of denitrification occurring during Ag-MAR flooding season, as a function of flooding magnitude.

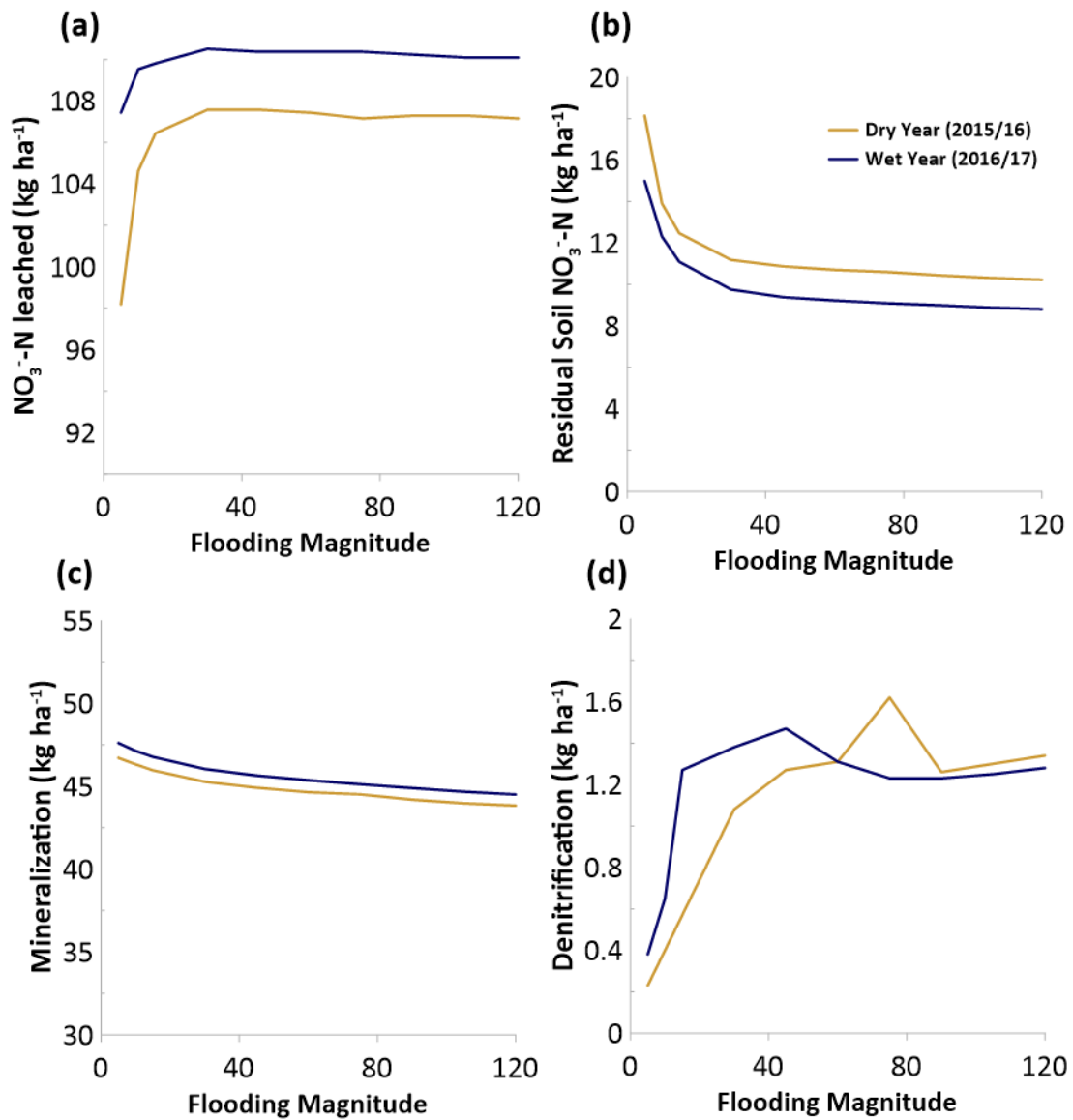


Fig. S4.9: Flooding magnitude scenarios for the sand soil at the 21-day flooding frequency. (a) sum of  $\text{NO}_3^-$  leached from model domain during Ag-MAR flooding season, (b) residual  $\text{NO}_3^-$  in soil profile following Ag-MAR flooding season, (c) amount of mineralization occurring during Ag-MAR flooding season, (d) amount of denitrification occurring during Ag-MAR flooding season, as a function of flooding magnitude.

## References

- Abiye, T. A., Sulieman, H., & Ayalew, M. (2009). Use of treated wastewater for managed aquifer recharge in highly populated urban centers: a case study in Addis Ababa, Ethiopia. *Environmental geology*, 58(1), 55-59.
- Ajdary, K., Singh, D. K., Singh, A. K., & Khanna, M. (2007). Modelling of nitrogen leaching from experimental onion field under drip fertigation. *Agricultural water management*, 89(1-2), 15-28.
- Andraski, T. W., Bundy, L. G., & Brye, K. R. (2000). *Crop management and corn nitrogen rate effects on nitrate leaching* (Vol. 29, No. 4, pp. 1095-1103). American Society of Agronomy, Crop Science Society of America, and Soil Science Society of America.
- Aronsson, P. G., & Bergström, L. F. (2001). Nitrate leaching from lysimeter-grown short-rotation willow coppice in relation to N-application, irrigation and soil type. *Biomass and Bioenergy*, 21(3), 155-164.
- Austin, A. T., Yahdjian, L., Stark, J. M., Belnap, J., Porporato, A., Norton, U., ... & Schaeffer, S. M. (2004). Water pulses and biogeochemical cycles in arid and semiarid ecosystems. *Oecologia*, 141(2), 221-235.
- Azam, F., Mahmood, T., & Malik, K. A. (1988). Immobilization-rem mineralization of NO<sub>3</sub>-N and total N balance during the decomposition of glucose, sucrose and cellulose in soil incubated at different moisture regimes. *Plant and Soil*, 107(2), 159-163.
- Bachand, P. A., Roy, S. B., Choperena, J., Cameron, D., & Horwath, W. R. (2014). Implications of using on-farm flood flow capture to recharge groundwater and mitigate flood risks along the Kings River, CA. *Environmental science & technology*, 48(23), 13601-13609.
- Bachand, P., Roy, S., Stern, N., Choperena, J., Cameron, D., & Horwath, W. (2016). On-farm flood capture could reduce groundwater overdraft in Kings River Basin. *California Agriculture*, 70(4), 200-207.
- Baram, S., Couvreur, V., Harter, T., Read, M., Brown, P. H., Hopmans, J. W., & Smart, D. R. (2016). Assessment of orchard N losses to groundwater with a vadose zone monitoring network. *Agricultural Water Management*, 172, 83-95.
- Barton, L., McLay, C. D. A., Schipper, L. A., & Smith, C. T. (1999). Annual denitrification rates in agricultural and forest soils: a review. *Soil Research*, 37(6), 1073-1094.
- Bateman, E. J., & Baggs, E. M. (2005). Contributions of nitrification and denitrification to N<sub>2</sub>O emissions from soils at different water-filled pore space. *Biology and fertility of soils*, 41(6), 379-388.

- Ben Moshe, S., Weisbrod, N., Barquero, F., Sallwey, J., Orgad, O., & Furman, A. (2020). On the role of operational dynamics in biogeochemical efficiency of a soil aquifer treatment system. *Hydrology and Earth System Sciences*, 417–426. Doi: 10.5194/hess-24-417-2020
- Ben Moshe, S., Weisbrod, N., & Furman, A. (2021). Optimization of soil aquifer treatment (SAT) operation using a reactive transport model. *Vadose Zone Journal*, 20(1), e20095.
- Bergström, L., & Johansson, R. (1991). Leaching of nitrate from monolith lysimeters of different types of agricultural soils. *Journal of environmental quality*, 20(4), 801-807.
- Booth, M. S., Stark, J. M., & Rastetter, E. (2005). Controls on nitrogen cycling in terrestrial ecosystems: a synthetic analysis of literature data. *Ecological monographs*, 75(2), 139-157.
- Borken, W., & Matzner, E. (2009). Reappraisal of drying and wetting effects on C and N mineralization and fluxes in soils. *Global change biology*, 15(4), 808-824.
- Botros, F. E., Onsoy, Y. S., Ginn, T. R., & Harter, T. (2012). Richards equation–based modeling to estimate flow and nitrate transport in a deep alluvial vadose zone. *Vadose Zone Journal*, 11(4).
- Bremner, J. M., & Shaw, K. (1958). Denitrification in soil. II. Factors affecting denitrification. *The Journal of Agricultural Science*, 51(1), 40-52.
- Burger, M., & Jackson, L. E. (2003). Microbial immobilization of ammonium and nitrate in relation to ammonification and nitrification rates in organic and conventional cropping systems. *Soil Biology and Biochemistry*, 35(1), 29-36.
- Butterbach-bahl, K., Baggs, E. M., Dannenmann, M., & Kiese, R. (n.d.). *Appendix : Nitrous oxide emissions from soils : How well do we understand the processes and their controls ?* 1–20.
- Butterbach-Bahl, K., & Dannenmann, M. (2011). Denitrification and associated soil N<sub>2</sub>O emissions due to agricultural activities in a changing climate. *Current Opinion in Environmental Sustainability*, 3(5), 389-395.
- Cabrera, M. L. (1993). Modeling the flush of nitrogen mineralization caused by drying and rewetting soils. *Soil Science Society of America Journal*, 57(1), 63-66.
- California Department of Water Resources (2017). Water Year 2017: What a difference a year makes.
- Cambardella, C. A., Moorman, T. B., Jaynes, D. B., Hatfield, J. L., Parkin, T. B., Simpkins, W. W., & Karlen, D. L. (1999). Water quality in Walnut Creek watershed: Nitrate-nitrogen in soils, subsurface drainage water, and shallow groundwater. *Journal of Environmental Quality*, 28(1), 25-34
- Cassman, K. G., & Munns, D. N. (1980). Nitrogen mineralization as affected by soil moisture, temperature, and depth. *Soil Science Society of America Journal*, 44(6), 1233-1237.

Ceriotti, G., Russian, A., Bolster, D., & Porta, G. (2019). A double-continuum transport model for segregated porous media: Derivation and sensitivity analysis-driven calibration. *Advances in Water Resources*, 128, 206-217.

Chau, JF., Bagtzoglou, AC., Willig, MR. 2011. The effect of soil texture on richness and diversity of bacterial communities. *Environ Forensics* 12:333-341

Cookson, W. R., Osman, M., Marschner, P., Abaye, D. A., Clark, I., Murphy, D. V., ... & Watson, C. A. (2007). Controls on soil nitrogen cycling and microbial community composition across land use and incubation temperature. *Soil Biology and Biochemistry*, 39(3), 744-756.

Dahlke, H., Brown, A., Orloff, S., Putnam, D., & O'Geen, T. (2018). Managed winter flooding of alfalfa recharges groundwater with minimal crop damage. *California Agriculture*, 72(1), 65-75.

Dahlke, H. E., LaHue, G. T., Mautner, M. R., Murphy, N. P., Patterson, N. K., Waterhouse, H., ... & Foglia, L. (2018). Managed aquifer recharge as a tool to enhance sustainable groundwater management in California: examples from field and modeling studies. In *Advances in Chemical Pollution, Environmental Management and Protection* (Vol. 3, pp. 215-275). Elsevier.

Dahan, O., Talby, R., Yechieli, Y., Adar, E., Lazarovitch, N., & Enzel, Y. (2009). In situ monitoring of water percolation and solute transport using a vadose zone monitoring system. *Vadose Zone Journal*, 8(4), 916-925.

Dalin, C., Taniguchi, M., & Green, T. R. (2019). Unsustainable groundwater use for global food production and related international trade. *Global Sustainability*, 2.

Di, H. J., & Cameron, K. C. (2002). Nitrate leaching in temperate agroecosystems: sources, factors and mitigating strategies. *Nutrient cycling in agroecosystems*, 64(3), 237-256.

Di, H. J., & Cameron, K. C. (2002). Nitrate leaching and pasture production from different nitrogen sources on a shallow stoney soil under flood-irrigated dairy pasture. *Soil Research*, 40(2), 317-334.

Diez, J. A., Caballero, R., Roman, R., Tarquis, A., Cartagena, M. C., & Vallejo, A. (2000). *Integrated fertilizer and irrigation management to reduce nitrate leaching in Central Spain* (Vol. 29, No. 5, pp. 1539-1547). American Society of Agronomy, Crop Science Society of America, and Soil Science Society of America.

Dillon, P. J., Pavelic, P., Page, D., Beringen, H., & Ward, J. (2009). Managed aquifer recharge. *An introduction waterlines report series*, 13, 1-64.

Dillon, P., Stuyfzand, P., Grischek, T., Lluria, M., Pyne, R. D. G., Jain, R. C., ... & Sapiano, M. (2019). Sixty years of global progress in managed aquifer recharge. *Hydrogeology journal*, 27(1), 1-30.

- Doane, T. A., & Horwath, W. R. (2003). Spectrophotometric determination of nitrate with a single reagent. *Analytical letters*, 36(12), 2713-2722.
- Domínguez-Niño, J. M., Arbat, G., Rajj-Hoffman, I., Kisekka, I., Girona, J., & Casadesús, J. (2020). Parameterization of soil hydraulic parameters for HYDRUS-3D simulation of soil water dynamics in a drip-irrigated orchard. *Water*, 12(7), 1858.
- D'odorico, P., Laio, F., Porporato, A., & Rodriguez-Iturbe, I. (2003). Hydrologic controls on soil carbon and nitrogen cycles. II. A case study. *Advances in Water Resources*, 26(1), 59-70.
- DWR. Groundwater. California Department of Water Resources (DWR), Sacramento, CA, USA (2019). <https://water.ca.gov/Water-Basics/Groundwater>
- Forster, J.C. **Soil physical analysis**. K. Alef, P. Nannipieri (Eds.) (1995). *Methods in Soil Microbiology and Biochemistry*, Academic Press, London, pp. 105-121
- Fraterrigo, J. M., Turner, M. G., Pearson, S. M., & Dixon, P. (2005). Effects of past land use on spatial heterogeneity of soil nutrients in southern Appalachian forests. *Ecological Monographs*, 75(2), 215-230.
- Gaines, T. P., & Gaines, S. T. (1994). Soil texture effect on nitrate leaching in soil percolates. *Communications in soil science and plant analysis*, 25(13-14), 2561-2570.
- Gårdenäs, A. I., Hopmans, J. W., Hanson, B. R., & Šimůnek, J. (2005). Two-dimensional modeling of nitrate leaching for various fertigation scenarios under micro-irrigation. *Agricultural water management*, 74(3), 219-242.
- Geisseler, D., Miller, K. S., Aegerter, B. J., Clark, N. E., & Miyao, E. M. (2019). Estimation of Annual Soil Nitrogen Mineralization Rates using an Organic-Nitrogen Budget Approach. *Soil Science Society of America Journal*, 83(4), 1227-1235.
- Gheysari, M., Mirlatifi, S. M., Homae, M., Asadi, M. E., & Hoogenboom, G. (2009). Nitrate leaching in a silage maize field under different irrigation and nitrogen fertilizer rates. *Agricultural water management*, 96(6), 946-954.
- Graham, P. H., & Vance, C. P. (2000). Nitrogen fixation in perspective: an overview of research and extension needs. *Field crops research*, 65(2-3), 93-106.
- Gorski, G., Fisher, A. T., Beganskas, S., Weir, W. B., Redford, K., Schmidt, C., & Saltikov, C. (2019). Field and Laboratory Studies Linking Hydrologic, Geochemical, and Microbiological Processes and Enhanced Denitrification during Infiltration for Managed Recharge. *Environmental science & technology*, 53(16), 9491-9501.
- Goren, O., Burg, A., Gavrieli, I., Negev, I., Guttman, J., Kraitzer, T., Kloppmann, W., and Lazar, B.: Biogeochemical processes in infiltration basins and their impact on the recharging effluent,

the soil aquifer treatment (SAT) system of the Shafdan plant, Israel, *Appl. Geochem.*, 48, 58–69, <https://doi.org/10.1016/j.apgeochem.2014.06.017>, 2014.

Gregorich, E. G., Voroney, R. P., & Kachanoski, R. G. (1991). Turnover of carbon through the microbial biomass in soils with different texture. *Soil Biology and Biochemistry*, 23(8), 799-805.

Greskowiak, J., Prommer, H., Massmann, G., Johnston, C. D., Nützmann, G., & Pekdeger, A. (2005). The impact of variably saturated conditions on hydrogeochemical changes during artificial recharge of groundwater. *Applied Geochemistry*, 20(7), 1409-1426.

Groffman, P.M., Holland, E.A., Myrold, D.D., Robertson, G.P., Zou, X. 1999. Denitrification. Pages 272-288 in G.P. Robertson, D.C. Coleman, C.S. Bledsoe, P. Sollins (editors). Standard soil methods for long-term ecological research. Oxford University Press, New York, NY, USA.

Groffman, P. M., Butterbach-Bahl, K., Fulweiler, R. W., Gold, A. J., Morse, J. L., Stander, E. K., ... & Vidon, P. (2009). Challenges to incorporating spatially and temporally explicit phenomena (hotspots and hot moments) in denitrification models. *Biogeochemistry*, 93(1-2), 49-77.

Gurdak, J. J., & Qi, S. L. (2012). Vulnerability of recently recharged groundwater in principle aquifers of the United States to NO<sub>3</sub>- contamination. *Environmental science & technology*, 46(11), 6004-6012.

Hanak, E., Lund, J., Arnold, B., Escrivá-Bou, A., Gray, B., Green, S., ... & Seavy, N. (2017). Water stress and a changing San Joaquin Valley. *Public Policy Institute of California*, 1, 5-48.

Hanson, B. R., Šimůnek, J., & Hopmans, J. W. (2006). Evaluation of urea–ammonium–nitrate fertigation with drip irrigation using numerical modeling. *Agricultural water management*, 86(1-2), 102-113.

Hargrove, W. L. (1988). Soil, environmental, and management factors influencing ammonia volatilization under field conditions. *Ammonia volatilization from urea fertilizers. Alabama: NFDC, TVA*, 2, 17-36.

Harter, T., Onsoy, Y., Heeren, K., Denton, M., Weissmann, G., Hopmans, J., & Horwath, W. (2005). Deep vadose zone hydrology demonstrates fate of nitrate in eastern San Joaquin Valley. *California agriculture*, 59(2), 124-132.

Harter, T., & Dahlke, H. (2014). Out of sight but not out of mind: California refocuses on groundwater. *California Agriculture*, 68(3), 54-55

Harter, T. (2015). California's agricultural regions gear up to actively manage groundwater use and protection. *California Agriculture*, 69(3), 193-201.

Hergert, G. W. (1986). *Nitrate leaching through sandy soil as affected by sprinkler irrigation management* (Vol. 15, No. 3, pp. 272-278). American Society of Agronomy, Crop Science Society of America, and Soil Science Society of America.

Hofstra, N., & Bouwman, A. F. (2005). Denitrification in agricultural soils: summarizing published data and estimating global annual rates. *Nutrient Cycling in Agroecosystems*, 72(3), 267-278.

Jiang, S., Pang, L., Buchan, G. D., Šimůnek, J., Noonan, M. J., & Close, M. E. (2010). Modeling water flow and bacterial transport in undisturbed lysimeters under irrigations of dairy shed effluent and water using HYDRUS-1D. *Water Research*, 44(4), 1050-1061.

Johnsson, H., Bergstrom, L., Jansson, P. E., & Paustian, K. (1987). Simulated nitrogen dynamics and losses in a layered agricultural soil. *Agriculture, Ecosystems & Environment*, 18(4), 333-356.

Kaiser, E. A., Mueller, T., Joergensen, R. G., Insam, H., & Heinemeyer, O. (1992). Evaluation of methods to estimate the soil microbial biomass and the relationship with soil texture and organic matter. *Soil biology and biochemistry*, 24(7), 675-683.

Kocis, T. N., & Dahlke, H. E. (2017). Availability of high-magnitude streamflow for groundwater banking in the Central Valley, California. *Environmental Research Letters*, 12(8), 084009.

Konikow, L. F., & Kendy, E. (2005). Groundwater depletion: A global problem. *Hydrogeology Journal*, 13(1), 317-320.

Kool, J. B., Parker, J. C., & Van Genuchten, M. T. (1985). Determining soil hydraulic properties from one-step outflow experiments by parameter estimation: I. Theory and numerical studies. *Soil Science Society of America Journal*, 49(6), 1348-1354.

Kosugi, K. I., Hopmans, J. W., & Dane, J. H. (2002). 3.3. 4 Parametric Models. *Methods of Soil Analysis: Part 4 Physical Methods*, 5, 739-757.

Kuypers, M. M., Marchant, H. K., & Kartal, B. (2018). The microbial nitrogen-cycling network. *Nature Reviews Microbiology*, 16(5), 263-276.

Lazicki, P., Geisseler, D., & Lloyd, M. (2020). *Nitrogen mineralization from organic amendments is variable but predictable* (Vol. 49, No. 2, pp. 483-495).

Levy, Z. F., Jurgens, B. C., Burow, K. R., Voss, S. A., Faulkner, K. E., Arroyo-Lopez, J. A., & Fram, M. S. (2021). Critical aquifer overdraft accelerates degradation of groundwater quality in California's Central Valley during drought. *Geophysical Research Letters*, 48(17), e2021GL094398.

Lewis, J., & Sjöström, J. (2010). Optimizing the experimental design of soil columns in saturated and unsaturated transport experiments. *Journal of contaminant hydrology*, 115(1-4), 1-13.

- Linn, D.M., Doran, J.W., 1984. Effect of water-filled pore space on carbon dioxide and nitrous oxide production in tilled and nontilled Soils1. *Soil Sci. Soc. Am. J.* 48, 1267. <http://dx.doi.org/10.2136/sssaj1984.03615995004800060013x>.
- Liu, Y., & Kitanidis, P. K. (2012). Applicability of the dual-domain model to nonaggregated porous media. *Groundwater*, 50(6), 927-934.
- Lotse, E. G., Jabro, J. D., Simmons, K. E., & Baker, D. E. (1992). Simulation of nitrogen dynamics and leaching from arable soils. *Journal of contaminant hydrology*, 10(3), 183-196.
- Lv, H., Lin, S., Wang, Y., Lian, X., Zhao, Y., Li, Y., ... & Butterbach-Bahl, K. (2019). Drip fertigation significantly reduces nitrogen leaching in solar greenhouse vegetable production system. *Environmental pollution*, 245, 694-701.
- Machefert, S. E., & Dise, N. B. (2004). Hydrological controls on denitrification in riparian ecosystems. *Hydrology and Earth System Sciences*, 8(4), 686-694.
- Mack, U. D., Feger, K. H., Gong, Y., & Stahr, K. (2005). Soil water balance and nitrate leaching in winter wheat–summer maize double-cropping systems with different irrigation and N fertilization in the North China Plain. *Journal of Plant Nutrition and Soil Science*, 168(4), 454-460.
- Miller, J. H., Ela, W. P., Lansey, K. E., Chipello, P. L., & Arnold, R. G. (2006). Nitrogen transformations during soil–aquifer treatment of wastewater effluent—Oxygen effects in field studies. *Journal of Environmental Engineering*, 132(10), 1298-1306.
- Miller, K. S., & Geisseler, D. (2018). Temperature sensitivity of nitrogen mineralization in agricultural soils. *Biology and Fertility of Soils*, 54(7), 853-860.
- Munch, J. C., & Velthof, G. L. (2007). Denitrification and agriculture. In *Biology of the nitrogen cycle* (pp. 331-341). Elsevier.
- Murphy, D. V., Sparling, G. P., & Fillery, I. R. P. (1998). Stratification of microbial biomass C and N and gross N mineralisation with soil depth in two contrasting Western Australian agricultural soils. *Soil Research*, 36(1), 45-56.
- Murphy, N. P., Waterhouse, H., & Dahlke, H. E. (2021). Influence of agricultural managed aquifer recharge on nitrate transport: The role of soil texture and flooding frequency. *Vadose Zone Journal*, 20(5), e20150.
- Noy-Meir, I. (1973). Desert ecosystems: environment and producers. *Annual review of ecology and systematics*, 4(1), 25-51.
- Nyamangara, J., Bergström, L. F., Piha, M. I., & Giller, K. E. (2003). Fertilizer use efficiency and nitrate leaching in a tropical sandy soil. *Journal of environmental quality*, 32(2), 599-606.

O'Geen, A. T., Saal, M., Dahlke, H., Doll, D., Elkins, R., Fulton, A., Fogg, G., Harter, T., Hopmans, J.W., Ingels, C., Niederholzer, F., Solis, S.S., Verdegaal, P., Walkinshaw, M. (2015). Soil suitability index identifies potential areas for groundwater banking on agricultural lands. *California Agriculture*, 69(2), 75-84.

Onsoy, Y. S., Harter, T., Ginn, T. R., & Horwath, W. R. (2005). Spatial variability and transport of nitrate in a deep alluvial vadose zone. *Vadose Zone Journal*, 4(1), 41-54.

Padilla, F. M., Gallardo, M., & Manzano-Agugliaro, F. (2018). Global trends in nitrate leaching research in the 1960–2017 period. *Science of the Total Environment*, 643, 400-413.

Parkhurst, D. L., & Appelo, C. A. J. (1999). User's guide to PHREEQC (Version 2): A computer program for speciation, batch-reaction, one-dimensional transport, and inverse geochemical calculations. *Water-resources investigations report*, 99(4259), 312.

Parkin, T. B. (1987). Soil microsites as a source of denitrification variability 1. *Soil Science Society of America Journal*, 51(5), 1194-1199.

Paul, E. A., & Clark, F. E. (2000). Soil microbiology and biochemistry. 1989.

Paul, K. I., Polglase, P. J., O'connell, A. M., Carlyle, J. C., Smethurst, P. J., & Khanna, P. K. (2003). Defining the relation between soil water content and net nitrogen mineralization. *European journal of soil science*, 54(1), 39-48.

Phogat, V., Skewes, M. A., Cox, J. W., Sanderson, G., Alam, J., & Šimůnek, J. (2014). Seasonal simulation of water, salinity and nitrate dynamics under drip irrigated mandarin (*Citrus reticulata*) and assessing management options for drainage and nitrate leaching. *Journal of Hydrology*, 513, 504-516.

Poeter, E. P., & Hill, M. C. (1999). UCODE, a computer code for universal inverse modeling. *Computers & Geosciences*, 25(4), 457-462.

Power, J. F. Y., & Schepers, J. S. (1989). NO<sub>3</sub><sup>-</sup> contamination of groundwater in North America. *Agriculture, ecosystems & environment*, 26(3-4), 165-187.

Porporato, A., D'odorico, P., Laio, F., & Rodriguez-Iturbe, I. (2003). Hydrologic controls on soil carbon and nitrogen cycles. I. Modeling scheme. *Advances in water resources*, 26(1), 45-58.

Quanrud, D. M., Arnold, R. G., Wilson, L. G., Gordon, H. J., Graham, D. W., & Amy, G. L. (1996). Fate of organics during column studies of soil aquifer treatment. *Journal of Environmental Engineering*, 122(4), 314-321.

Ransom, K. M., Bell, A. M., Barber, Q. E., Kourakos, G., & Harter, T. (2018). A Bayesian approach to infer nitrogen loading rates from crop and land-use types surrounding private wells in the Central Valley, California. *Hydrology and Earth System Sciences*, 22(5), 2739-2758.

- Recous, S., Mary, B., & Faurie, G. (1990). Microbial immobilization of ammonium and nitrate in cultivated soils. *Soil Biology and Biochemistry*, 22(7), 913-922.
- Ritter, W. F. (1989). Nitrate leaching under irrigation in the United States—a review. *Journal of Environmental Science & Health Part A*, 24(4), 349-378.
- Romero, C. M., Engel, R., Chen, C., & Wallander, R. (2015). Microbial immobilization of nitrogen-15 labelled ammonium and nitrate in an agricultural soil. *Soil Science Society of America Journal*, 79(2), 595-602.
- Rukh, S., Akhtar, M. S., Mehmood, A., Hoghooghi, N., & Radcliffe, D. E. (2018). Evaluating Nonequilibrium Solute Transport through Four Soils of Pakistan using a HYDRUS Model and Nonparametric Indices. *Soil Science Society of America Journal*, 82(5), 1071-1084.
- Schaap, M. G., Leij, F. J., & Van Genuchten, M. T. (2001). Rosetta: A computer program for estimating soil hydraulic parameters with hierarchical pedotransfer functions. *Journal of hydrology*, 251(3-4), 163-176.
- Schmidt, C. M., Fisher, A. T., Racz, A. J., Lockwood, B. S., & Huertos, M. L. (2011). Linking denitrification and infiltration rates during managed groundwater recharge. *Environmental science & technology*, 45(22), 9634-9640.
- Simunek, J., Sejna, M., Van Genuchten, M. T., Šimůnek, J., Šejna, M., Jacques, D., ... & Sakai, M. (1998). HYDRUS-1D. *Simulating the one-dimensional movement of water, heat, and multiple solutes in variably-saturated media, version, 2*.
- Šimůnek, J., & van Genuchten, M. T. (2008). Modeling nonequilibrium flow and transport processes using HYDRUS. *Vadose Zone Journal*, 7(2), 782-797.
- Smith, M. S., Firestone, M. K., & Tiedje, J. M. (1978). The acetylene inhibition method for short-term measurement of soil denitrification and its evaluation using nitrogen-13. *Soil Science Society of America Journal*, 42(4), 611-615.
- SoilWeb, 2015. SoilWeb - Interactive map of USDA-NCSS soil survey data for locations throughout most of the U.S. [WWW Document]. Calif. Soil Resour. Lab UC Davis UC- ANR Collab. with USDA Nat. Resour. Conserv. Serv. URL (<http://casoilresource.lawr.ucdavis.edu/gmap> (accessed 10.15.17)).
- Sogbedji, J. M., van Es, H. M., Yang, C. L., Geohring, L. D., & Magdoff, F. R. (2000). Nitrate leaching and nitrogen budget as affected by maize nitrogen rate and soil type. *Journal of Environmental Quality*, 29(6), 1813-1820.
- Springob, G., & Kirchmann, H. (2003). Bulk soil C to N ratio as a simple measure of net N mineralization from stabilized soil organic matter in sandy arable soils. *Soil Biology and Biochemistry*, 35(4), 629-632.

Van Genuchten, M. T., & Nielsen, D. R. (1985). On describing and predicting the hydraulic properties. In *Annales Geophysicae* (Vol. 3, No. 5, pp. 615-628).

Vázquez, N., Pardo, A., Suso, M. L., & Quemada, M. (2006). Drainage and nitrate leaching under processing tomato growth with drip irrigation and plastic mulching. *Agriculture, ecosystems & environment*, 112(4), 313-323.

Verdouw, H., Van Echteld, C. J. A., & Dekkers, E. M. J. (1978). Ammonia determination based on indophenol formation with sodium salicylate. *Water Research*, 12(6), 399-402.

Wada, Y., Wisser, D., & Bierkens, M. F. (2014). Global modeling of withdrawal, allocation and consumptive use of surface water and groundwater resources. *Earth System Dynamics*, 5(1), 15-40.

Waddell, J. T., Gupta, S. C., Moncrief, J. F., Rosen, C. J., & Steele, D. D. (2000). Irrigation-and nitrogen-management impacts on nitrate leaching under potato. *Journal of Environmental Quality*, 29(1), 251-261.

Wade, J., Horwath, W. R., & Burger, M. B. (2016). Integrating soil biological and chemical indices to predict net nitrogen mineralization across California agricultural systems. *Soil Science Society of America Journal*, 80(6), 1675-1687.

Wade, J., Waterhouse, H., Roche, L. M., & Horwath, W. R. (2018). Structural equation modeling reveals iron (hydr) oxides as a strong mediator of N mineralization in California agricultural soils. *Geoderma*, 315, 120-129.

Wang, H., Ju, X., Wei, Y., Li, B., Zhao, L., & Hu, K. (2010). Simulation of bromide and nitrate leaching under heavy rainfall and high-intensity irrigation rates in North China Plain. *Agricultural water management*, 97(10), 1646-1654.

Wang, Y., Ying, H., Yin, Y., Zheng, H., & Cui, Z. (2019). Estimating soil nitrate leaching of nitrogen fertilizer from global meta-analysis. *Science of the total Environment*, 657, 96-102.

Waterhouse, H., Bachand, S., Mountjoy, D., Choperena, J., Bachand, P., Dahlke, H., & Horwath, W. (2020). Agricultural managed aquifer recharge—water quality factors to consider. *California Agriculture*, 74(3), 144-154.

Waterhouse, H., Arora, B., Spycher, N. F., Nico, P. S., Ulrich, C., Dahlke, H. E., & Horwath, W. R. (2021). Influence of Agricultural Managed Aquifer Recharge (AgMAR) and Stratigraphic Heterogeneities on Nitrate Reduction in the Deep Subsurface. *Water Resources Research*, e2020WR029148.

Wen-Zhi, Z., Jie-Sheng, H., Jing-Wei, W., & Xi, C. (2013). Modeling soil salt and nitrogen transport under different fertigation practices with Hydrus-1D. *Adv J Food Sci Technol*, 5(5), 592-599.

Willmott, C. J. (1982). Some comments on the evaluation of model performance. *Bulletin of the American Meteorological Society*, 63(11), 1309-1313.

Yetbarek, E., Kumar, S., & Ojha, R. (2020). Effects of soil heterogeneity on subsurface water movement in agricultural fields: A numerical study. *Journal of Hydrology*, 590, 125420.

Yu, S., & Ehrenfeld, J. G. (2009). The effects of changes in soil moisture on nitrogen cycling in acid wetland types of the New Jersey Pinelands (USA). *Soil Biology and Biochemistry*, 41(12), 2394-2405.

Zektser, S., Loáiciga, H. A., & Wolf, J. T. (2005). Environmental impacts of groundwater overdraft: selected case studies in the southwestern United States. *Environmental Geology*, 47(3), 396-404.

Zhou, J., Gu, B., Schlesinger, W. H., & Ju, X. (2016). Significant accumulation of nitrate in Chinese semi-humid croplands. *Scientific reports*, 6(1), 1-8.